Benjamin Kollmitzer

Elasticity and interactions of liquid-ordered/liquid-disordered domains

DOCTORAL THESIS

For obtaining the academic degree of

Doktor der technischen Wissenschaften

Doctoral Programme of Technical Sciences
Technical Physics

Graz University of Technology

Supervisor:
Assoz. Prof. Dr. Georg Pabst

Institute of Materials Physics

Graz, April 2015

Affidavit

I declare that I have authored this thesis independently, that I have not used other than the declared sources/resources, and that I have explicitly indicated all material which has been quoted either literally or by content from the sources used. The text document uploaded to TUGRAZonline is identical to the present doctoral dissertation.

Graz, _____ _____

Date Signature

Eidesstattliche Erklärung[1]

Ich erkläre an Eides statt, dass ich die vorliegende Arbeit selbstständig verfasst, andere als die angegebenen Quellen/Hilfsmittel nicht benutzt, und die den benutzten Quellen wörtlich und inhaltlich entnommenen Stellen als solche kenntlich gemacht habe. Das in TUGRAZonline hochgeladene Textdokument ist mit der vorliegenden Dissertation identisch.

Graz, am _____ _____

Datum Unterschrift

[1] Beschluss der Curricula-Kommission für Bachelor-, Master- und Diplomstudien vom 10.11.2008; Genehmigung des Senates am 1.12.2008

Acknowledgments

I was absurdly fortunate to conduct the research presented in this thesis in a unique environment. I am enormously grateful for the possibility of working in such an amazing team, which taught me the beauties of interdisciplinarity and modern science; but obviously, my deepest gratitude extends to Georg and Peter.

Innumerable travels abroad, to conferences and labs in different parts of the world, and especially the international experiments conducted within the "Asymmetry-team" expanded my horizons. Without support by the Austrian Science Fund FWF, Project no. P24459-B20, and several scholarships, this would never have happened. I am also thankful for having had access to the Vienna Scientific Cluster (VSC).

I am grateful beyond words for my family and some very special friends, but most of all I would like to thank Andrea, who still listens ...

Abstract

Lateral inhomogeneities are a common feature in cell membranes and facilitate a variety of active processes, e.g. cell signaling and trafficking. For biophysical studies, lipid-only vesicles showing liquid-ordered/liquid-disordered (Lo/Ld) phase-separation seem an ideal model system, especially since the size of their inhomogeneities, the domains, can be tuned from nano- to macroscopic regimes. Although the present knowledge on phase behavior and structural details in such systems is enormous, quantitative information on their elastic properties and fundamental interactions are still sparse. The necessary means for obtaining these data by small angle X-ray scattering (SAXS) are derived in the present thesis, and subsequently applied on phase-separated lipid model membranes.

Specifically, we determined the monolayer spontaneous curvature of the physiologically relevant lipids cholesterol, DOPE, POPE, DOPC, DPPC, DSPC, POPC, SOPC and egg sphingomyelin in a broad temperature range from 15–55 °C. This data allowed us to estimate the preferential curvature of Lo/Ld phase-separated lipid mixtures.

Exploiting the domain registration in multibilayers of certain lipid mixtures enabled us to measure the fundamental surface interactions between coexisting Lo/Ld phases and their corresponding elastic curvature bending moduli. In order to analyze such osmotic stress SAXS experiments, we applied a novel Monte Carlo (MC) simulation based technique, which allowed us to treat the repulsion due to thermal undulations exactly.

Finally, we applied these experimentally determined quantities to calculate domain line tensions and the mechanical influences of lipid bilayers on protein partitioning.

Contents

List of Figures

1. Introduction

1.1. Lipid model membranes

All biological cells possess an outer barrier, the so-called plasma membrane [1, pp. 8–9]. Apart from confining and protecting the cell interior, plasma membranes have to selectively pass all nutrition, by-products and signaling information to or from the cell interior. Eukaryotic cells consist of several further membranes, which provide means to separate different cell compartments, for example the nucleus or the endoplasmic reticulum [1, pp. 565–598]. This abundance of membrane motives in nature calls for an in-depth understanding of their properties.

The major building element of membrane structure are lipid molecules [2, 3]. These amphiphilic molecules form few nanometer thick, flexible, and highly dynamic boundaries, thereby providing also the appropriate environment for membrane proteins.

Biological cell membranes consist of thousands of different lipid species, whose compositions are adjusted to environmental conditions [4]. Although lipids are nearly free to diffuse laterally in the prevalently fluid-like membranes, they are not mixed randomly [5–8]. Lateral inhomogeneities in plasma membranes were observed with a multitude of different methods, but their characteristic sizes and compositions are still heavily debated [8, 9]. In light of the astonishing complexity of real cells, just the consensus on the existence of some kind of membrane lipid demixing is remarkable.

Contrary to experiments on whole cells, using reduced model membrane systems tremendously simplifies quantitative and reproducible analyses. Because very pure lipids are readily available, lipid-only vesicles are among the cleanest and best defined membrane mimics [10]. Even at small concentrations, lipids spontaneously form aggregates in aqueous solutions, in order to shield their hydrophobic tails from the surrounding water. In doing so, many

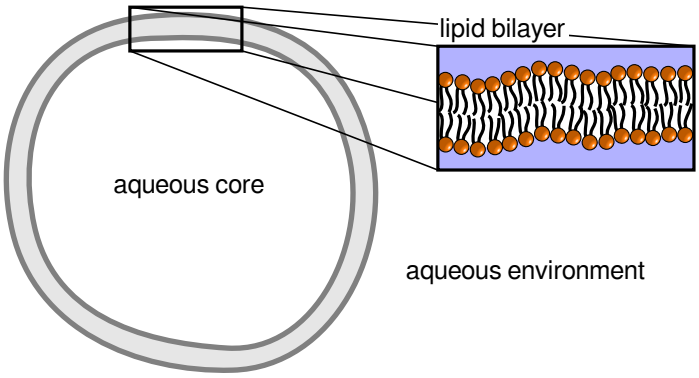

Figure 1.1.: An unilamellar vesicle (gray) consisting of a single lipid bilayer (inset).

physiologically relevant lipid species prefer the planar bilayer phase at standard conditions. To prevent the lipid tails on the membrane's circumference from becoming exposed to the surrounding water, the edges fuse, resulting in usually micrometer-sized vesicles consisting of one (uni-) or multiple lipid bilayers (multilamellar vesicles, MLV), see Fig. 1.1.

In order to gear these lipid-only systems closer towards biological membranes, one can introduce mixtures of different lipid species [3]. Even for simple binary mixtures, deviations from the ideal mixing behavior like in cell membranes can be observed [11, 12]. Especially relevant in this respect are however ternary mixtures consisting of cholesterol (chol), a saturated high-melting, and an unsaturated low-melting lipid. By changing the compositions, these mixtures can be driven through several regimes, including the physiologically highly interesting liquid/liquid phase coexistence (Fig. 1.2) [13]. While the lateral lipid diffusion remains high in this regime, two distinct phases are formed: Most of the low-melting lipid partitions into the liquid-disordered (Ld) phase, while the liquid-ordered (Lo) phase contains prevalently the high-melting lipid and is enriched in cholesterol [14, 15].

Experiments performed on vesicles with coexisting domains are naturally delicate. Usually one would like to determine the properties of individual phases separately, instead of measuring only averaged values for the whole vesicle. If the tie lines, i.e. the lines connecting the compositions of coexisting phases, are known, one can measure instead single phase samples prepared at the tie line endpoints. One difficulty with that approach is obviously the precise determination of the tie lines, which is a subtle and intricate

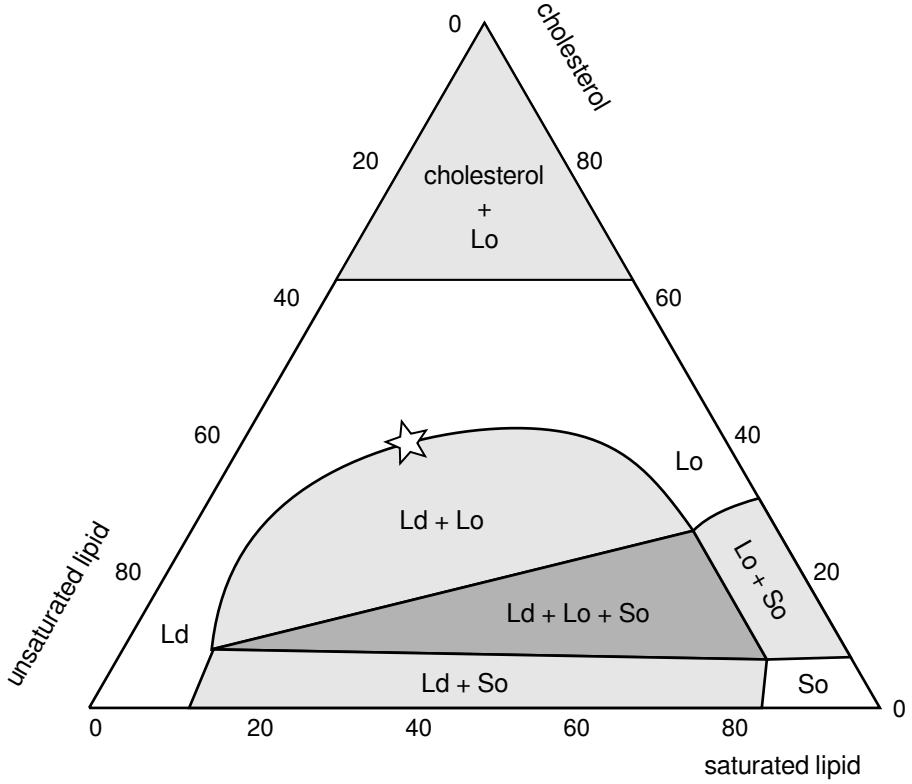

Figure 1.2.: A typical phase diagram for a ternary lipid mixture, consisting of cholesterol (top), an unsaturated (left bottom), and a saturated lipid (right bottom). Homogeneous phases are drawn in white and regions of two/three phase coexistence in light/dark gray. The star indicates a critical point.

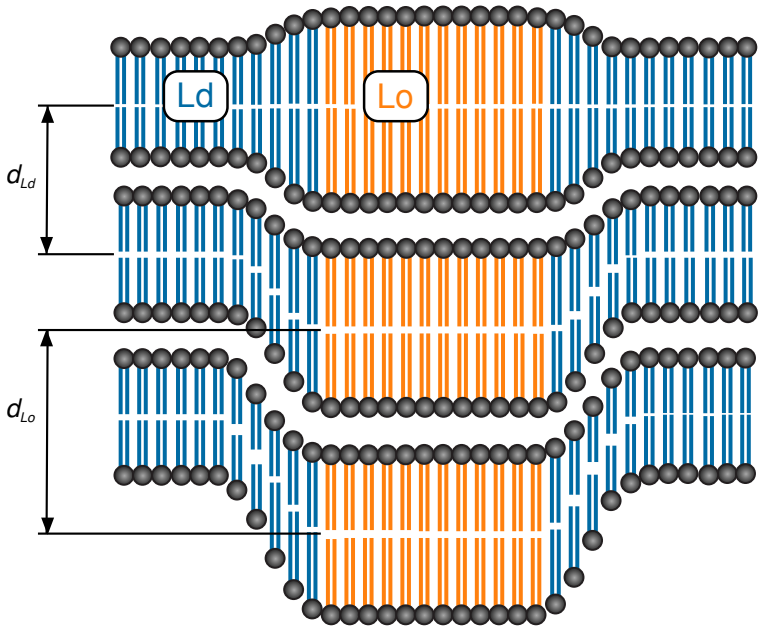

Figure 1.3.: Domain alignment of in lipid multibilayers, giving rise to two distinct lamellar repeat distances, d_{Ld} and d_{Lo}. Adapted from [25].

problem, but even the preparation of samples with a precise composition is by itself demanding [15]. Better suited for investigating lipid phase demixing are therefore techniques, which are able to differentiate between coexisting phases [16, 17].

Small angle X-ray scattering (SAXS) on MLV offers, under certain prerequisites, the possibility to distinguish coexisting Lo/Ld domains from each other [17]. This advantage over many other techniques is based on an interesting and not yet understood phenomenon of domain alignment [17–24]: Like domains of certain lipid mixtures align laterally across multiple membranes, thereby forming two separate bilayer lattices with different periodicities d, see Fig. 1.3. Consequently, two distinct reciprocal Bragg lattices are detectable with diffraction techniques, such as for example SAXS. With sophisticated analysis methods, it is then possible to determine the bilayer structure and the repeat distance together with its mean square deviation for the two coexisting lipid phases [17].

1.2. Theoretical membrane models

In this thesis, I will make use of continuum mechanical descriptions for lipid aggregates. Such representations are appropriate for modeling mesoscopic effects, particularly thermal bilayer fluctuations, generation of bilayer stress due to protein insertion or due to protein conformational changes, as well as molecular interactions of macromolecular surfaces. In order to apply continuum mechanics on such interesting and physiologically highly relevant problems, however, quantitative values for parameters describing structural and elastic properties of membranes are necessary. The present section introduces a few relevant moduli and explains their connection to experiments.

1.2.1. Spontaneous monolayer curvature

One important parameter connected with lipid stress in bilayers is the spontaneous/intrinsic curvature J_0. Spontaneous curvature is an effective lipid property, describing preferential curvature in unstressed monolayers [26–28]. Lipids with $J_0 \approx 0$ are approximately cylindrical, meaning they prefer planar monolayer structures, realized for example in bilayers. Phosphatidylcholine (PC) lipids are typical examples for this group. Compared to PC, phosphatidylethanolamine (PE) lipids have smaller headgroups. This leads to a – by definition negative – spontaneous curvature, $J_0 < 0$. Such lipids prefer intrinsically negatively curved phases, for example the inverted hexagonal phase H_{II}.

The H_{II} phase is preferably employed for measuring lipid spontaneous curvature [27, 29–36]. Bilayer phases are unsuited for this purpose because the two monolayers constituting a lipid bilayer are not free to curve independently from each other. Such a behavior would create unphysical voids between the monolayers, which – if filled by the aqueous phase – would in turn expose the hydrophobic hydrocarbon chains to water. The H_{II} phase, depicted in Fig. 1.4, however consists of rolled up monolayers, whose curvatures are nearly unrestrained. In order to protect the outward pointing lipid tails from water, these tubes densely pack in a hexagonal pattern. This hexagonal lattice is usually well ordered and leads to a distinct series of Bragg peaks in SAXS, thereby easing the detection of H_{II} phases and in turn the reconstruction of electron density profiles [37]. This way, the tubes radii and therefore curvature can be measured precise and probe-free.

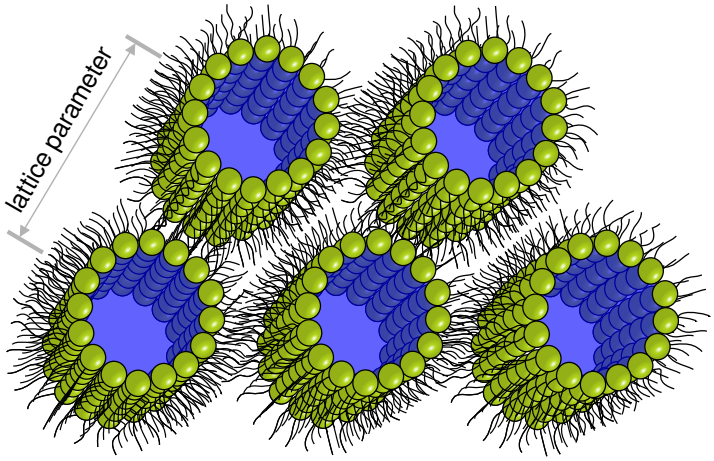

Figure 1.4.: Sketch of an inverted hexagonal phase H_{II}. Rolled up lipid monolayers are arranged in a hexagonal lattice and enclose water cylinders (blue).

Even spontaneous curvatures of usually bilayer forming lipids can be measured with H_{II} phases [31, 34, 38–40]. To this end, an otherwise bilayer forming lipid-of-interest is mixed in various concentrations χ with a H_{II} forming "host" lipid, see Fig. 1.5. For well-behaved mixtures in the H_{II} phase, the spontaneous curvature $J_0(\chi)$ can be determined. Upon the assumption of a linear dependence of J_0 on χ, the spontaneous curvature of the pure lipid-of-interest, $J_0(\chi = 1)$, is then readily extrapolated.

1.2.2. Bilayer mechanics

The possible fundamental deformations for a single, perfectly fluid lipid bilayer are stretching, tilt, curvature, and further nonlinear contributions [42, 43], see Fig. 1.6. The influences of lateral stretching, lipid tilt and nonlinear deformations are often neglected in applications of biomembrane mechanics, where the focus mostly lies on elastic curvature, i.e. bending deformations [44, pp. 37–38]. The omission of stretching effects is usually valid due to the high energetic costs of stretching strain [45] and furthermore because lipid bilayers rupture already at small membrane tensions [46]. Similarly, nonlinear deformations can be safely ignored for sufficiently small deformations.

Matters are however more intricate regarding tilt, which bears a close con-

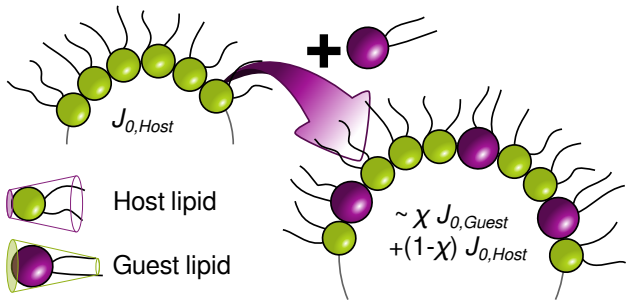

Figure 1.5.: Incorporation of bilayer-forming "guest" lipid (purple) at a concentration χ in the "host" H_{II} template phase. Reproduced from [41].

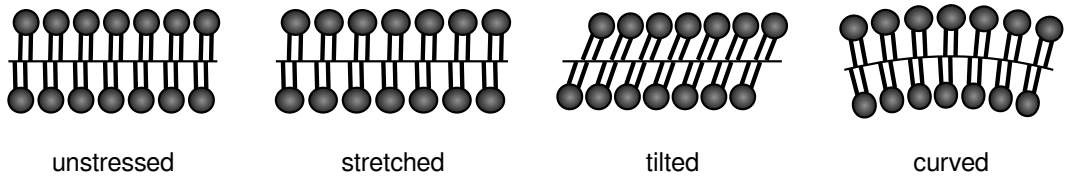

Figure 1.6.: Fundamental elastic deformations of fluid bilayers.

nection to curvature. Membrane bending and the divergence of the tilt field enter the free energy in fact by the same elastic moduli and their effects are additive [47]. Lipid tilt is expected to be important for diverse biological effects, for preserving domain boundaries, and for height fluctuation spectra in molecular dynamics (MD) simulations [48, 49]. Experimental validations for the underlying theories were however lacking until recently, when Jablin *et al.* showed that accounting for lipid tilt by an additional fitting parameter improved the agreement between a theoretical model and diffuse scattering intensities from SAXS experiments of aligned samples [50]. The effect of lipid tilt on the fluctuation spectra of powder diffraction samples, for example free floating MLV, is at the time of writing this thesis unknown, but several remarkably good fits for MLV [17, 51] seem to contradict a big influence. Therefore and because investigations of lipid tilt were beyond the scope of this thesis, they are not considered for fluctuation spectra henceforth.

Local bending of a two-dimensional membrane can be parameterized in general by the two principle radii c_1 and c_2. This description allows one to cast the energy of bending per unit area A in the form

$$\mathcal{H}/A = \frac{K_c}{2}\left(c_1 + c_2 - J_{0,B}\right)^2 + K_g\, c_1 c_2, \tag{1.1}$$

where K_c denotes the bilayer's bending curvature modulus, K_g the Gaussian curvature modulus, and $J_{0,B}$ the bilayer spontaneous curvature [43]. The Gaussian modulus describes the membrane's resistivity against saddle splay deformations and is only for topology changes of concern, for example for the formation or annihilation of holes.[1] Similarly, also the bilayer spontaneous curvature $J_{0,B}$, which quantifies the membrane's propensity to bend, is irrelevant for most artificial lipid bilayers because it vanishes if they are symmetric [52–57].

For sufficiently flat membranes, one can simplify Eq. (1.1) even further by making use of local membrane displacement $u(x, y)$ instead of principal curvature radii, which yields [58]

$$\mathcal{H}/A = \frac{K_c}{2}\left(\nabla^2 u\right)^2. \tag{1.2}$$

[1] According to the Gauss–Bonnet theorem, closed integrals over $c_1 c_2$ depend only on the genus of the surface, i.e. the number of holes.

This form is convenient for deriving fluctuation spectra, which are related to the mean square fluctuations of u and depend strongly on the bending rigidity K_c.

This connection between K_c and membrane undulations is exploited by different experimental methods, in order to quantify the bending modulus. The most prominent are probably diffuse SAXS on aligned multibilayers and aspiration or flicker analysis of giant unilamellar vesicles (GUV), which are well-suited for measuring K_c of homogeneous samples [59–61]. These techniques are however unable to determine individual bending moduli for coexisting lipid phases, unless tie line endpoint samples are used for that purpose. But direct measurements of K_c for coexisting phases are possible with other techniques, for example inelastic neutron scattering [62] or combined SAXS/osmotic pressure experiments [23, 40, 63, 64], see also Sec. 1.2.3.

Despite all possible simplifications, the full form of Eq. (1.1) is still relevant because – upon exchanging the bilayer material properties for their monolayer counterparts – it describes individual bilayer leaflets. Here the concept of spontaneous curvature becomes important: Even for artifical, symmetric bilayers, the monolayer spontaneous curvatures can be finite, leading to an intrinsic lipid stress which can influence for example the conformation of intermembrane proteins [23, 40, 65–70].

1.2.3. Bilayer interactions

Depending on their lipid compositions, spontaneously formed and equilibrated MLV exhibit different lamellar repeat distances d [71]. These equilibrium distances are set by a subtle balance between attractive and repulsive surface interactions, acting across the interbilayer aqueous phase. The distance-dependence of the sum of these interactions can be probed for example by osmotic stress experiments, in which the bilayers of MLV are compressed by application of osmotic pressure [72–74]. A typical isotherm, as can be obtained by such an experiment, is sketched in Fig. 1.7. An in-depth description of the relevant surface forces can be found in [75, pp. 341-378,577–599].

For very small separations, steric repulsions due to lipid headgroup protrutions dominate the isotherm. These interactions were found to obey an exponential distance dependence $P(d_W) \approx A \exp(-d_W/\lambda)$, with a large amplitude $A_{st} \approx 3.6\,\mathrm{GPa}$ and a small decay length $\lambda_{st} \approx 0.6\,\text{Å}$ [77].

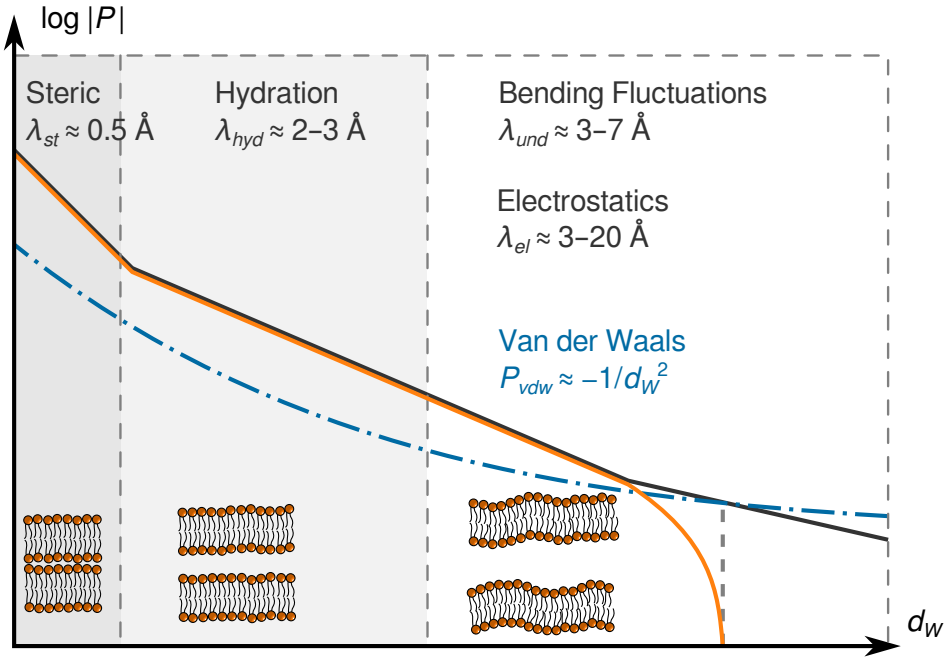

Figure 1.7.: Pressure P between bilayers as function of bilayer separation d_W (solid orange line). Separately plotted are repulsive (solid black line) and attractive (dash-dotted blue line) contributions. The most important fundamental repulsive (black) and attractive (blue) interactions are listed together with their exponential decay lengths λ or distance dependence. Adapted from [76].

The solvent-mediated hydration interaction is the strongest contribution at intermediate bilayer separations. It was found to depend on the hydrophobicity of the corresponding macromolecular surfaces and seems to be related to order in the water structure [78–80]. The empirical equation describing the hydration pressure is also an exponential repulsion, but with decay lengths λ_{hyd} of 2–3 Å and roughly an order of magnitude smaller amplitudes than steric interactions.

For charged lipids, for example phosphatidylglycerol (PG) or phosphatidylserine (PS), long-ranging electrostatic repulsions become important at large separations. Due to screening effects, they strongly depend on the salt concentration of the aqueous phase, as well as on the pH [81]. For the electrically neutral PE and PC lipids investigated in this thesis, electrostatic interactions originating from residual charges are however orders of magnitude smaller than other surface forces and will be neglected henceforth [82].

In order to stabilize a finite value of the lamellar repeat spacing d, some attractive interactions must be present. For lipid bilayers, the dominating attractive interactions are van der Waals [83]. They originate from restrictions of quantum mechanical fluctuations between two surfaces and follows roughly an $P_{vdw}(d_W) \sim 1/d_W^3$ dependence for planar surfaces.

The interactions mentioned above are additive and can be described within the DLVO framework [84], but their presence gives rise to another interaction for lipid bilayers. Two adjacent bilayers exert the above mentioned surface forces upon each other not only at their average separation, but at all separations within a certain range due to thermal bending fluctuations. Together with the distance dependence of the bare forces, this leads to an entropic, effectively exponential repulsion, the so-called undulation interaction [84–86]. It is longer ranged than the hydration interaction, with an effective decay length λ_{und} of 3–7 Å and therefore, determines together with van der Waals interactions the equilibrium spacing of charge-neutral, fluid lipid bilayers. The intricate connection between undulation forces and thermal fluctuations, which depend on the membrane elasticity, opens furthermore the possibility of deducing K_c from osmotic pressure experiments [76].

Extracting microscopic properties from osmotic stress experiments is however nontrivial. The interplay of bare surface forces with thermal fluctuations complicates the calculation of macroscopic observables, but solutions to such calculations are vital. Experimentally, only the cumulative effects of all present forces are accessible and one has to fit theoretical models to these results

in order to tell the contributions from the individual interactions apart [23, 40, 72, 73, 87–93]. A suitable model to this end has to combine the bending degrees of freedom of multiple flexible membranes, compare Eq. (1.2), with the bare interactions described before.

Analytical solutions of such models are available, but they are all based on some crudely justified assumptions [85, 86, 94–96]. Usually, these calculations assume a certain distribution of height fluctuations and henceforth treat the undulation interactions mean-field like. By using numerical simulations, one can however overcome these flaws and calculate the effect of bilayer fluctuations exactly [97, 98]. In contrast to analytical solutions, simulations obviously come at the expense of computational effort and are harder to fit to experimental data. Despite these shortcomings, they enable the precise and consistent analysis of osmotic stress experiments [64].

Osmotic stress experiments can also be performed on MLV showing phase coexistence [23, 40]. Together with the possibility of SAXS to characterize two phases simultaneously, this enabled us recently to determine separate bending moduli K_c for coexisting Lo and Ld phases, together with the relevant forces between like domains [63, 64].

2. Methods

This chapter focuses on a rather general description of the applied methods, their underlying principles and possible problems, which are usually not considered for publication. The original articles, which are attached at the end of this thesis, contain further elaborations on technical details, used materials and mathematical subtleties.

2.1. Sample preparation

In principle, thin film hydration, which is the standard lipid sample preparation for SAXS, is straight-forward: After mixing the lipids, which are dissolved in an organic solvent, one dries them by evaporating the solvent and subsequently hydrates the thus created lipid films with water and by introduction of mechanical energy through vortexing. There are however several potential pitfalls connected with this procedure, especially for lipid mixtures, of which I will discuss a few subsequently.

In order to prepare lipid mixtures of a precise concentration, one has to start by combining well-defined quantities of different lipid species. To this end, one can weigh the lipid powder, dissolve it in an organic solvent up to a certain solution volume and estimate the lipid molar fraction of this stock solution from the molar weight M_W of the lipid. This procedure is problematic because ambient water molecules tend to adsorb especially on unsaturated lipids, thereby increasing the lipids' effective molar weights. While a simple workaround is to just increase M_W of unsaturated lipids by one or two water molecules in the calculation, higher precisions are possible, for example by performing inorganic phosphate assays [15, 99, 100]. Because we were able to analyze phase-coexisting samples directly instead of having to prepare precise tie line endpoints, we just increased M_W for the unsaturated lipid DOPC effectively by one water molecule.

Another problem arises during the evaporation of the organic solvent. In the course of such dehydration processes, artificial phase separations can be induced due to differences in the components' miscibilities [101]. Thus generated precipitates might inhibit lipid redistribution during hydration, thereby preventing the formation of lipid aggregates of equal and uniform compositions. This problem is especially pronounced for cholesterol-rich mixtures [101–104]. In order to circumvent this difficulty, one can employ alternative preparation methods, for example rapid solvent exchange (RSE) [101, 105, 106]. With RSE, the sample is never dried down, but is rapidly transfered from the fluid organic solvent to the fluid aqueous phase. By avoiding the intermediate solid phase, the formation of concentration gradients is reduced [101]. Because the necessary equipment for RSE was missing in our laboratory at the time of preparation, the samples described in this thesis were prepared by ordinary thin film hydration.

The homogeneity of lipid vesicles can also be improved during hydration. Repeatedly freezing and thawing the sample above T_m[1] with concurrent vortexing facilitates hydration, homogenizes the vesicles [107], and is routinely performed upon hydration of lipid mixtures [15]. We performed multiple freeze/thaw cycles for all our samples during hydration.

2.1.1. Osmotically stressed samples

A possible way of exerting pressure on a stack of membranes is by addition of large neutral polymers, for example poly-ethylene-glycol (PEG) [23, 40, 72, 73, 87–93]. At an average molar weight of 8000 g mol^{-1}, PEG molecules are much too big to insert interstitially between PC bilayers and therefore dehydrate MLV through osmosis. Experimental data and theoretical interpretations are available for calculating the exerted osmotic pressure from a given PEG concentration [108, 109].

Unfortunately, PEG has a considerable X-ray scattering cross-section in water. Ideally, only the osmotically stressed lipid bilayers and not the PEG solutions would be irradiated in SAXS experiments. By centrifuging MLV down before carefully overlaying them with PEG, one can separate both components spatially to some extent. After incubation for several days, we removed the

[1] T_m is the main phase transitions, above which the liquid bilayer phase is thermodynamically stable.

overlay just before the actual measurement in order to obtain as-pure-as-possible MLV samples. During the short measurement time of a few minutes, the bilayers can only rehydrate minimally.

2.1.2. Investigated mixtures

Because the techniques for analyzing SAXS spectra from phase coexisting liquid/liquid samples were just developed at that time [17], we aimed for support by homogeneous tie line endpoint samples. Obviously, only the few lipid mixtures, for which reliable phase diagrams and tie line information had been published, were appropriate for such studies.

Specifically, we investigated the 3 component mixtures POPC/eggSM/Chol [110], DOPC/DPPC/Chol [24] and DOPC/DSPC/Chol [15], and the 4 component mixture DOPC/POPC/DSPC/Chol [111]. The actual sample concentrations can be found in the original publications [17, 64].

The 4-component system is especially interesting because upon exchanging POPC with DOPC at fixed ratios of DSPC (39 mol%) and Chol (22 mol%), the average size of coexisting domains can be driven from nanoscopic to macroscopic [112]. The amount of DOPC in the low-melting lipid fraction is parameterized by $\rho = \chi_{DOPC}/(\chi_{DOPC} + \chi_{POPC})$, which increases from 0 (POPC) to 1 (DOPC) upon the transition from nanoscopic to macroscopic domains.

2.2. Small angle X-ray scattering

Soft X-rays are photons with a wavelength on the order of Å and therefore sensitive to the electron density ρ. They are used in SAXS [113], which is sensitive to spatial variations of the electron density on the order of a few tens to hundreds of Å. The detectable signal intensity is however not directly related to $\rho(\boldsymbol{r})$ in real-space, but only to the absolute square of its Fourier transform.

Real-space information can be either reconstructed by inverse Fourier transformation of the detected signal, or by fitting a theoretical model to the data.

The loss of phase information during detection and the possible noise amplification due to the nonlinearity of the inverse Fourier transform disfavor the former method for many soft materials; although it might be well suited for strongly ordered samples, for example protein crystals.

Correlations ("periodicities") in the electron density create interference patterns in the detected intensity. For a lattice of periodicity d, one expects peaks according to Bragg's law at wave-vectors $\boldsymbol{q}_n$ with magnitudes $q_n = (2\pi/d) \cdot n$ and diffraction order $n \in \mathbb{N}_0$. Usual soft materials, in particular those exhibiting smectic-like order, are only weakly correlated at small distances due to thermal fluctuations, and completely lack long-range order. Instead positional correlations decay according to a power-law, leading to interference patterns with characteristic line-shapes. This behavior is often referred to as quasi-long range order. The generated interference patterns are therefore smeared out and vanish already after a few orders of diffraction.

Quasiperiodic structures are conveniently described in terms of their crystal structure and unit cell. While the former determines the observed interference pattern, the unit cell modulates the signal intensity. In real-space, the mathematical equivalent to this description is the convolution, which copies the unit cell to points in space determined by the crystal structure. The Fourier transform of the convolution is a multiplication, i.e. one only has to multiply the Fourier transformed crystal structure with the Fourier transformed unit cell to obtain the total amplitude. The scattering intensity is then given by the absolute square of this amplitude.

Random orientation of structures is common for samples in excess water, as investigated in this thesis, and gives rise to rotationally averaged scattering termed powder diffraction. Although the use of aligned samples would yield additionally in-plane information, its use complicates sample preparation. All samples described in this thesis were measured in excess water, therefore yielding powder diffraction spectra.

2.2.1. Inverted hexagonal phase

Because the Fourier transform of a hexagonal structure is itself hexagonal, the H_{II} lipid phase gives rise to a hexagonal interference pattern. Bragg peaks emerge at wave-vectors fulfilling the reflection law $\sqrt{3}aq_{h,k}/4\pi = \sqrt{h^2+hk+k^2} = 1, \sqrt{3}, 2, \sqrt{7}\ldots$, where h, k denote the Miller indices and a is

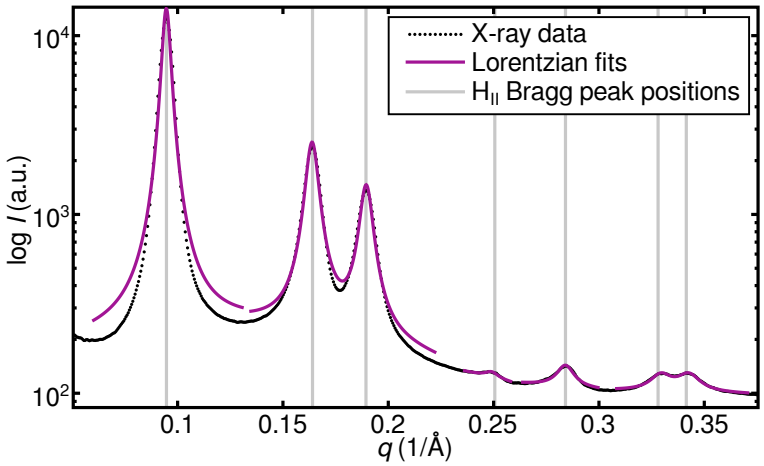

Figure 2.1.: Locations of constructive interference (gray solid lines) in a typical SAXS signal obtained from an H_{II} phase (black dotted line). Bragg peaks were fitted for real-space reconstruction (magenta solid lines). Adapted from [41].

the lattice parameter [114]. A typical SAXS spectrum for a H_{II} lipid phase is plotted in Fig. 2.1.

Fourier-based analyses are actually feasible for H_{II} phases due to their higher structural order, as compared to fluid lamellar bilayers. The necessary procedures for such an analysis have already been excellently described [114–117]. A typical H_{II} phase electron density profile, as can be obtained by a Fourier-based reconstruction, is plotted in Fig. 2.2.

The H_{II} phase data described in this thesis were analyzed with self-made procedures, which were implemented in Matlab [118]. Further details on them are given in [41].

2.2.2. Liquid lamellar phase

The crystal lattice of the bilayer phase is one-dimensional with the lamellar repeat distance d, giving rise to Bragg reflections at integer multiples of $2\pi/d$. Due to the considerable amount of disorder present in the liquid phase, the Bragg peaks' intensities fade-out rapidly for higher diffraction orders, thereby hindering Fourier-based analyses. But thermal and structural disorder of liquid bilayers gives also rise to a specific line-shape of Bragg peaks [119, 120],

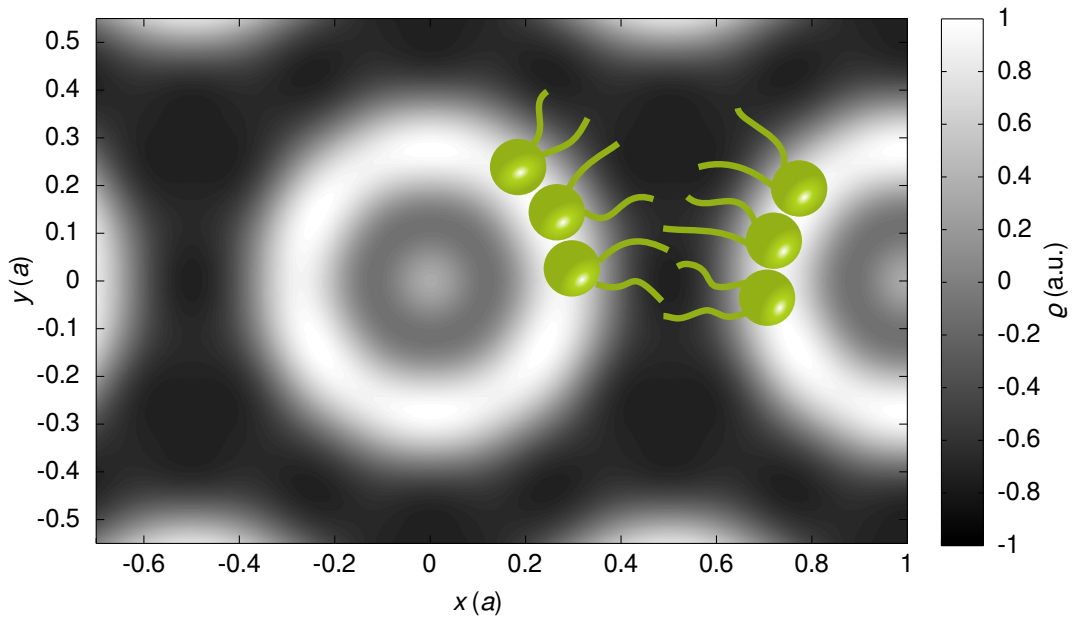

Figure 2.2.: Real-space electron density $\rho(x, y)$ reconstructed from the SAXS spectrum in Fig. 2.1 for a lipid H_{II} phase. Spatial coordinates are given in units of the lattice parameter a. A few lipid molecules are schematically overlayed (green) Adapted from [41].

which can be used to quantify the degree of bilayer fluctuations [121]. These descriptions use the line-shape parameter η, from which the mean square fluctuation of the membrane spacing $\Delta^2 = \eta d^2/\pi^2$ can be derived [91].

Apart from the Bragg peaks, SAXS spectra of fluid bilayers contain considerable amounts of diffuse scattering from uncorrelated lipid bilayers as well. Model-based methods can simultaneously analyze both effects and are thus well-suited for such samples [122–124]. Such a combined analysis is also necessary for describing scattering data from coexisting Lo/Ld domains [17]. To this end, each phase is separately described in terms of its bilayer structure and lattice, and the thus calculated contributions to the scattering intensity are weighed and summed-up. A detailed explanation of this method can be found in the original publication [17]. With only slight adjustments, which are described in [64], we were able to employ this method for analyzing scattering data obtained from osmotically stressed samples showing Lo/Ld phase coexistence.

This method allowed us to determine the repeat distance d and the line-shape parameter η separately for the Lo and the Ld phase as a function of osmotic pressure. We also succeeded in obtaining detailed structural information on the lipid bilayer for fully hydrated samples. Specifically, we derived values for the steric bilayer thickness d_B for both phases, which were used to calculate the interbilayer separations $d_W = d - d_B$. The bilayer structures depended only marginally on the osmotic pressure.

2.3. Monolayer spontaneous curvature

The spontaneous curvature J_0 of an unstressed monolayer is defined via the radius of its *neutral plane* [27, 28]. Stress-free monolayers are routinely obtained by adding small amounts of free alkanes or alkenes to the lipid samples, which partition into the interstitial sites in the H_{II} phase and thus release the hexagonal packing frustration [31, 35, 125, 126]. Further explanations on this topic are given in [41].

2.3.1. Locating the neutral plane

More important in the definition of J_0 is however the concept of the neutral plane. At this specific position, bending and stretching modes are decoupled [26], which explains why the neutral plane is used so frequently in calculations. One can stretch and bend the lipid monolayers in H_{II} phases by application of osmotic pressure and thereby determine experimentally the location of the neutral plane [27], but only a few lipid species have been investigated with this elaborate procedure [27, 29–35]. They found that the neutral plane of the well-studied lipid DOPE is located close to the glycerol backbone, which is reasonable due to the high rigidity of this molecular subgroup [28] and was also observed in simulations [127]. Experimental follow-up studies have consequently measured J_0 by locating the glycerol backbone, instead of actually determining the neutral plane by osmotic stress experiments [39, 40, 117].

We used a similar procedure, based on highly resolved structural data from combined neutron and X-ray studies [128–131], to locate the glycerol backbone. Specifically, we determined the radius R_p of the lipid headgroups from electron density maps and adjusted it by a constant value d_{H1} obtained from the aforementioned studies, to account for the distance between headgroup and glycerol backbone. Further details and comparisons to neutral plane locations obtained from osmotic stress experiments are given in the original publication [41].

2.3.2. Bilayer-forming lipids in H_{II} templates

As already explained in Sec. 1.2.1, H_{II} phases can be used as templates to determine the monolayer spontaneous curvature of bilayer-forming lipid molecules. For this procedure, experimental values for the spontaneous curvature $J_0(\chi)$ as a function of guest-lipid concentration are fit with a model function, which yields with $J_0(1)$ the spontaneous curvature of the lipid-of-interest.

The simplest available model explaining spontaneous curvatures of mixtures is given by a linear dependence of J_0 on χ [132–135],

$$J_0^{mix} = \sum_i \chi_i J_0^i, \tag{2.1}$$

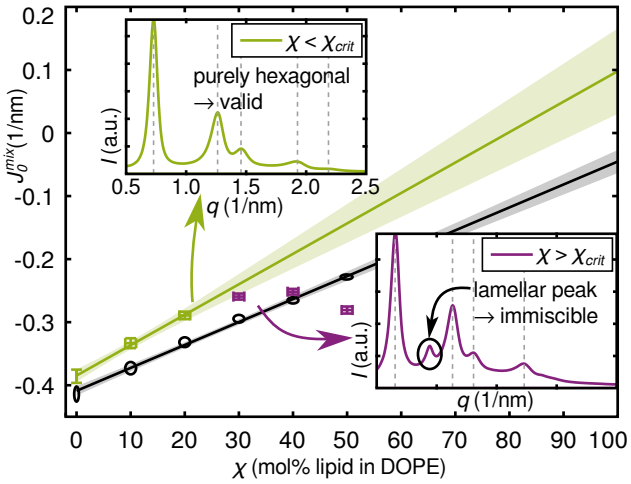

Figure 2.3.: Extrapolation of spontaneous curvature J_0 for the bilayer-forming lipids DPPC at 25 °C (crosses) and for POPC at 45 °C (ellipses) mixed in a DOPE template. The insets show SAXS spectra for the highest miscible (top left) and the first immiscible DPPC concentration (bottom right). Reproduced from [41].

where χ_i and J_0^i denote the molar fraction and the spontaneous curvature of the i-th component. We applied this form to obtain J_0 of bilayer-forming lipids [41]. Although a detailed model based on continuum elastic calculations would exist [136], its correctness and applicability to experiments remain debatable [41, 137].

Usually, such models do not account for the possibility of phase separation, but especially upon adding lipids which prefer to aggregate in different phases, an immiscibility gap must be expected at some critical composition χ_{crit}. With SAXS experiments, phase demixing is often accompanied by the appearance of a second interference pattern, see Fig. 2.3. Although this is the safest evidence for immiscibility, other possible indications have to be respected as well [41].

2.3.3. Temperature dependence

For elevated temperatures, one expects an increased flexibility and disorder of the lipid tail's hydrocarbon chains. In terms of monolayer spontaneous curvature J_0, further spread-out lipid tails would correspond qualitatively

to more negative values. In order to quantify and compare the temperature dependences for different lipids, we measured J_0 at various temperatures from 15–55 °C and described these data by the linear relationship

$$J_0(T) = k\,(T - T^{av}) + J_0^{av}, \tag{2.2}$$

where $T^{av} = 35\,°\mathrm{C}$ is an average temperature, k denotes the coefficient of thermal curvature change, and J_0^{av} the spontaneous curvature at T^{av}. All acquired data could be well described by Eq. (2.2), see [41, Sec. S5].

2.4. Membrane simulations

2.4.1. Fundamentals of Monte Carlo simulations

As several textbooks on the use of Monte Carlo (MC) simulations for physical applications are already available [138–140], there is no need to introduce them in great detail. Quite generally, MC simulations are used to generate random numbers according to a given distribution in many dimensions. Because we are interested in solving statistical mechanics problems, the distribution is given in our case by the Boltzmann weight of microstates. In order to compute thermodynamic observables with MC simulations, one draws a number of microstates, calculates at each MC step the observables of interest, and finally averages them.

The precision of such averages is largely determined by the statistical uncertainty due to the finite sample size. The relevant sample size is however not the number n of realized microstates, but an "effective" size $n_{eff} = n/2\tau_{int}$, where τ_{int} is the integrated autocorrelation time [138–140]. Roughly speaking, τ_{int} describes how many samples have to be drawn before an additional independent sample is available. Its value depends strongly on the procedure for generating new samples. The autocorrelation time is commonly measured in MC steps (MCS), with 1 MCS corresponding to updating on average every degree-of-freedom once.

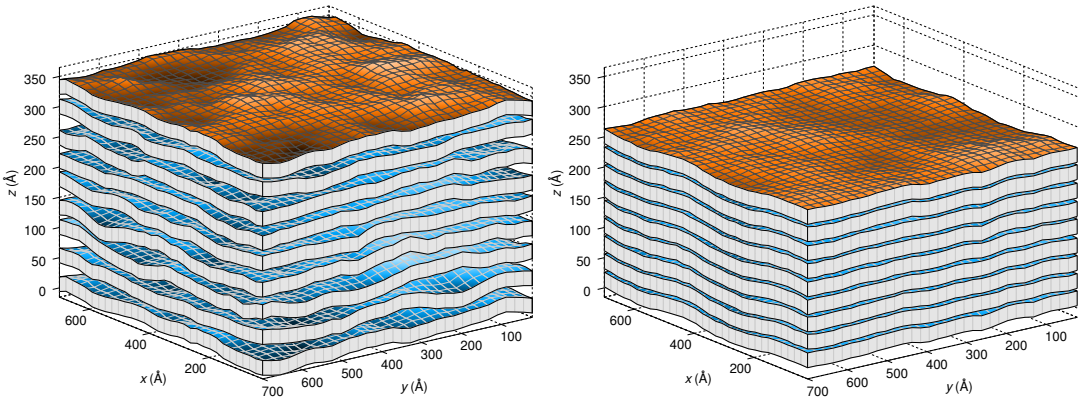

Figure 2.4.: Membrane simulation snapshots at zero (left) and finite (5.5 MPa, right) ambient pressure P. Membranes are drawn with their actual thickness d_B as determined by SAXS. The orange membranes equal the bottom-most membranes due to periodic boundary conditions. The most prominent effects of pressure, being a compression of the stack and reduction of fluctuations, are evident. Reproduced from [64].

2.4.2. Fourier membrane simulation

The membrane MC simulation code, which was used in the present thesis, has already been described in detail elsewhere [64, 97, 98, 141]. I will therefore excerpt only the most relevant concepts and refer the interested reader to the original publications.

The simulation models a stack of flexible and interacting membranes, as depicted in Fig. 2.4, which is the appropriate description for osmotic stress experiments on MLV.

It accounts for M membranes of size $L \times L$ and bending elasticity K_c, whose local deviations $u_m(x, y)$ from the average membrane position are considered. The average membrane separation is given by $\bar{a}$, which allows us to cast the local distance between the membranes m and $(m+1)$ in the form $a_m(x, y) = u_{m+1}(x, y) - u_m(x, y) + \bar{a}$. The bare interactions between neighboring membranes are modeled by potentials $\Phi(a)$. To avoid membrane interpenetration, we require $a_m(x, y) \geq 0$. Furthermore, periodic boundary conditions (pbc) are imposed in all three dimensions, meaning $u_{m+M}(x + L, y + L) = u_m(x, y)$.

With these definitions, we can write down the Hamiltonian

$$\mathcal{H} = \sum_{m=0}^{M-1} \int \left(\frac{K_c}{2} (\nabla^2 u_m)^2 + \Phi(a_m) \right) \mathrm{d}x \, \mathrm{d}y, \tag{2.3}$$

which basically combines the bending energy term known from Eq. (1.2) for several membranes with the bare interactions from Sec. 1.2.3.

The bare potential between two neighboring membranes at separation a is given by

$$\Phi(a) \simeq A_{hyd} \lambda_{hyd} \exp\left(-\frac{a}{\lambda_{hyd}} \right) - \frac{H}{12\pi a^2}, \tag{2.4}$$

where the first term models the hydration and the second term the van der Waals interactions. H denotes the Hamaker coefficient, which depends in general, however weakly, on a and can be calculated from dielectric spectra [83, 142]. The bare interaction pressures discussed in Sec. 1.2.3 are related to the potentials via $P(a) = -\partial\Phi(a)/\partial a$.

Rather than varying $u_m(x, y)$ directly, MC updates are proposed in Fourier space $u_m(q_x, q_y)$ [98]. Within this description, a single MC update corresponds to exciting or damping a specific fluctuation mode (q_x, q_y) of the m-th membrane. The simulations of this thesis are performed in the isothermal–isobaric ensemble, i.e. at constant temperature T and pressure P [98, 143]. The spatial variables (x, y) are quantized on a square lattice with $N \times N$ sites to reduce the degrees-of-freedom.

The two observables relating such simulations to osmotic stress experiments are the average bilayer separation $d_W = \langle \bar{a} \rangle$, and its fluctuations

$$\Delta^2 = \left\langle \left(u_{m+1}(x, y) - u_m(x, y) \right)^2 \right\rangle + \left\langle m \cdot (\bar{a} - d_W)^2 \right\rangle, \tag{2.5}$$

where the brackets $\langle . \rangle$ denote temporal and spatial (m, x, y) averaging.

2.4.3. Fitting simulations to data

Several well-written articles highlight the difficulties, but also the benefits, of optimizing simulations towards a goal, as compared to using analytical models [144–147].

The computational effort for running simulations is usually much higher than for just evaluating an analytical solution. This immediately disfavors purely stochastic optimization algorithms, for example genetic algorithms, which usually rely on an enormous number of model evaluations to pinpoint the global optimum. But also standard gradient-based algorithms are imperfectly suited for optimizing simulations because how can one obtain reliable gradients? Finite difference approaches have a hard time due to the stochastic nature of simulation. A viable alternative might be the histogram reweighting method [148–150], which can efficiently compute derivatives by reweighting the realized samples of a single simulation run. But also this method is effected by stochastic noise. A further problem is that gradients of well-behaved functions become small close to extrema, which slows down the convergence and amplifies the influence of noise, the closer one approaches the optimal solution. Alternatively, several algorithms specifically designed for optimizing simulations do exist, but their current implementations are far from perfect [146].

Despite these difficulties, some problems are only tractable with simulations, which clearly indicates why optimizing simulations can be necessary. Particularly for our case, optimizing the membrane simulations enabled us to take the intricate interactions between bare potentials and membrane fluctuations into account without having to rely heavily on approximations or assumptions. To this end, we combined a general-purpose gradient-based optimization algorithm with the histogram reweighting method for obtaining the necessary gradients. The problem of slow convergence towards the end was dealt with by running multiple optimizations from different, randomly chosen starting points, which resulted in the optimal region being heavily sampled by the different runs.

Simulation can be optimized towards a specific goal by adjusting their parameters. The variety of them, on which our membrane simulations depend on, shall be briefly reviewed in this paragraph. Obviously, the pressure P and temperature T are externally specified parameters for the simulations, as well as for the experiments. Next, there are the number M and size L^2 of membranes and the number of lattice sites N^2, which limit the simulations' degrees-of-freedom. The corresponding values in experiments, $M = \mathcal{O}(100)$, $L = \mathcal{O}(\mu\mathrm{m})$, and $N/L = \mathcal{O}(\mathrm{nm}^{-1})$, are much larger than what is computationally feasible, thus calling for careful finite-size extrapolations [64, 98]. The last group consists of the actual model parameters describing the physical properties of the membranes and their interactions. These are the bending

modulus K_c, the hydration interaction's amplitude A_{hyd} and decay length λ_{hyd}, and finally the Hamaker coefficient H.

This group represents the set of free parameters $\mathbf{\Lambda}$, which should be adjusted in order to minimize the misfit between simulational and experimental results. The misfit is given by the sum of squared residues,

$$\chi^2(\mathbf{\Lambda}) = \sum_i \left(\frac{d_{W,i} - d_W(P_i;\mathbf{\Lambda})}{U_{\text{eff}}(d_{W,i})} \right)^2 + \left(\frac{\Delta_i - \Delta(P_i;\mathbf{\Lambda})}{U_{\text{eff}}(\Delta_i)} \right)^2 . \tag{2.6}$$

The sum runs over the set of osmotic pressures P_i, for which experimental results for the interbilayer separation $d_{W,i}$ and the fluctuations Δ_i were obtained. The corresponding simulational results are denoted by $d_W(P_i;\mathbf{\Lambda})$ and $\Delta(P_i;\mathbf{\Lambda})$, respectively, and the effective errors U_{eff} account for experimental and simulational uncertainties, see [64]. The quantitative agreement between simulations and experiments is then given by the reduced $\chi^2_{red} = \chi^2/\tilde{N}$, where $\tilde{N}$ equals the number of experimental data points minus the number of free parameters [151, p. 268]. If the model fits the experimental data well with respect to the measurement uncertainty, χ^2_{red} is roughly one; for worse fits, χ^2_{red} is considerably larger.

Instead of fitting the Hamaker coefficient H together with the other parameters, we calculated its value theoretically [142]. This allowed us to eliminate one free fitting parameters and minimized ambiguities in the optimization process.

2.5. Applications

2.5.1. Line tension

The bilayer thicknesses of coexisting Lo and Ld phases differ in general from each other due to their different lipid compositions. In order to shield the hydrophobic region of lipids in the thicker phase from being exposed to water, lipids have to deform at the phase boundaries. Such deformations are usually energetically unfavorable compared to an unperturbed, flat bilayer and co-determine the energy cost per unit length of the boundary, the line tension γ.

Its value is connected to the size and shape of domains [152, 153] and also influences domain boundary fluctuations [154, 155]. For high values of γ, large, circular domains form due to the energetic cost of maintaining domain boundaries, while nanoscopic domains seem to be only stable for small line tensions [112].

The elastic deformations occurring at domain boundaries can be modeled by continuum mechanics, starting from the monolayer form of Eq. (1.1). After an elaborate calculation, Kuzmin *et al.* [49] arrived at a fairly simple relation for calculating the line tension γ from monolayer properties of the two phases (1 and 2), which is given by

$$\gamma = \frac{\Delta h^2}{Z\, h_0^2} \sqrt{k_{c,1}\, k_{t,1}\, k_{c,2}\, k_{t,2}} - \frac{1}{2\, Z} \left(J_{0,1}\, k_{c,1} - J_{0,2}\, k_{c,2} \right)^2 , \tag{2.7}$$

with $Z = \sqrt{k_{c,1} k_{t,1}} + \sqrt{k_{c,2} k_{t,2}}$. The parameters entering Eq. (2.7) are the monolayer bending k_c and tilt moduli k_t, the monolayer spontaneous curvatures J_0, and the structural quantities $\Delta h = h_2 - h_1$ and $h_0 = (h_1 + h_2)/2$ relating the positions h of the monolayer neutral planes. We denote the first term of Eq. (2.7) γ_h and the second term γ_J. While γ_h describes an elastic influence of height mismatch to the line tension, γ_J accounts for hidden stress due to spontaneous curvature.

2.5.2. Protein partitioning and conformation

In light of the discussion whether rafts exist in cell membranes and if, with what molecules they are enriched, see Sec. 1.1, investigating the partitioning behavior of transmembrane proteins in various (model) membranes seems worthwhile. In cooled giant plasma membrane vesicles (GPMV), which have similar lipid and protein compositions as plasma membranes of intact cells [156, 157], several usually raft-associated proteins were found to be enriched in the more ordered, *ergo* raft-like, phase [7, 158–160]. Contrary to these finding, most peptides and proteins, which are reconstituted into lipid-only membranes, rather partition in the liquid-disordered phase [160–163]. A simple continuum mechanical model published by Cantor [66] allows us to calculate the protein insertion penalty for different lipid phases, helping us to understand the reasons for this unrealistic partitioning. The same model is also suitable for computing the mechanical implications of internal bilayer stress on protein conformations.

The derivation [66] starts from the work W, which has to be performed against the lipid bilayer upon inserting a protein of cross-section $A(z)$. It is given by the equation

$$W = \int_{-d_B/2}^{d_B/2} A(z)\, p(z)\, \mathrm{d}z, \tag{2.8}$$

where z is the spatial coordinate normal to the bilayer plane and $p(z)$ is the lateral pressure profile [164]. A sketch of the model is shown in Fig. 2.5.

Expanding – separately for the two leaflets – the protein cross section into power series yields

$$A(z) = a_0 + a_1^{\pm} \cdot |z| + a_2^{\pm} \cdot |z|^2 + \mathcal{O}(z^3), \tag{2.9}$$

where $\pm$ denotes the upper/lower monolayer. Inserting this relation into Eq. (2.8) gives $W = \sum a_j^{\pm}\, p_j$ for symmetric bilayers, where the sum runs over $\pm$ and j. The quantities p_j are given by the j-th moment of $p(z)$, i.e. $p_j = \int_0^{d_B/2} z^j\, p(z)\, \mathrm{d}z$, and depend only on continuum elastic parameters [166, 167]

$$p_0 = -\sigma \qquad p_1 = J_0\, k_c \qquad p_2 = 2\, k_m\, J_0\, h - k_g. \tag{2.10}$$

Specifically, these are the bilayer surface tension σ, which vanishes for common free-floating vesicles [168], the monolayer spontaneous curvature J_0, bending curvature modulus k_c and Gaussian curvature modulus k_g, and the position of the neutral plane h. Instead of the lateral pressure profile, these parameters can be quantitatively determined with experiments of modest complexity.

Finally, the equilibrium K between the states 1 and 2, for example two protein conformations or partitioning in two coexisting phases, can be calculated. Upon neglecting all further contributions of lipid–protein or protein–protein interactions, the equilibrium K is proportional to $\exp(-\Delta W/kT)$ [65, 169], where ΔW is the energy difference $\Delta W = W_2 - W_1$ and kT is the thermal energy.

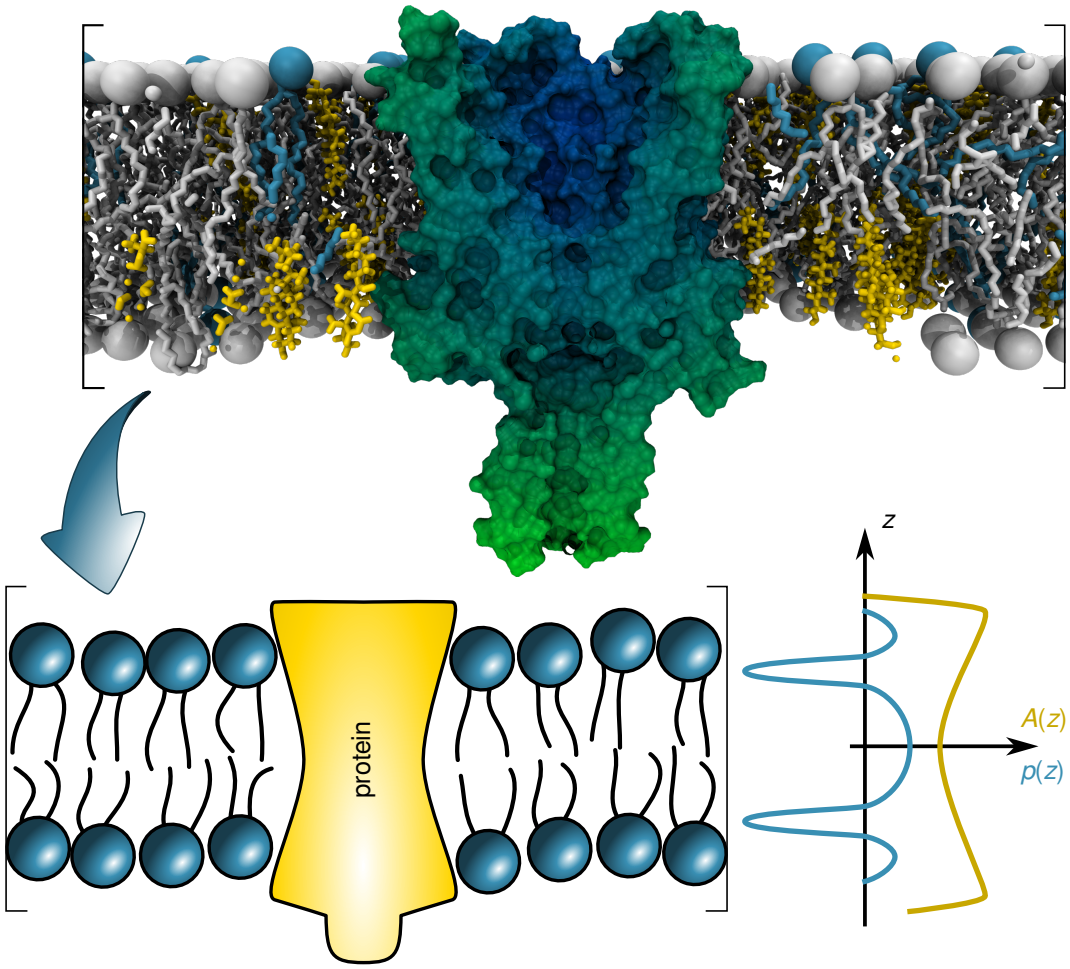

Figure 2.5.: Schematic overview for calculating the mechanical work necessary for inserting a transmembrane protein in a lipid bilayer. Instead of complex MD simulations (top), we use a simple continuum description of the bilayer (bottom). The important quantities for this model are the internal bilayer pressure $p(z)$ and the protein cross section $A(z)$ as function of the vertical coordinate z. Adapted from [165].

3. Results

3.1. Elastic properties of coexisting domains

3.1.1. Spontaneous curvature of single lipids

Before being able to compute monolayer spontaneous curvatures J_0 for coexisting lipid domains, we had to determine J_0 for their individual components, as outlined in Sec. 2.3. The spontaneous curvatures of the H_{II} phase forming lipids DOPE and POPE[1] could be determined directly. For the remaining, mostly bilayer-forming lipids, we had to resort to using DOPE-rich H_{II} templates.

We were able to determine lipid spontaneous curvatures in a broad temperature range from 15–55 °C, for all lipids except for POPE. The obtained data could be well described by Eq. (2.2), thereby yielding the numbers listed in Tab. 3.1. Such information on the temperature dependence of J_0 is indeed important because of the big range of physiologically relevant temperatures in different organisms.

Unsurprisingly, we obtained strongly negative values for the spontaneous curvature of PEs, which are prone to form negatively curved phases. Also the general trend of nearly vanishing curvatures for the bilayer-forming PC lipids and eggSM was anticipated. The differences obtained for the individual lipids however turned out to be very interesting.

For example, comparing the results for DPPC, DSPC and eggSM shows, how marginal changes in the chemical structure can alter lipid spontaneous curvatures. DPPC and DSPC are chemically very similar lipids, with the only difference that DSPC has slightly longer hydrocarbon chains. Still, this

[1] Due to addition of tricosene, the H_{II} phase was already at 37 °C thermodynamically stable, instead of 74 °C for pure POPE [170].

Table 3.1.: Temperature dependence of monolayer spontaneous curvature $J_0(T)$ as described by Eq. (2.2), with $T^{av} = 35\,^{\circ}\mathrm{C}$, except for (*) where $T^{av} = 37\,^{\circ}\mathrm{C}$. Adapted from [41].

lipid	J_0^{av} (nm^{-1})	k ($10^{-3}\,\mathrm{nm}^{-1}\,^{\circ}\mathrm{C}^{-1}$)
DOPE	$-0.399(5)$	$-1.3(4)$
POPE (*)	$-0.316(7)$	$-2.7(7)$
Chol	$-0.494(13)$	$-3.5(9)$
DOPC	$-0.091(8)$	$-1.1(6)$
POPC	$-0.022(10)$	$-1.8(7)$
SOPC	$-0.010(18)$	$-2.2(13)$
DPPC	$+0.068(32)$	$-3.5(23)$
DSPC	$-0.100(44)$	$-0.2(34)$
eggSM	$-0.134(72)$	$+1.4(51)$

minor change in the chain length suffices to reduce the spontaneous curvature from roughly $+0.1\,\mathrm{nm}^{-1}$ for DPPC to $-0.1\,\mathrm{nm}^{-1}$ for DSPC at $35\,^{\circ}\mathrm{C}$. But apart from the importance of headgroup and chains, also the influence of the lipid backbone attracts attention. For example, the predominant lipid species in eggSM solely differs from DPPC by having a sphingosine instead of a glycerol backbone. Also this change is enough to reduce $J_0(35\,^{\circ}\mathrm{C})$ to roughly $-0.1\,\mathrm{nm}^{-1}$.

3.1.2. Monolayer spontaneous curvature of domains

Inserting the single lipid spontaneous curvatures in Eq. (2.1) allowed us to calculate effective monolayer spontaneous curvatures for well-behaving lipid mixtures. In the presence of phase separation, however, we had to rely on miscibility boundaries and tie lines from published phase diagrams. Parameterizing the tie lines from $u = 0$ at the critical point to $u = 1$ next to the three phase coexistence region[2] allowed for comparisons of J_0 for coexisting phases. The results of such calculations for three different ternary lipid mixtures are plotted in Fig. 3.1.

Most interesting, we obtained more positive values of J_0 for the Lo phase in the DOPC/DPPC/Chol system, as compared to the coexisting Ld phase. Common sense would suggest the contrary, as realized for the other two

[2]See [112] for a more specific definition of u.

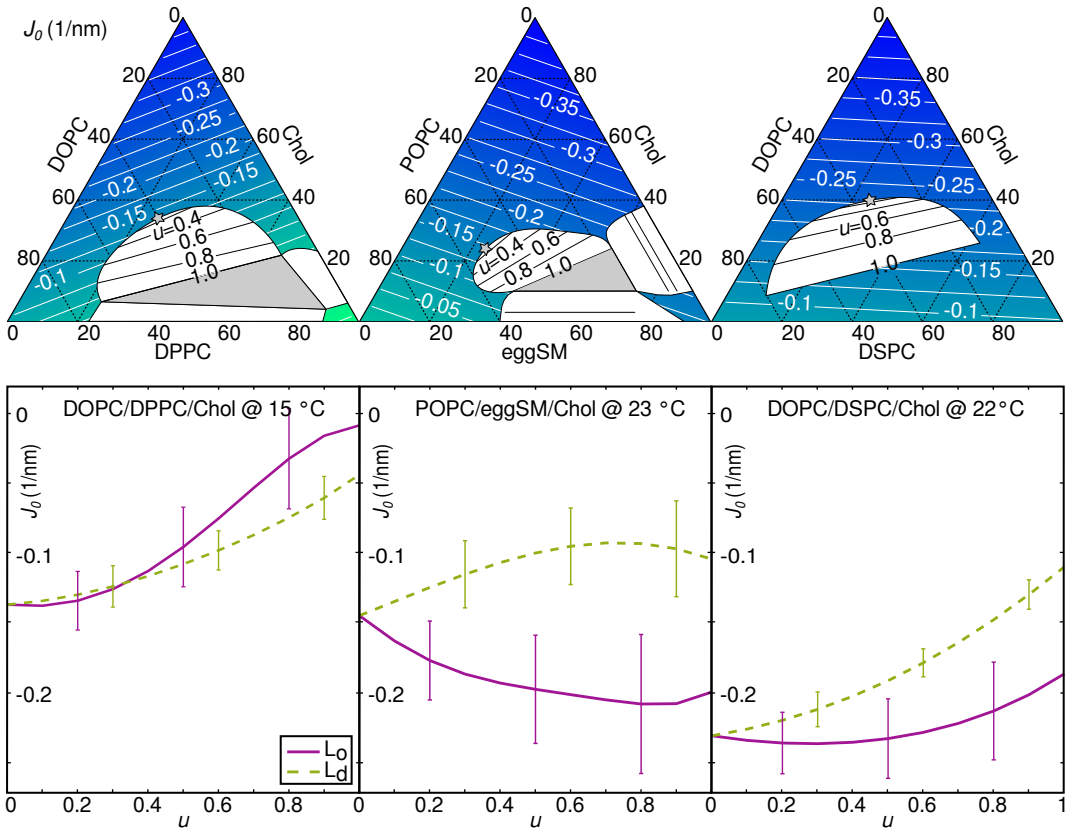

Figure 3.1.: Top: Effective monolayer spontaneous curvatures J_0 in nm^{-1} (white contours) for ternary lipid mixtures overlayed on published phase diagrams [15, 24, 110]. The tie lines corresponding to $u \in \{0, 0.2, \ldots, 1\}$ are plotted in the liquid/liquid phase coexistence region. Bottom: Comparison of J_0 for the coexisting Lo/Ld phases according to these tie lines. Adapted from [41].

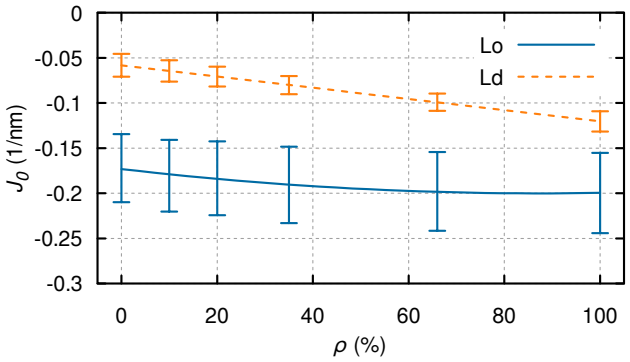

Figure 3.2.: Effective monolayer spontaneous curvature J_0 for coexisting Lo/Ld phases in DOPC/POPC/DSPC/Chol, according to published tie lines.

mixtures, because Lo phases are usually enriched in cholesterol, for which we measured a strongly negative curvature, see Tab. 3.1. The abnormal behavior of the DOPC/DPPC/Chol mixture can be traced back to the positive J_0 of the high-melting lipid component DPPC, which is the actually the major constituent in the Lo phase for $u \geq 0.4$.

Information about one tie line are also available for the quaternary lipid mixture DOPC/POPC/DSPC/Chol [111, 112, 171]. This allowed us to calculate J_0 as a function of ρ, which is the DOPC concentration in the low-melting lipid fraction. The results are plotted in Fig. 3.2. The trend of decreasing J_0 with increasing amounts of DOPC comes from DOPC's more negative curvature as compared to POPC.

3.1.3. Bending elastic modulus of domains

We determined the bending elasticity moduli K_c of coexisting Lo/Ld domains from a MC simulation-based analysis of SAXS/osmotic-stress experiments. While some explanations of this technique are outlined in Secs. 1.2.3 and 2.4, more detailed descriptions are available in the original publication [64].

For the macroscopically phase separated samples ($\rho \geq 0.35$) of the mixture DOPC/POPC/DSPC/Chol, domain alignment allowed for a straightforward analysis of the acquired data. The obtained bending moduli for Lo and Ld domains are plotted in Fig. 3.3. At the time of writing this thesis, an

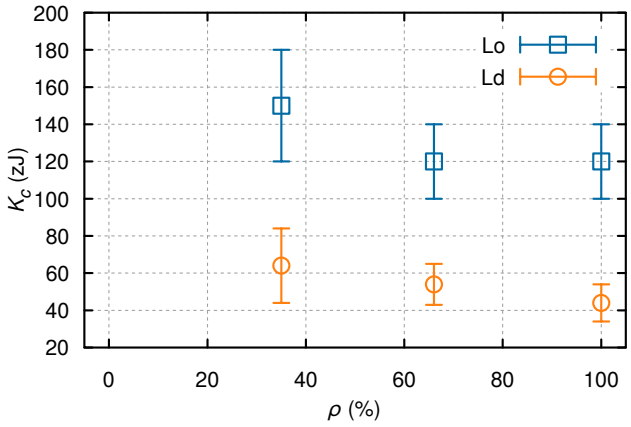

Figure 3.3.: Bending curvature modulus K_c obtained from coexisting Lo/Ld phases in DOPC/POPC/DSPC/Chol.

indisputable analysis was however lacking for the remaining samples, in which the coexisting domains were at least partially unaligned.

Liquid-ordered phases are usually enriched in cholesterol and saturated, high-melting lipids. Compared to their coexisting Ld phases, which contain mostly unsaturated, low-melting lipids and smaller amounts of cholesterol, Lo bilayers should be much more rigid. In accordance with this reasoning, we found 2–3 fold larger elastic bending moduli K_c for Lo phases, as compared to Ld.

3.2. Domain interactions

Apart from bending moduli, the simulation-driven analysis of SAXS/osmotic-stress experiments allowed us also to measure the individual fundamental surface interactions between coexisting domains, see Sec. 2.4 or [64]. We applied this technique on the macroscopically phase separated samples of the quaternary mixture DOPC/POPC/DSPC/Chol.

While experimental data and simulations agreed perfectly for the Ld phases ($\chi^2_{red} \approx 1$), we obtained slightly worse fits for Lo ($\chi^2_{red} \approx 5$), see Fig. 3.4 and Tab. 3.2. These bigger deviations originate probably from a limited

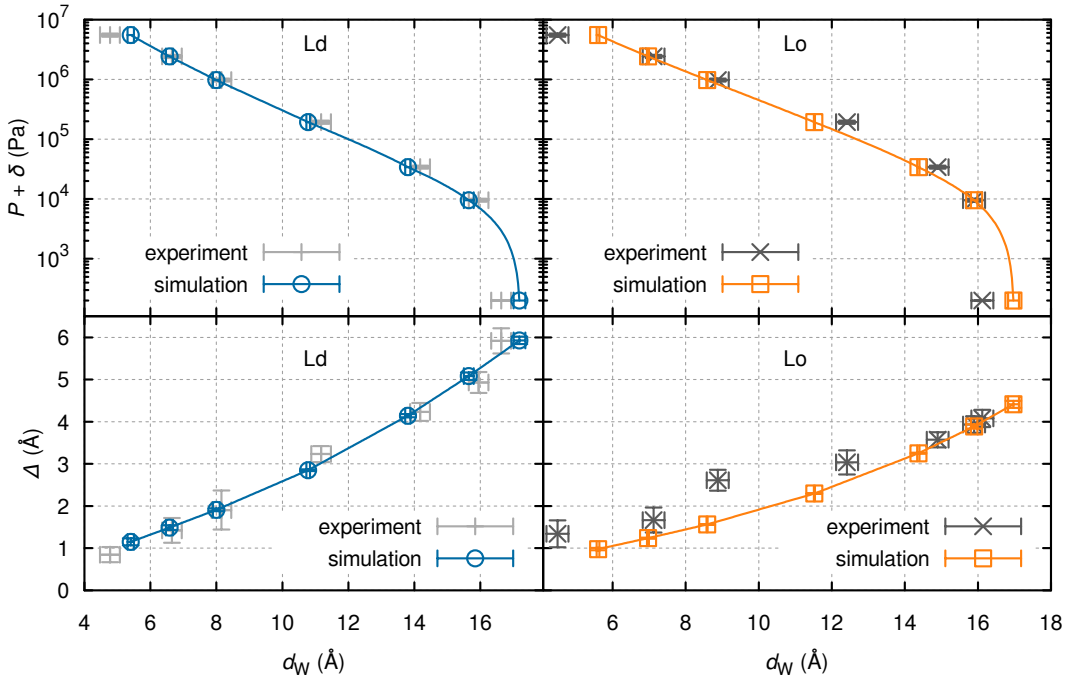

Figure 3.4.: Pressure P (top) and fluctuations Δ (bottom) vs water-layer thickness d_W. Plotted are the best fits of membrane MC simulations against SAXS data for coexisting Lo/Ld domains at $\rho = 1$ (see Tab. 3.2). Reproduced from [64].

applicability of the line-shape model in the SAXS analysis for highly ordered systems [64]. Figure 3.4 showcases the agreement between experimental and simulational results for the $\rho = 1$ sample.

The obtained interdomain forces are listed in Tab. 3.2 and their contributions to the cumulative isotherms are plotted exemplarily for $\rho = 1$ in Fig. 3.5. Specifically, the listed quantities are the Hamaker coefficient H describing the strength of van der Waals interactions, and the amplitudes A and decay-lengths λ of hydration (hyd) and undulation (und) interactions[3].

All three reported samples exhibited alignment of like domains. This common motive suggests that also their interdomain forces might be similar. Indeed, only a single parameter (A_{hyd} in the Ld phase at $\rho = 0.35$) deviated

[3]While the undulation interactions were treated exactly in the simulational analysis, their effective intermembrane pressures could be roughly described by an exponential function.

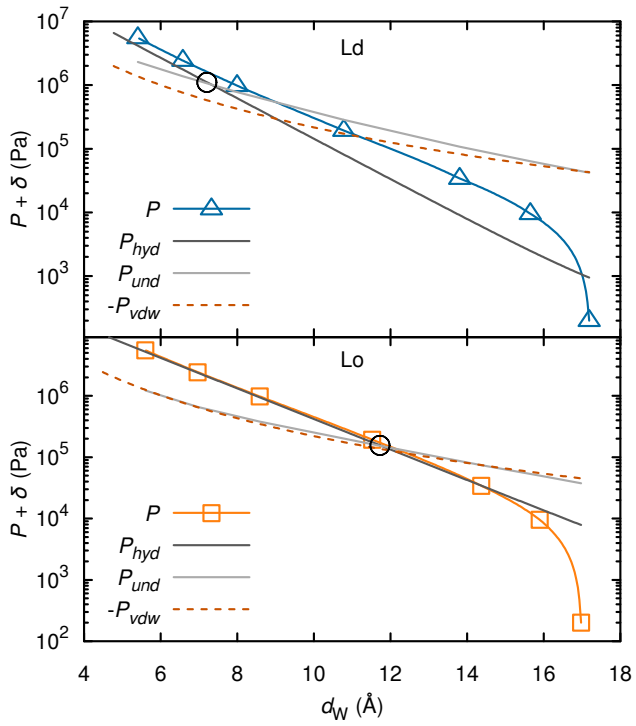

Figure 3.5.: Dissecting the isotherms from coexisting Lo/Ld domains at $\rho = 1$ into contributions from hydration P_{hyd}, undulation P_{und}, and van der Waals P_{vdw} interactions. The black circles highlight the interbilayer separation d_W, at which $P_{hyd} = P_{und}$. Reproduced from [64].

Table 3.2.: Domain interactions determined from coexisting Lo/Ld domains in DOPC/POPC/DSPC/Chol. The corresponding goodness of fit χ^2_{red} and bilayer thickness d_B are also listed.

	Ld			Lo		
ρ/%	35	65	100	35	65	100
K_c/zJ	64(20)	54(11)	44(10)	150(30)	120(20)	120(20)
H/zJ	4.09	4.09	4.08	4.13	4.15	4.15
A_{hyd}/Pa	$10^{8.8(2)}$	$10^{8.4(3)}$	$10^{8.3(2)}$	$10^{8.0(2)}$	$10^{8.0(2)}$	$10^{8.1(2)}$
λ_{hyd}/Å	1.28(12)	1.39(15)	1.37(15)	1.86(15)	1.82(15)	1.74(15)
A_{und}/Pa	$10^{7.1(2)}$	$10^{6.9(2)}$	$10^{6.8(2)}$	$10^{6.5(2)}$	$10^{6.5(2)}$	$10^{6.6(2)}$
λ_{und}/Å	3.0(3)	3.3(3)	3.3(3)	3.9(4)	3.8(4)	3.7(4)
χ^2_{red}	1.2(5)	0.9(5)	1.5(5)	4.5(5)	3.8(5)	5.8(5)
d_B/Å	48.8(10)	48.9(10)	48.5(10)	60.0(12)	61.1(12)	61.3(12)

significantly, while all other quantities were unaffected within experimental uncertainty by changes of ρ.

We found however astonishing differences in the hydration and undulation interactions between different domains. The hydration interactions for Ld phases decay much faster than for the corresponding Lo phases, see Tab. 3.2 or Fig. 3.5. Furthermore, the smaller bending rigidities of Ld, see Fig. 3.3, lead to an increase of undulation interactions compared with Lo phases. These difference imply that undulations are for Ld phases the dominant interaction over a much larger range of bilayer separations than they are for Lo, see Fig. 3.5.

3.3. Line tension of coexisting domains

Line tension and elastic curvature energies seem to determine the size and also the shape of domains in the quaternary lipid mixture DOPC/POPC/DSPC/Chol [172]. A previous attempt [112] to calculate the line tension in this system yielded just the qualitative trend because the relevant elastic parameters had to be estimated at that time. Measuring monolayer spontaneous curvatures and bending moduli as described in Sec. 3.1 enabled us to actually calculate the line tension quantitatively with Eq. (2.7) as function of ρ [64]. The necessary

Table 3.3.: Necessary parameters for line tension calculations and (interim) results according to Eq. (2.7). The input parameters are given by the position of the neutral plane h, the monolayer spontaneous curvature J_0, and the monolayer bending k_c and tilt moduli k_t.* Results are the elastic (γ_h) and curvature-induced (γ_J) contributions and the final line tension γ.

ρ/%	0	10	20	35	66	100
$h^{\ddagger}_{Ld}$/nm	1.85(4)	1.80(4)	1.75(4)	1.69(3)	1.70(3)	1.68(3)
$h^{\ddagger}_{Lo}$/nm	2.03(4)	2.06(4)	2.11(4)	2.05(4)	2.11(4)	2.12(4)
$-J_{0,Ld}$/nm^{-1}	0.06(1)	0.06(1)	0.07(1)	0.08(1)	0.10(1)	0.12(1)
$-J_{0,Lo}$/nm^{-1}	0.17(4)	0.18(4)	0.18(4)	0.19(4)	0.20(4)	0.20(4)
$k_{c,Ld}$/zJ	32(10)†	32(10)†	32(10)†	32(10)	27(6)	22(5)
$k_{c,Lo}$/zJ	75(15)†	75(15)†	75(15)†	75(15)	60(10)	60(10)
γ_h/pN	0.3(2)	0.7(3)	1.3(4)	1.4(5)	1.6(5)	1.7(5)
γ_J/pN	−0.2(2)	−0.3(2)	−0.3(2)	−0.3(2)	−0.2(1)	−0.2(2)
γ/pN	0.1(3)	0.4(4)	1.0(5)	1.2(5)	1.4(5)	1.5(5)

* The tilt moduli k_t of 70(5) and 540(20) zJ^2 nm^{-1} for Ld and Lo, respectively, were obtained from MD simulations at $\rho = 1$ [173].
† Assumed to equal $k_c(\rho = 35\,\%)$.
‡ The neutral plane positions were obtained from the SAXS analyses.

parameters and obtained results are summarized in Tab. 3.3. A graphical representation of the results is given in Fig. 3.6.

We found a strong increase of line tension in the nanoscopic regime ($\rho < 0.35$) and considerably higher tensions for macropscopically sized domains ($\rho \geq 0.35$), see Fig. 3.6. This functional dependence is mainly determined by the decrease of the bilayer thickness in the Ld phase with increasing ρ, which is especially pronounced for nanoscopic domains, see Tab. 3.3. On the other hand, the spontaneous curvature-induced contribution γ_J remained constant over the whole range of ρ. These results emphasize the importance of domain height mismatch on line tension, and therefore also on domain size [64, 112].

3.4. Protein partitioning in coexisting domains

The continuum mechanical model described in Sec. 2.5.2 allowed us to estimate the mechanical work required for inserting protein-like shapes into

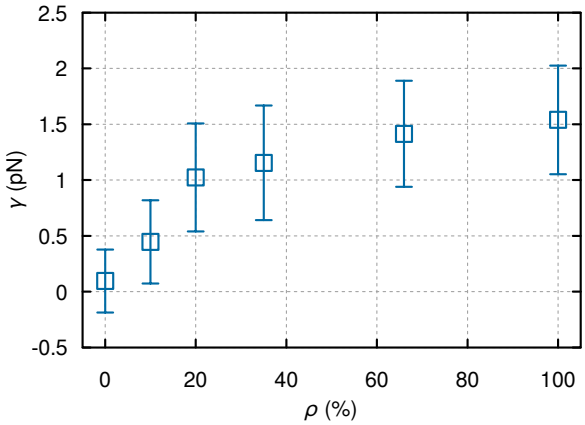

Figure 3.6.: Calculated line tensions γ from Tab. 3.3 for coexisting Lo/Ld phases in DOPC/POPC/DSPC/Chol. Adapted from [41].

lipid bilayer phases. Although one could make use of the detailed structural information available for many transmembrane proteins [174], a more general understanding can be gained by the application of simple model shapes [66].

We therefore resorted to two previously published protein models, see Fig. 3.7. The first geometrical model describes a cone of angle $\varphi_c = 0.14$ and radius $r_c = 2.4\,\mathrm{nm}$ at the bilayer center [66]. Expanding this model's cross section into the power series given by Eq. (2.9) yields $a_1^+ = -(a_1^-)$, i.e. the first-order contribution vanishes for a symmetrical bilayer, and $a_2^\pm = \pi \tan^2 \varphi_c$ [66]. The second considered shape resembles an hourglass with a radius of $r_h = 2.0\,\mathrm{nm}$ at the bilayer midplane, which expands at an angle of $\varphi_h = 0.20$ away from the center [23]. For this structure, $a_1^\pm = 2\pi r_h \tan \varphi_h$ and $a_2^\pm = \pi \tan^2 \varphi_h$ were reported [23].

Calculating the mechanical work of insertion in the quaternary lipid mixture required first the moments of the bilayer pressure profiles. While the zeroth moments vanished, we calculated the first and second moments by inserting the parameters listed in Tab. 3.3 into Eq. (2.10).[4] The resulting values are given in Tab. 3.4.

[4]The necessary Gaussian moduli k_g were estimated from the relation $k_g/k_c \approx -0.80(5)$ for that purpose [45].

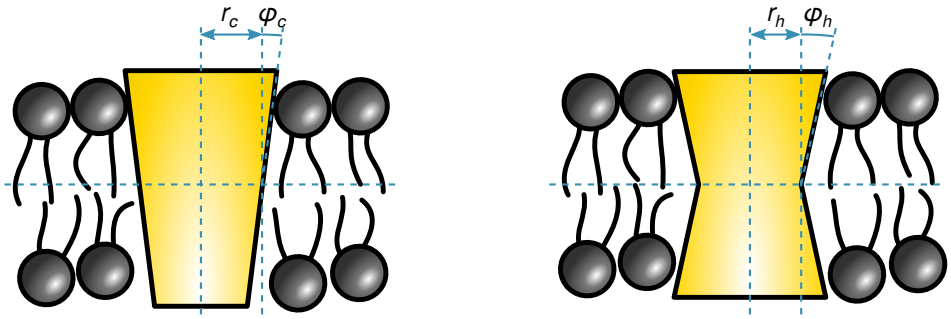

Figure 3.7.: The two geometrical protein models, representing a cone (left) or an hourglass (right) structure of radii $r_{c/h}$ at the bilayer midplane and opening angles $\varphi_{c/h}$.

Table 3.4.: The first and second moment of the bilayer pressure profile according to Eq. (2.10).

ρ/%	0	10	20	35	66	100
$-p_{1,Ld}$/pN	1.9(7)	2.1(7)	2.3(8)	2.6(9)	2.7(6)	2.6(7)
$-p_{1,Lo}$/pN	12.9(38)	13.5(40)	13.8(41)	14.3(43)	11.9(33)	12.0(33)
$p_{2,Ld}$/zJ	19(10)	18(10)	18(10)	17(10)	13(5)	9(5)
$p_{2,Lo}$/zJ	8(17)	4(18)	2(18)	1(18)	−2(14)	−3(14)

Having obtained these moments p_j and the coefficients $a_j^{\pm}$ of the protein model cross sections allowed us to calculate the mechanical insertion energies $W_{Lo/Ld}$ for both models in the corresponding Lo/Ld phases. Their difference $\Delta W = W_{Lo} - W_{Ld}$ corresponds consistently to the energetic penalty ($\Delta W > 0$) or gain (ΔW) upon transferring the protein model shapes from the Ld into the Lo phase and is plotted in Fig. 3.8.

We obtained consistently over the whole investigated range of ρ values of ΔW close to zero for the cone model protein and significantly negative values for the hourglass shape. These findings imply only a minor effect of internal bilayer stress on cone-like protein shapes, but a preferential contribution of considerable magnitude towards partitioning into the Lo phase for hourglass-shapes proteins in the quaternary mixture DOPC/POPC/DSPC/Chol.

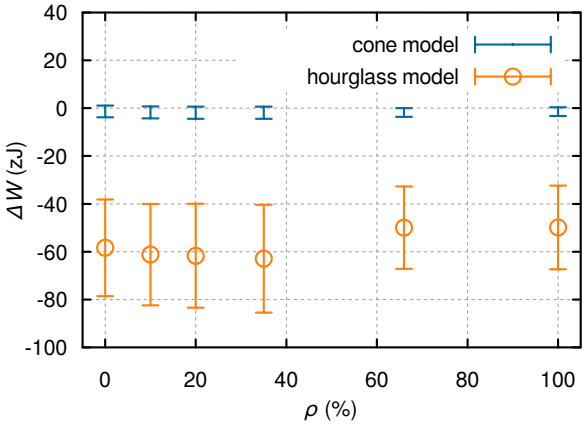

Figure 3.8.: Mechanical work $\Delta W = W_{Lo} - W_{Ld}$ required for transferring model proteins from the Ld into the Lo phase.

4. Conclusion

We quantified the elastic parameters of and fundamental interactions between phase-separated Lo/Ld lipid-only membranes. The obtained quantities should prove useful for numerous biophysical applications. Exemplarily, we showed their applicability with two continuum mechanical calculations.

The preferential lipid curvature J_0 of several different physiologically relevant lipids was measured with SAXS in H_{II} template phases. We obtained strongly negative values for lipids with PE headgroups and for cholesterol, and curvatures closer to zero for PC and SM lipids. The temperature dependence dJ_0/dT was found to be -1 to $-3 \times 10^{-3}\,\mathrm{nm}^{-1}\,^{\circ}\mathrm{C}$ in the range of 15–55 °C for most of the investigated lipids.

We derived bending moduli and interdomain forces from SAXS/osmotic pressure experiments, which were analyzed by a novel MC simulation-based method. This new technique allowed us to treat the entropic undulation interactions exactly, without having to resort to barely justifiable assumptions. Because the underlying full q-range SAXS analysis was capable of modeling coexisting Lo and Ld phases in MLV, we could further determine these quantities independently from phase diagrams; thereby reducing the necessary effort for measuring previously unconsidered lipid mixtures and eliminating the influence of tie line uncertainties.

We obtained roughly 3-fold higher bending elasticity moduli for Lo phases compared to Ld. With increasing domain size, the bending elasticity moduli slightly decreased for both phases in the quaternary lipid system DOPC/POPC/DSPC/Chol. The van der Waals interactions turned out very similar for all investigated samples, with the largest difference being only 2 %. In contrast, hydration, as well as undulation interactions differed significantly between Lo and Ld phases. For the softer Ld phases, the measured undulation interactions were of larger magnitude than for Lo. We also found that hydration interactions were shorter ranged for Ld than for Lo phases, which further emphasizes the importance of undulation interactions for soft bilayers. These

findings should prove valuable for pinpointing the source of the observed long-range positional order between like domains in several multilamellar bilayer assemblies.

The usefulness of all obtained parameters was demonstrated by continuum mechanical calculations of domain line tension and bilayer induced effects on protein partitioning. We found an increase in line tension for larger domains in the DOPC/POPC/DSPC/Chol mixture. Although this property changed with domain size, no significant trends could be observed in the mechanical contribution to model protein partitioning.

5. Outlook

The present thesis contains results which were obtained in the course of three years. Obviously, science, technology and my own experience has evolved in the meantime, thus favoring different approaches if similar research had to be performed again. On the other hand, the time span proved naturally insufficient to answer all questions posed by ourselves, colleagues, and the scientific community on the covered topics. I will therefore propose a few ideas and suggestions for prospective research in the following paragraphs.

Regarding the monolayer spontaneous curvature determination, three difficulties come to mind. The most fundamental problem is the low miscibility threshold for some of the lipids in the H_{II} template phase. As already pointed out in chapter 2.1, using RSE instead of thin film hydration for sample preparation could expand the miscibility towards larger concentrations. Furthermore, one could try other template lipids than DOPE, for which miscibility boundaries might be different. The SAXS analysis could also be considerably improved. Instead of performing a direct Fourier reconstruction of the electron density, the use of model-based reconstructions might allow for a direct detection of the glycerol backbone, thereby eliminating the need to estimate its position based on electron density maps.

The third weak point of the current procedure is the use of Eq. (2.1), which assumes a linear dependence of curvature on concentrations. Instead of this very simplistic model, one could try extrapolating based on more detailed theories [136], or preferably even reach out towards MD or MC simulations [127, 175]. By simulating and experimentally measuring the nominally same H_{II} phase mixtures and pure lipid bilayers, one would first have to verify the applicability of simulations for the interesting molecules.[1] Even if one might have to tweak the underlying force fields in order to obtain concurrent results, simulations could still be superior to continuum mechanical extrapolations

[1] Standard molecular simulations suffer from several restrictions, e.g. use of Newtonian mechanics or imperfect force fields.

because they intrinsically account for many body effects. Subsequently, one could obtain the monolayer spontaneous curvature directly from the bilayer simulations, or actually simulate experimentally unrealizable structures, e.g. "unstressed monolayers" of otherwise bilayer-forming lipids.

Osmotic pressure experiments could benefit a lot from decreasing the concentration of additive solutes during measurements. The probably cleanest approach are dedicated osmotic cells [176], but even conventional preparations with improved sample handling might suffice to conceal additives below the detection limit. Also the analysis of osmotic pressure experiments could still be improved. At the moment, the membrane MC simulations are restricted to stacks of like membranes. Generalizing the code towards mixed membrane stacks should allow for analyzing even osmotic stress experiments on nanoscopic, unregistered domains. Such results would come in handy for formulating and verifying theories explaining the observed transitions in long-range domain alignment.

Further, possibly fruitful research topics might be testing the limitations of continuum mechanical calculations by comparing their results to experimental observations, or application of the presented methods to other lipids and/or different solutions than pure water.

Appendix A.

List of publication

A.1. Attached publications

- B. Kollmitzer, P. Heftberger, M. Rappolt, and G. Pabst. "Monolayer spontaneous curvature of raft-forming membrane lipids." In: *Soft Matter* 9.45 (2013), pp. 10877–10884. ISSN: 1744-6848. DOI: 10.1039/C3SM51829A
  Author contributions:
  B.K. designed and performed research, analyzed data, and wrote the paper
  P.H. designed and performed research
  M.R. performed research
  G.P. designed and performed research, and wrote the paper

- B. Kollmitzer, P. Heftberger, R. Podgornik, J. F. Nagle, and G. Pabst. "Bending rigidities and interdomain forces in membranes with coexisting lipid domains." In: *Biophys. J.* (Submitted)
  Author contributions:
  B.K. designed and performed research, analyzed data (except X-ray analysis), and wrote the paper
  P.H. designed and performed research, and analyzed X-ray data
  R.P. contributed analytic tools and wrote the paper
  J.F.N. contributed analytic tools and wrote the paper
  G.P. designed and performed research, and wrote the paper

A.2. Further publications

- G. Khelashvili, B. Kollmitzer, P. Heftberger, G. Pabst, and D. Harries. "Calculating the Bending Modulus for Multicomponent Lipid Membranes in Different Thermodynamic Phases." In: *J. Chem. Theory Comput.* 9.9 (2013), pp. 3866–3871. ISSN: 1549-9618. DOI: 10.1021/ct400492e
- P. Heftberger, B. Kollmitzer, F. A. Heberle, J. Pan, M. Rappolt, H. Amenitsch, N. Kučerka, J. Katsaras, and G. Pabst. "Global small-angle X-ray scattering data analysis for multilamellar vesicles: the evolution of the scattering density profile model." In: *J. Appl. Crystallogr.* 47.1 (2013), pp. 173–180. ISSN: 1600-5767. DOI: 10.1107/S1600576713029798
- P. Heftberger, B. Kollmitzer, A. A. Rieder, H. Amenitsch, and G. Pabst. "In Situ Determination of Structure and Fluctuations of Coexisting Fluid Membrane Domains." In: *Biophys. J.* 108.4 (2015), pp. 854–862. ISSN: 0006-3495. DOI: 10.1016/j.bpj.2014.11.3488

Bibliography

[1] B. Alberts, A. Johnson, J. Lewis, D. Morgan, M. C. Raff, K. Roberts, P. Walter, J. Wilson, and T. Hunt. *Molecular biology of the cell*. 2015. ISBN: 0815344325 9780815344322.

[2] R. Lipowsky. *Structure and dynamics of membranes*. Vol. 1. North Holland, 1995.

[3] F. A. Heberle and G. W. Feigenson. "Phase Separation in Lipid Membranes." In: *Cold Spring Harb. Perspect. Biol.* 3.4 (2011), a004630. ISSN: , 1943-0264. DOI: 10.1101/cshperspect.a004630.

[4] A. A. Spector and M. A. Yorek. "Membrane lipid composition and cellular function." In: *J. Lipid Res.* 26.9 (1985), pp. 1015–1035. ISSN: 0022-2275, 1539-7262.

[5] M. J. Karnovsky, A. M. Kleinfeld, R. L. Hoover, and R. D. Klausner. "The concept of lipid domains in membranes." In: *J. Cell Biol.* 94.1 (1982), pp. 1–6. ISSN: 0021-9525, 1540-8140. DOI: 10.1083/jcb.94.1.1.

[6] K. Simons and E. Ikonen. "Functional rafts in cell membranes." In: *Nature* 387.6633 (1997), pp. 569–572. ISSN: 0028-0836. DOI: 10.1038/42408.

[7] D. Lingwood and K. Simons. "Lipid rafts as a membrane-organizing principle." In: *Science* 327.5961 (2010), pp. 46–50.

[8] K. Simons and J. L. Sampaio. "Membrane Organization and Lipid Rafts." In: *Cold Spring Harb. Perspect. Biol.* 3.10 (2011), a004697. ISSN: , 1943-0264. DOI: 10.1101/cshperspect.a004697.

[9] M. L. Kraft. "Plasma membrane organization and function: moving past lipid rafts." In: *Mol. Biol. Cell* 24.18 (2013), pp. 2765–2768. ISSN: 1059-1524, 1939-4586. DOI: 10.1091/mbc.E13-03-0165.

[10] E. Sackmann. "Physical Basis of Self-Organization and Function of Membranes: Physics of Vesicles." In: *Handbook of Biological Physics*. Ed. by E. Sackmann and R. Lipowsky. Vol. 1. Structure and Dynamics of Membranes From Cells to Vesicles. North-Holland, 1995, pp. 213–304.

[11] E. J. Shimshick and H. M. McConnell. "Lateral phase separation in phospholipid membranes." In: *Biochemistry* 12.12 (1973), pp. 2351–2360.

[12] S. Mabrey and J. M. Sturtevant. "Investigation of phase transitions of lipids and lipid mixtures by sensitivity differential scanning calorimetry." In: *PNAS* 73.11 (1976), pp. 3862–3866. ISSN: 0027-8424, 1091-6490.

[13] S. L. Veatch and S. L. Keller. "Separation of Liquid Phases in Giant Vesicles of Ternary Mixtures of Phospholipids and Cholesterol." In: *Biophys. J.* 85.5 (2003), pp. 3074–3083. ISSN: 0006-3495. DOI: 10.1016/S0006-3495(03)74726-2.

[14] S. L. Veatch and S. L. Keller. "Seeing spots: Complex phase behavior in simple membranes." In: *Biochim. Biophys. Acta, Mol. Cell Res.* 1746.3 (2005), pp. 172–185. ISSN: 01674889. DOI: 10.1016/j.bbamcr.2005.06.010.

[15] F. A. Heberle, J. Wu, S. L. Goh, R. S. Petruzielo, and G. W. Feigenson. "Comparison of Three Ternary Lipid Bilayer Mixtures: FRET and ESR Reveal Nanodomains." In: *Biophys. J.* 99.10 (2010), pp. 3309–3318. ISSN: 00063495. DOI: 10.1016/j.bpj.2010.09.064.

[16] J. Pan, F. A. Heberle, R. S. Petruzielo, and J. Katsaras. "Using small-angle neutron scattering to detect nanoscopic lipid domains." In: *Chemistry and Physics of Lipids* 170–171 (2013), pp. 19–32. ISSN: 0009-3084. DOI: 10.1016/j.chemphyslip.2013.02.012.

[17] P. Heftberger, B. Kollmitzer, A. A. Rieder, H. Amenitsch, and G. Pabst. "In Situ Determination of Structure and Fluctuations of Coexisting Fluid Membrane Domains." In: *Biophys. J.* 108.4 (2015), pp. 854–862. ISSN: 0006-3495. DOI: 10.1016/j.bpj.2014.11.3488.

[18] L. Tayebi, Y. Ma, D. Vashaee, G. Chen, S. K. Sinha, and A. N. Parikh. "Long-range interlayer alignment of intralayer domains in stacked lipid bilayers." In: *Nat. Mater.* 11.12 (2012), pp. 1074–1080. ISSN: 1476-1122. DOI: 10.1038/nmat3451.

[19] S. Karmakar and V. A. Raghunathan. "Structure of phospholipid-cholesterol membranes: An x-ray diffraction study." In: *Phys. Rev. E* 71.6 (2005), p. 061924. DOI: 10.1103/PhysRevE.71.061924.

[20] L. Chen, Z. Yu, and P. J. Quinn. "The partition of cholesterol between ordered and fluid bilayers of phosphatidylcholine: A synchrotron X-ray diffraction study." In: *Biochim. Biophys. Acta, Biomembr.* 1768.11 (2007), pp. 2873–2881. ISSN: 0005-2736. DOI: 10.1016/j.bbamem.2007.07.023.

[21] T. T. Mills, S. Tristram-Nagle, F. A. Heberle, N. F. Morales, J. Zhao, J. Wu, G. E. S. Toombes, J. F. Nagle, and G. W. Feigenson. "Liquid-Liquid Domains in Bilayers Detected by Wide Angle X-Ray Scattering." In: *Biophys. J.* 95.2 (2008), pp. 682–690. ISSN: 0006-3495. DOI: 10.1529/biophysj.107.127910.

[22] G. Staneva, C. Chachaty, C. Wolf, K. Koumanov, and P. J. Quinn. "The role of sphingomyelin in regulating phase coexistence in complex lipid model membranes: Competition between ceramide and cholesterol." In: *Biochim. Biophys. Acta, Biomembr.* 1778.12 (2008), pp. 2727–2739. ISSN: 0005-2736. DOI: 10.1016/j.bbamem.2008.07.025.

[23] G. Pabst, B. Boulgaropoulos, E. Gander, B. R. Sarangi, H. Amenitsch, V. A. Raghunathan, and P. Laggner. "Effect of Ceramide on Nonraft Proteins." In: *J. Membr. Biol.* 231.2 (2009), pp. 125–132. ISSN: 0022-2631, 1432-1424. DOI: 10.1007/s00232-009-9211-3.

[24] P. Uppamoochikkal, S. Tristram-Nagle, and J. F. Nagle. "Orientation of Tie-Lines in the Phase Diagram of DOPC/DPPC/Cholesterol Model Biomembranes." In: *Langmuir* 26.22 (2010), pp. 17363–17368. ISSN: 0743-7463, 1520-5827. DOI: 10.1021/la103024f.

[25] B. Bechinger. "Lipid multilayers: Domains stack up." In: *Nat. Mater.* 11.12 (2012), pp. 1005–1006. ISSN: 1476-1122. DOI: 10.1038/nmat3507.

[26] M. M. Kozlov and M. Winterhalter.
"Elastic moduli and neutral surface for strongly curved monolayers. Analysis of experimental results."
In: *Journal de Physique II* 1.9 (1991), pp. 1085–1100.

[27] S. Leikin, M. M. Kozlov, N. L. Fuller, and R. P. Rand.
"Measured effects of diacylglycerol on structural and elastic properties of phospholipid membranes." In: *Biophys. J.* 71.5 (1996), pp. 2623–2632.

[28] M. M. Kozlov. "Determination of lipid spontaneous curvature from X-ray examinations of inverted hexagonal phases."
In: *Methods in Membrane Lipids*. Springer, 2007, pp. 355–366.

[29] S. M. Gruner, V. A. Parsegian, and R. P. Rand. "Directly measured deformation energy of phospholipid HII hexagonal phases."
In: *Faraday Discuss.* 81 (1986), pp. 29–37. ISSN: 0301-7249.
DOI: 10.1039/DC9868100029.

[30] M. W. Tate and S. M. Gruner. "Temperature dependence of the structural dimensions of the inverted hexagonal (HII) phase of phosphatidylethanolamine-containing membranes."
In: *Biochemistry* 28.10 (1989), pp. 4245–4253.

[31] R. P. Rand, N. L. Fuller, S. M. Gruner, and V. A. Parsegian.
"Membrane curvature, lipid segregation, and structural transitions for phospholipids under dual-solvent stress."
In: *Biochemistry* 29.1 (1990), pp. 76–87.

[32] M. M. Kozlov, S. Leikin, and R. P. Rand.
"Bending, hydration and interstitial energies quantitatively account for the hexagonal-lamellar-hexagonal reentrant phase transition in dioleoylphosphatidylethanolamine."
In: *Biophys. J.* 67.4 (1994), pp. 1603–1611. ISSN: 0006-3495.
DOI: 10.1016/S0006-3495(94)80633-2.

[33] R. P. Rand and N. L. Fuller. "Structural dimensions and their changes in a reentrant hexagonal-lamellar transition of phospholipids."
In: *Biophys. J.* 66.6 (1994), pp. 2127–2138.

[34] Z. Chen and R. P. Rand. "The influence of cholesterol on phospholipid membrane curvature and bending elasticity."
In: *Biophys. J.* 73.1 (1997), pp. 267–276. ISSN: 0006-3495.
DOI: 10.1016/S0006-3495(97)78067-6.

[35] Z. Chen and R. P. Rand. "Comparative Study of the Effects of Several n-Alkanes on Phospholipid Hexagonal Phases."
In: *Biophys. J.* 74.2 (1998), pp. 944–952.

[36] J. Zimmerberg and M. M. Kozlov.
"How proteins produce cellular membrane curvature."
In: *Nat. Rev. Mol. Cell Biol.* 7.1 (2005), pp. 9–19.
ISSN: 1471-0072, 1471-0080. DOI: 10.1038/nrm1784.

[37] M. Rappolt.
"The biologically relevant lipid mesophases as 'seen' by X-rays."
In: *Adv. Planar Lipid Bilayers Liposomes* 5 (2006), pp. 253–283.

[38] E. E. Kooijman, V. Chupin, N. L. Fuller, M. M. Kozlov, B. de Kruijff, K. N. J. Burger, and R. P. Rand. "Spontaneous Curvature of Phosphatidic Acid and Lysophosphatidic Acid."
In: *Biochemistry* 44.6 (2005), pp. 2097–2102. ISSN: 0006-2960, 1520-4995.
DOI: 10.1021/bi0478502.

[39] S. H. Alley, O. Ces, M. Barahona, and R. H. Templer.
"X-ray diffraction measurement of the monolayer spontaneous curvature of dioleoylphosphatidylglycerol."
In: *Chem. Phys. Lipids* 154.1 (2008), pp. 64–67. ISSN: 00093084.
DOI: 10.1016/j.chemphyslip.2008.03.007.

[40] B. Boulgaropoulos, M. Rappolt, B. Sartori, H. Amenitsch, and G. Pabst. "Lipid Sorting by Ceramide and the Consequences for Membrane Proteins." In: *Biophys. J.* 102.9 (2012), pp. 2031–2038. ISSN: 00063495.
DOI: 10.1016/j.bpj.2012.03.059.

[41] B. Kollmitzer, P. Heftberger, M. Rappolt, and G. Pabst.
"Monolayer spontaneous curvature of raft-forming membrane lipids."
In: *Soft Matter* 9.45 (2013), pp. 10877–10884. ISSN: 1744-6848.
DOI: 10.1039/C3SM51829A.

[42] P. B. Canham. "The minimum energy of bending as a possible explanation of the biconcave shape of the human red blood cell."
In: *J. Theor. Biol.* 26.1 (1970), pp. 61–81.

[43] W. Helfrich. "Elastic Properties of Lipid Bilayers: Theory and Possible Experiments." In: *Z. Naturforsch., C: J. Biosci.* 28 (1973), pp. 693–703.

[44] J. Thimmel. "Quellen und Trennen von Lipidvielschichtsystemen: Untersuchung des Prozesses und neuer Membranstrukturen."
PhD thesis. 2000.

[45] D. Marsh.
"Elastic curvature constants of lipid monolayers and bilayers."
In: *Chem. Phys. Lipids* 144.2 (2006), pp. 146–159. ISSN: 0009-3084.
DOI: 10.1016/j.chemphyslip.2006.08.004.

[46] D. V. Zhelev. "Material property characteristics for lipid bilayers containing lysolipid." In: *Biophys. J.* 75.1 (1998), pp. 321–330.

[47] M. Hamm and M. M. Kozlov.
"Elastic energy of tilt and bending of fluid membranes."
In: *Eur. Phys. J. E* 3.4 (2000), pp. 323–335.

[48] M. C. Watson, E. S. Penev, P. M. Welch, and F. L. H. Brown.
"Thermal fluctuations in shape, thickness, and molecular orientation in lipid bilayers." In: *J. Chem. Phys.* 135.24 (2011), p. 244701.
ISSN: 0021-9606, 1089-7690. DOI: 10.1063/1.3660673.

[49] P. I. Kuzmin, S. A. Akimov, Y. A. Chizmadzhev, J. Zimmerberg, and F. S. Cohen. "Line Tension and Interaction Energies of Membrane Rafts Calculated from Lipid Splay and Tilt."
In: *Biophys. J.* 88.2 (2005), pp. 1120–1133. ISSN: 0006-3495.
DOI: 10.1529/biophysj.104.048223.

[50] M. S. Jablin, K. Akabori, and J. F. Nagle. "Experimental Support for Tilt-Dependent Theory of Biomembrane Mechanics." In: (2014).

[51] P. Heftberger, B. Kollmitzer, F. A. Heberle, J. Pan, M. Rappolt, H. Amenitsch, N. Kučerka, J. Katsaras, and G. Pabst.
"Global small-angle X-ray scattering data analysis for multilamellar vesicles: the evolution of the scattering density profile model."
In: *J. Appl. Crystallogr.* 47.1 (2013), pp. 173–180. ISSN: 1600-5767.
DOI: 10.1107/S1600576713029798.

[52] M. P. Sheetz and S. J. Singer. "Biological Membranes as Bilayer Couples. A Molecular Mechanism of Drug-Erythrocyte Interactions."
In: *PNAS* 71.11 (1974), pp. 4457–4461. ISSN: 0027-8424, 1091-6490.

[53] E. Evans. "Bending Resistance and Chemically Induced Moments in Membrane Bilayers." In: *Biophys. J.* 14.12 (1974), pp. 923–931.
ISSN: 0006-3495. DOI: 10.1016/S0006-3495(74)85959-X.

[54] S. Svetina, A. Ottova-Leitmannová, and R. Glaser. "Membrane bending energy in relation to bilayer couples concept of red blood cell shape transformations." In: *J. Theor. Biol.* 94.1 (1982), pp. 13–23. ISSN: 0022-5193. DOI: 10.1016/0022-5193(82)90327-7.

[55] S. Svetina and B. Žekš. "Membrane bending energy and shape determination of phospholipid vesicles and red blood cells." In: *Eur. Biophys. J.* 17.2 (1989), pp. 101–111. ISSN: 0175-7571, 1432-1017. DOI: 10.1007/BF00257107.

[56] B. Bozic, S. Svetina, B. Zeks, and R. E. Waugh. "Role of lamellar membrane structure in tether formation from bilayer vesicles." In: *Biophys. J.* 61.4 (1992), pp. 963–973. ISSN: 0006-3495. DOI: 10.1016/S0006-3495(92)81903-3.

[57] L. Miao, U. Seifert, M. Wortis, and H.-G. Döbereiner. "Budding transitions of fluid-bilayer vesicles: The effect of area-difference elasticity." In: *Phys. Rev. E* 49.6 (1994), pp. 5389–5407. DOI: 10.1103/PhysRevE.49.5389.

[58] F. Brochard and J. F. Lennon. "Frequency spectrum of the flicker phenomenon in erythrocytes." In: *Journal de Physique* 36.11 (1975), pp. 1035–1047.

[59] E. Evans and W. Rawicz. "Entropy-driven tension and bending elasticity in condensed-fluid membranes." In: *Phys. Rev. Lett.* 64.17 (1990), pp. 2094–2097. DOI: 10.1103/PhysRevLett.64.2094.

[60] P. Méléard, C. Gerbeaud, T. Pott, L. Fernandez-Puente, I. Bivas, M. D. Mitov, J. Dufourcq, and P. Bothorel. "Bending elasticities of model membranes: influences of temperature and sterol content." In: *Biophys. J.* 72.6 (1997), pp. 2616–2629. ISSN: 0006-3495. DOI: 10.1016/S0006-3495(97)78905-7.

[61] Y. Lyatskaya, Y. Liu, S. Tristram-Nagle, J. Katsaras, and J. F. Nagle. "Method for obtaining structure and interactions from oriented lipid bilayers." In: *Phys. Rev. E* 63.1 (2000), p. 011907. DOI: 10.1103/PhysRevE.63.011907.

[62] J. D. Nickels, M. Ohl, X. Cheng, C. Stanley, F. Heberle, R. Standaert, and J. Katsaras. "Experiment and Simulation Reveal the Bending Properties of Nanoscopic Lipid Domains." In: 108.2 (2015), 31a. ISSN: 0006-3495. DOI: 10.1016/j.bpj.2014.11.197.

[63] B. Kollmitzer, P. Heftberger, H. Amenitsch, R. Podgornik, J. F. Nagle, and G. Pabst. "Membrane Domain Interactions by Monte Carlo Type Analysis of Osmotic Stress Data." In: 108.2 (2015), 86a. ISSN: 0006-3495. DOI: 10.1016/j.bpj.2014.11.502.

[64] B. Kollmitzer, P. Heftberger, R. Podgornik, J. F. Nagle, and G. Pabst. "Bending rigidities and interdomain forces in membranes with coexisting lipid domains." In: *Biophys. J.* (Submitted).

[65] R. S. Cantor. "The Lateral Pressure Profile in Membranes: A Physical Mechanism of General Anesthesia."
In: *Biochemistry* 36.9 (1997), pp. 2339–2344. ISSN: 0006-2960.
DOI: 10.1021/bi9627323.

[66] R. S. Cantor. "The influence of membrane lateral pressures on simple geometric models of protein conformational equilibria."
In: *Chem. Phys. Lipids* 101.1 (1999), pp. 45–56.

[67] S. A. Safran.
"Statistical thermodynamics of surfaces, interfaces, and membranes."
In: *J. Stat. Phys.* 78.3 (1995), pp. 1175–1177. ISSN: 0022-4715, 1572-9613.
DOI: 10.1007/BF02183712.

[68] R. Brewster and S. A. Safran.
"Line Active Hybrid Lipids Determine Domain Size in Phase Separation of Saturated and Unsaturated Lipids."
In: *Biophys. J.* 98.6 (2010), pp. L21–L23. ISSN: 0006-3495.
DOI: 10.1016/j.bpj.2009.11.027.

[69] J. A. Lundbæk, P. Birn, J. Girshman, A. J. Hansen, and O. S. Andersen. "Membrane Stiffness and Channel Function†."
In: *Biochemistry* 35.12 (1996), pp. 3825–3830. ISSN: 0006-2960.
DOI: 10.1021/bi952250b.

[70] D. Marsh.
"Lateral Pressure Profile, Spontaneous Curvature Frustration, and the Incorporation and Conformation of Proteins in Membranes."
In: *Biophys. J.* 93.11 (2007), pp. 3884–3899. ISSN: 00063495.
DOI: 10.1529/biophysj.107.107938.

[71] G. Pabst, F. A. Heberle, and J. Katsaras.
"X-Ray Scattering of Lipid Membranes." In: *Encyclopedia of Biophysics*. Springer, 2013, pp. 2785–2791.

[72] D. M. LeNeveu and R. P. Rand.
"Measurement and modification of forces between lecithin bilayers." In: *Biophys. J.* 18.2 (1977), pp. 209–230.

[73] V. A. Parsegian, N. Fuller, and R. P. Rand.
"Measured work of deformation and repulsion of lecithin bilayers." In: *PNAS* 76.6 (1979), pp. 2750–2754. ISSN: 0027-8424, 1091-6490.

[74] V. A. Parsegian and R. P. Rand. "Interaction in membrane assemblies." In: *Handbook of biological physics*. Ed. by R. Lipowsky and E. Sackmann. Vol. 1. North-Holland, 1995, pp. 643–690.

[75] J. N. Israelachvili. *Intermolecular and surface forces*.
Burlington, MA: Academic Press, 2011.
ISBN: 9780123751829 0123751829 9780080923635 0080923631 9780123919274 0123919274 9780123919335 0123919339.

[76] G. Pabst.
"Coupling Membrane Elasticity and Structure to Protein Function." In: *Advances in Planar Lipid Bilayers and Liposomes*. Vol. 18. Elsevier, 2013, pp. 81–109. ISBN: 9780124115156.

[77] T. J. McIntosh, A. D. Magid, and S. A. Simon.
"Steric repulsion between phosphatidylcholine bilayers." In: *Biochemistry* 26.23 (1987), pp. 7325–7332.

[78] S. Marčelja and N. Radić.
"Repulsion of interfaces due to boundary water." In: *Chem. Phys. Lett.* 42.1 (1976), pp. 129–130. ISSN: 0009-2614.
DOI: 10.1016/0009-2614(76)80567-2.

[79] M. Kanduč, E. Schneck, and R. R. Netz. "Hydration interaction between phospholipid membranes: insight into different measurement ensembles from atomistic molecular dynamics simulations." In: *Langmuir* 29.29 (2013), pp. 9126–9137.

[80] M. Kanduč, A. Schlaich, E. Schneck, and R. R. Netz.
"Hydration repulsion between membranes and polar surfaces: Simulation approaches versus continuum theories." In: *Adv. Colloid Interface Sci.* 208 (2014), pp. 142–152.

[81] D. Andelman. "Electrostatic properties of membranes: the Poisson-Boltzmann theory." In: *Handbook of biological physics*. Vol. 1. 1995, pp. 603–642.

[82] F. Pincet, S. Cribier, and E. Perez. "Bilayers of neutral lipids bear a small but significant charge." In: *Eur. Phys. J. B* 11.1 (1999), pp. 127–130. ISSN: 1434-6028, 1434-6036. DOI: 10.1007/BF03219162.

[83] V. A. Parsegian. *Van der Waals forces*. Cambridge university press Cambridge etc., 2006.

[84] J. N. Israelachvili. "Interactions of Biological Membranes and Structures." In: *Intermolecular and surface forces*. Burlington, MA: Academic Press, 2011, pp. 577–616. ISBN: 9780123751829 0123751829 9780080923635 0080923631 9780123919274 0123919274 9780123919335 0123919339.

[85] W. Helfrich. "Steric Interaction of Fluid Membranes in Multilayer Systems." In: *Z. Naturforsch., A: Phys. Sci.* 33 (1978), p. 305. ISSN: 0932-0784.

[86] R. Podgornik and V. A. Parsegian. "Thermal-mechanical fluctuations of fluid membranes in confined geometries: the case of soft confinement." In: *Langmuir* 8.2 (1992), pp. 557–562. ISSN: 0743-7463. DOI: 10.1021/la00038a041.

[87] V. A. Parsegian, R. P. Rand, N. L. Fuller, and D. C. Rau. "Osmotic stress for the direct measurement of intermolecular forces." In: *Methods in Enzymology*. Ed. by Lester Packer. Vol. 127. Biomembranes Part O: Protons and Water: Structure and Translocation. Academic Press, 1986, pp. 400–416. ISBN: 0076-6879.

[88] T. J. McIntosh and S. A. Simon. "Hydration force and bilayer deformation: a reevaluation." In: *Biochemistry* 25.14 (1986), pp. 4058–4066.

[89] T. J. McIntosh and S. A. Simon. "Contributions of hydration and steric (entropic) pressures to the interactions between phosphatidylcholine bilayers: Experiments with the subgel phase." In: *Biochemistry* 32.32 (1993), pp. 8374–8384. ISSN: 0006-2960. DOI: 10.1021/bi00083a042.

[90] R. P. Rand and V. A. Parsegian.
"Hydration Forces Between Phospholipid Bilayers."
In: *Biochim. Biophys. Acta* 988.3 (1989), pp. 351–376. ISSN: 0006-3002.
DOI: 10.1016/0304-4157(89)90010-5.

[91] H. I. Petrache, N. Gouliaev, S. Tristram-Nagle, R. Zhang, R. M. Suter, and J. F. Nagle.
"Interbilayer interactions from high-resolution x-ray scattering."
In: *Phys. Rev. E* 57.6 (1998), pp. 7014–7024.
DOI: 10.1103/PhysRevE.57.7014.

[92] G. Pabst, S. Danner, R. Podgornik, and J. Katsaras.
"Entropy-Driven Softening of Fluid Lipid Bilayers by Alamethicin."
In: *Langmuir* 23.23 (2007), pp. 11705–11711. ISSN: 0743-7463, 1520-5827.
DOI: 10.1021/la701586c.

[93] G. Pabst, N. Kučerka, M.-P. Nieh, M. C. Rheinstädter, and J. Katsaras.
"Applications of neutron and X-ray scattering to the study of biologically relevant model membranes."
In: *Chem. Phys. Lipids* 163.6 (2010), pp. 460–479.

[94] D. Sornette and N. Ostrowsky.
"Importance of membrane fluidity on bilayer interactions."
In: *J. Chem. Phys.* 84.7 (1986), pp. 4062–4067. ISSN: 00219606.
DOI: doi:10.1063/1.450067.

[95] E. A. Evans and V. A. Parsegian. "Thermal-mechanical fluctuations enhance repulsion between bimolecular layers."
In: *PNAS* 83.19 (1986), pp. 7132–7136.

[96] K. R. Mecke, T. Charitat, and F. Graner.
"Fluctuating Lipid Bilayer in an Arbitrary Potential: Theory and Experimental Determination of Bending Rigidity."
In: *Langmuir* 19.6 (2003), pp. 2080–2087. ISSN: 0743-7463.
DOI: 10.1021/la026606d.

[97] N. Gouliaev and J. F. Nagle. "Simulations of Interacting Membranes in the Soft Confinement Regime."
In: *Phys. Rev. Lett.* 81.12 (1998), pp. 2610–2613. ISSN: 0031-9007.
DOI: 10.1103/PhysRevLett.81.2610.

[98] N. Gouliaev and J. F. Nagle. "Simulations of a single membrane between two walls using a Monte Carlo method."
In: *Phys. Rev. E* 58.1 (1998), pp. 881–888.
DOI: 10.1103/PhysRevE.58.881.

[99] P. S. Chen Jr, T. Toribara, and H. Warner.
"Microdetermination of phosphorus."
In: *Anal. Chem.* 28.11 (1956), pp. 1756–1758.

[100] P. B. Kingsley and G. W. Feigenson. "The synthesis of a perdeuterated phospholipid: 1,2-dimyristoyl-sn-glycero-3-phosphocholine-d72."
In: *Chem. Phys. Lipids* 24.2 (1979), pp. 135–147. ISSN: 0009-3084.
DOI: 10.1016/0009-3084(79)90083-5.

[101] J. T. Buboltz and G. W. Feigenson. "A novel strategy for the preparation of liposomes: rapid solvent exchange."
In: *Biochim. Biophys. Acta, Biomembr.* 1417.2 (1999), pp. 232–245.
ISSN: 0005-2736. DOI: 10.1016/S0005-2736(99)00006-1.

[102] R. M. Epand, R. F. Epand, D. W. Hughes, B. G. Sayer, N. Borochov, D. Bach, and E. Wachtel. "Phosphatidylcholine structure determines cholesterol solubility and lipid polymorphism."
In: *Chem. Phys. Lipids* 135.1 (2005), pp. 39–53. ISSN: 0009-3084.
DOI: 10.1016/j.chemphyslip.2005.01.008.

[103] A. Hodzic, M. Rappolt, H. Amenitsch, P. Laggner, and G. Pabst. "Differential Modulation of Membrane Structure and Fluctuations by Plant Sterols and Cholesterol."
In: *Biophys. J.* 94.10 (2008), pp. 3935–3944. ISSN: 0006-3495.
DOI: 10.1529/biophysj.107.123224.

[104] E. Baykal-Caglar, E. Hassan-Zadeh, B. Saremi, and J. Huang. "Preparation of giant unilamellar vesicles from damp lipid film for better lipid compositional uniformity."
In: *Biochim. Biophys. Acta, Biomembr.* 1818.11 (2012), pp. 2598–2604.
ISSN: 0005-2736. DOI: 10.1016/j.bbamem.2012.05.023.

[105] J. T. Buboltz. "A more efficient device for preparing model-membrane liposomes by the rapid solvent exchange method."
In: *Rev. Sci. Instrum.* 80.12 (2009), p. 124301. ISSN: 0034-6748.
DOI: 10.1063/1.3264073.

[106] A. A. Rieder, D. Koller, K. Lohner, and G. Pabst. "Optimizing rapid solvent exchange preparation of multilamellar vesicles." In: *Chemistry and Physics of Lipids* 186 (2015), pp. 39–44. ISSN: 0009-3084. DOI: 10.1016/j.chemphyslip.2014.12.001.

[107] L. D. Mayer, M. J. Hope, P. R. Cullis, and A. S. Janoff. "Solute distributions and trapping efficiencies observed in freeze-thawed multilamellar vesicles." In: *Biochim. Biophys. Acta, Biomembr.* 817.1 (1985), pp. 193–196. ISSN: 0005-2736. DOI: 10.1016/0005-2736(85)90084-7.

[108] C. B. Stanley and H. H. Strey. "Measuring Osmotic Pressure of Poly(ethylene glycol) Solutions by Sedimentation Equilibrium Ultracentrifugation." In: *Macromolecules* 36.18 (2003), pp. 6888–6893. ISSN: 0024-9297. DOI: 10.1021/ma034079e.

[109] J. A. Cohen, R. Podgornik, P. L. Hansen, and V. A. Parsegian. "A Phenomenological One-Parameter Equation of State for Osmotic Pressures of PEG and Other Neutral Flexible Polymers in Good Solvents†." In: *J. Phys. Chem. B* 113.12 (2009), pp. 3709–3714.

[110] I. V. Ionova, V. A. Livshits, and D. Marsh. "Phase Diagram of Ternary Cholesterol/Palmitoylsphingomyelin/Palmitoyloleoyl-Phosphatidylcholine Mixtures: Spin-Label EPR Study of Lipid-Raft Formation." In: *Biophys. J.* 102.8 (2012), pp. 1856–1865. ISSN: 00063495. DOI: 10.1016/j.bpj.2012.03.043.

[111] T. M. Konyakhina, J. Wu, J. D. Mastroianni, F. A. Heberle, and G. W. Feigenson. "Phase diagram of a 4-component lipid mixture: DSPC/DOPC/POPC/chol." In: *Biochimica et Biophysica Acta (BBA) - Biomembranes* 1828.9 (2013), pp. 2204–2214. ISSN: 0005-2736. DOI: 10.1016/j.bbamem.2013.05.020.

[112] F. A. Heberle, R. S. Petruzielo, J. Pan, P. Drazba, N. Kučerka, R. F. Standaert, G. W. Feigenson, and J. Katsaras. "Bilayer Thickness Mismatch Controls Domain Size in Model Membranes." In: *J. Am. Chem. Soc.* 135.18 (2013), pp. 6853–6859. ISSN: 0002-7863. DOI: 10.1021/ja3113615.

[113] O. Glatter and O. Kratky. *Small angle X-ray scattering*. Vol. 102. London: Academic Press, 1982.

[114] B. E. Warren. *X-ray diffraction*.
Reading, Mass.: Addison-Wesley Pub. Co., 1969.

[115] D. C. Turner and S. M. Gruner. "X-ray diffraction reconstruction of the inverted hexagonal (HII) phase in lipid-water systems."
In: *Biochemistry* 31.5 (1992), pp. 1340–1355.

[116] P. E. Harper, D. A. Mannock, R. N. Lewis, R. N. McElhaney, and S. M. Gruner.
"X-Ray Diffraction Structures of Some Phosphatidylethanolamine Lamellar and Inverted Hexagonal Phases*."
In: *Biophys. J.* 81.5 (2001), pp. 2693–2706. ISSN: 0006-3495.
DOI: 10.1016/S0006-3495(01)75912-7.

[117] M. Rappolt, A. Hodzic, B. Sartori, M. Ollivon, and P. Laggner.
"Conformational and hydrational properties during the-to-and-to HII-phase transition in phosphatidylethanolamine."
In: *Chem. Phys. Lipids* 154.1 (2008), pp. 46–55.

[118] *MATLAB v. 7.12 (R2011a)*. Version 7.12 (R2011a). 2011.

[119] A. Caillé. "Physique cristalline: remarques sur la diffusion des rayons X dans les smectiques."
In: *C. R. Acad. Sc. Paris Sie B.* 274 (1972), pp. 891–893.

[120] R. Zhang, R. M. Suter, and J. F. Nagle.
"Theory of the structure factor of lipid bilayers."
In: *Phys. Rev. E* 50.6 (1994), pp. 5047–5060.
DOI: 10.1103/PhysRevE.50.5047.

[121] R. Zhang, S. Tristram-Nagle, W. Sun, R. L. Headrick, T. C. Irving, R. M. Suter, and J. F. Nagle.
"Small-angle x-ray scattering from lipid bilayers is well described by modified Caillé theory but not by paracrystalline theory."
In: *Biophys. J.* 70.1 (1996), pp. 349–357. ISSN: 0006-3495.
DOI: 10.1016/S0006-3495(96)79576-0.

[122] G. Pabst, M. Rappolt, H. Amenitsch, and P. Laggner.
"Structural information from multilamellar liposomes at full hydration: full q-range fitting with high quality x-ray data."
In: *Phys. Rev. E* 62.3 (2000), p. 4000.

[123] M. Rappolt and G. Pabst.
"Flexibility and structure of fluid bilayer interfaces." In: *Structure and Dynamics of Membranous Interfaces. Wiley, Hoboken (NJ) USA*.
Ed. by K. Nag. John Wiley & Sons, 2008, pp. 45–81.

[124] F. A. Heberle, J. Pan, R. F. Standaert, P. Drazba, N. Kučerka, and J. Katsaras. "Model-based approaches for the determination of lipid bilayer structure from small-angle neutron and X-ray scattering data." In: *Eur. Biophys. J.* 41.10 (2012), pp. 875–890. ISSN: 0175-7571, 1432-1017. DOI: 10.1007/s00249-012-0817-5.

[125] G. L. Kirk and S. M. Gruner. "Lyotropic effects of alkanes and headgroup composition on the Lα-Hii lipid liquid crystal phase transition: hydrocarbon packing versus intrinsic curvature." In: *Journal de Physique* 46.5 (1985), pp. 761–769.

[126] H. Vacklin, B. J. Khoo, K. H. Madan, J. M. Seddon, and R. H. Templer. "The Bending Elasticity of 1-Monoolein upon Relief of Packing Stress." In: *Langmuir* 16.10 (2000), pp. 4741–4748. ISSN: 0743-7463, 1520-5827. DOI: 10.1021/la991408g.

[127] A. J. Sodt and R. W. Pastor. "Bending Free Energy from Simulation: Correspondence of Planar and Inverse Hexagonal Lipid Phases." In: *Biophys. J.* 104.10 (2013), pp. 2202–2211. ISSN: 0006-3495. DOI: 10.1016/j.bpj.2013.03.048.

[128] N. Kučerka, S. Tristram-Nagle, and J. F. Nagle. "Closer Look at Structure of Fully Hydrated Fluid Phase DPPC Bilayers." In: *Biophys. J.* 90.11 (2006), pp. L83–L85. ISSN: 00063495. DOI: 10.1529/biophysj.106.086017.

[129] N. Kučerka, S. Tristram-Nagle, and J. F. Nagle. "Structure of Fully Hydrated Fluid Phase Lipid Bilayers with Monounsaturated Chains." In: *J. Membr. Biol.* 208.3 (2006), pp. 193–202. ISSN: 0022-2631, 1432-1424. DOI: 10.1007/s00232-005-7006-8.

[130] N. Kučerka, J. F. Nagle, J. N. Sachs, S. E. Feller, J. Pencer, A. Jackson, and J. Katsaras. "Lipid Bilayer Structure Determined by the Simultaneous Analysis of Neutron and X-Ray Scattering Data." In: *Biophys. J.* 95.5 (2008), pp. 2356–2367. ISSN: 00063495. DOI: 10.1529/biophysj.108.132662.

[131] N. Kučerka, M.-P. Nieh, and J. Katsaras.
"Fluid phase lipid areas and bilayer thicknesses of commonly used phosphatidylcholines as a function of temperature."
In: *Biochim. Biophys. Acta, Biomembr.* 1808.11 (2011), pp. 2761–2771. ISSN: 0005-2736. DOI: 10.1016/j.bbamem.2011.07.022.

[132] S. A. Safran, P. Pincus, and D. Andelman.
"Theory of spontaneous vesicle formation in surfactant mixtures."
In: *Science* 248.4953 (1990), p. 354.

[133] M. M. Kozlov and W. Helfrich. "Effects of a cosurfactant on the stretching and bending elasticities of a surfactant monolayer."
In: *Langmuir* 8.11 (1992), pp. 2792–2797.

[134] S. L. Keller, S. M. Bezrukov, S. M. Gruner, M. W. Tate, I. Vodyanoy, and V. A. Parsegian. "Probability of alamethicin conductance states varies with nonlamellar tendency of bilayer phospholipids."
In: *Biophys. J.* 65.1 (1993), pp. 23–27.

[135] G. Khelashvili, D. Harries, and H. Weinstein.
"Modeling Membrane Deformations and Lipid Demixing upon Protein-Membrane Interaction: The BAR Dimer Adsorption."
In: *Biophys. J.* 97.6 (2009), pp. 1626–1635. ISSN: 0006-3495.
DOI: 10.1016/j.bpj.2009.07.006.

[136] S. May and A. Ben-Shaul. "Spontaneous curvature and thermodynamic stability of mixed amphiphilic layers."
In: *J. Chem. Phys.* 103.9 (1995), p. 3839. ISSN: 00219606.
DOI: 10.1063/1.470062.

[137] M. Gradzielski, D. Langevin, T. Sottmann, and R. Strey. "Droplet microemulsions at the emulsification boundary: The influence of the surfactant structure on the elastic constants of the amphiphillic film."
In: *J. Chem. Phys.* 106.19 (1997), pp. 8232–8238. ISSN: 00219606.
DOI: doi:10.1063/1.473888.

[138] D. P. Landau and K. Binder.
A guide to Monte Carlo simulations in statistical physics.
Cambridge; New York: Cambridge University Press, 2009.
ISBN: 9780511651762 0511651767 9780511994944 051199494X 9780511632532 0511632533.

[139] K. Binder and D. W. Heermann.
Monte Carlo simulation in statistical physics an introduction.
Heidelberg; New York: Springer-Verlag, 2010.
ISBN: 9783642031632 3642031633 9783642031625 3642031625.

[140] B. A. Berg. *Markov chain Monte Carlo simulations and their statistical analysis with web-based Fortran code*.
Hackensack, NJ: World Scientific, 2004.
ISBN: 9812703632 9789812703637.

[141] N. Gouliaev. "Monte-Carlo simulations of membrane systems."
PhD thesis. Pittsburgh, Pennsylvania, USA: Carnegie Mellon University, 1998.

[142] R. Podgornik, R. H. French, and V. A. Parsegian.
"Nonadditivity in van der Waals interactions within multilayers."
In: *J. Chem. Phys.* 124 (2006), p. 044709.

[143] I. McDonald.
"NpT-ensemble Monte Carlo calculations for binary liquid mixtures."
In: *Mol. Phys.* 23.1 (1972), pp. 41–58. ISSN: 0026-8976.
DOI: 10.1080/00268977200100031.

[144] A. Ben-Tal and A. Nemirovski.
"Robust solutions of uncertain linear programs."
In: *Operations Research Letters* 25.1 (1999), pp. 1–13. ISSN: 0167-6377.
DOI: 10.1016/S0167-6377(99)00016-4.

[145] A. Ben-Tal and A. Nemirovski. "Robust solutions of Linear Programming problems contaminated with uncertain data."
In: *Math. Program.* 88.3 (2000), pp. 411–424. ISSN: 0025-5610, 1436-4646.
DOI: 10.1007/PL00011380.

[146] M. C. Fu.
"Feature Article: Optimization for simulation: Theory vs. Practice."
In: *INFORMS Journal on Computing* 14.3 (2002), pp. 192–215.
ISSN: 1091-9856. DOI: 10.1287/ijoc.14.3.192.113.

[147] A. Ben-Tal, A. Goryashko, E. Guslitzer, and A. Nemirovski.
"Adjustable robust solutions of uncertain linear programs."
In: *Math. Program., Ser. A* 99.2 (2004), pp. 351–376.
ISSN: 0025-5610, 1436-4646. DOI: 10.1007/s10107-003-0454-y.

[148] Z. W. Salsburg, J. D. Jacobson, W. Fickett, and W. W. Wood. "Application of the Monte Carlo Method to the Lattice-Gas Model. I. Two-Dimensional Triangular Lattice." In: *J. Chem. Phys.* 30.1 (1959), pp. 65–72. ISSN: 0021-9606, 1089-7690. DOI: 10.1063/1.1729945.

[149] A. M. Ferrenberg and R. H. Swendsen. "New Monte Carlo technique for studying phase transitions." In: *Phys. Rev. Lett.* 61.23 (1988), pp. 2635–2638. DOI: 10.1103/PhysRevLett.61.2635.

[150] A. M. Ferrenberg and R. H. Swendsen. "Optimized Monte Carlo data analysis." In: *Phys. Rev. Lett.* 63.12 (1989), pp. 1195–1198. DOI: 10.1103/PhysRevLett.63.1195.

[151] J. Taylor. *Introduction to Error Analysis, the Study of Uncertainties in Physical Measurements, 2nd Edition*. Vol. 1. 1 vols. New York: University Science Books, 1997.

[152] A. J. García-Sáez, S. Chiantia, and P. Schwille. "Effect of Line Tension on the Lateral Organization of Lipid Membranes." In: *J. Biol. Chem.* 282.46 (2007), pp. 33537–33544. ISSN: 0021-9258, 1083-351X. DOI: 10.1074/jbc.M706162200.

[153] D. W. Lee, Y. Min, P. Dhar, A. Ramachandran, J. N. Israelachvili, and J. A. Zasadzinski. "Relating domain size distribution to line tension and molecular dipole density in model cytoplasmic myelin lipid monolayers." In: *PNAS* 108.23 (2011), pp. 9425–9430. ISSN: 0027-8424, 1091-6490. DOI: 10.1073/pnas.1106368108.

[154] B. L. Stottrup, A. M. Heussler, and T. A. Bibelnieks. "Determination of Line Tension in Lipid Monolayers by Fourier Analysis of Capillary Waves." In: *J. Phys. Chem. B* 111.38 (2007), pp. 11091–11094. ISSN: 1520-6106. DOI: 10.1021/jp074898r.

[155] C. Esposito, A. Tian, S. Melamed, C. Johnson, S.-Y. Tee, and T. Baumgart. "Flicker Spectroscopy of Thermal Lipid Bilayer Domain Boundary Fluctuations." In: *Biophys. J.* 93.9 (2007), pp. 3169–3181. ISSN: 0006-3495. DOI: 10.1529/biophysj.107.111922.

[156] R. E. Scott, R. G. Perkins, M. A. Zschunke, B. J. Hoerl, and P. B. Maercklein. "Plasma membrane vesiculation in 3T3 and SV3T3 cells. I. Morphological and biochemical characterization." In: *J. Cell Sci.* 35.1 (1979), pp. 229–243. ISSN: 0021-9533, 1477-9137.

[157] E. K. Fridriksson, P. A. Shipkova, E. D. Sheets, D. Holowka, B. Baird, and F. W. McLafferty. "Quantitative Analysis of Phospholipids in Functionally Important Membrane Domains from RBL-2H3 Mast Cells Using Tandem High-Resolution Mass Spectrometry." In: *Biochemistry* 38.25 (1999), pp. 8056–8063. ISSN: 0006-2960. DOI: 10.1021/bi9828324.

[158] I. Levental, D. Lingwood, M. Grzybek, Ü. Coskun, and K. Simons. "Palmitoylation regulates raft affinity for the majority of integral raft proteins." In: *PNAS* 107.51 (2010), pp. 22050–22054. ISSN: 0027-8424, 1091-6490. DOI: 10.1073/pnas.1016184107.

[159] T. Baumgart, A. T. Hammond, P. Sengupta, S. T. Hess, D. A. Holowka, B. A. Baird, and W. W. Webb. "Large-scale fluid/fluid phase separation of proteins and lipids in giant plasma membrane vesicles." In: *PNAS* 104.9 (2007), pp. 3165–3170. ISSN: 0027-8424, 1091-6490. DOI: 10.1073/pnas.0611357104.

[160] H.-J. Kaiser, D. Lingwood, I. Levental, J. L. Sampaio, L. Kalvodova, L. Rajendran, and K. Simons. "Order of lipid phases in model and plasma membranes." In: *PNAS* 106.39 (2009), pp. 16645–16650. ISSN: 0027-8424, 1091-6490. DOI: 10.1073/pnas.0908987106.

[161] H. Shogomori, A. T. Hammond, A. G. Ostermeyer-Fay, D. J. Barr, G. W. Feigenson, E. London, and D. A. Brown. "Palmitoylation and Intracellular Domain Interactions Both Contribute to Raft Targeting of Linker for Activation of T Cells." In: *J. Biol. Chem.* 280.19 (2005), pp. 18931–18942. ISSN: 0021-9258, 1083-351X. DOI: 10.1074/jbc.M500247200.

[162] N. Kahya, D. A. Brown, and P. Schwille. "Raft Partitioning and Dynamic Behavior of Human Placental Alkaline Phosphatase in Giant Unilamellar Vesicles." In: *Biochemistry* 44.20 (2005), pp. 7479–7489. ISSN: 0006-2960. DOI: 10.1021/bi047429d.

[163] K. Bacia, C. G. Schuette, N. Kahya, R. Jahn, and P. Schwille. "SNAREs Prefer Liquid-disordered over 'Raft' (Liquid-ordered) Domains When Reconstituted into Giant Unilamellar Vesicles." In: *J. Biol. Chem.* 279.36 (2004), pp. 37951–37955. ISSN: 0021-9258, 1083-351X. DOI: 10.1074/jbc.M407020200.

[164] A. Ben-Shaul, L. Szleifer, and W. M. Gelbart. "Molecular Theory for Amphiphile Packing and Elastic Properties of Monolayers and Bilayers." In: *Physics of Amphiphilic Layers*. Ed. by D. J. Meunier, D. D. Langevin, and P. N. Boccara. Springer Proceedings in Physics 21. Springer Berlin Heidelberg, 1987, pp. 2–8. ISBN: 978-3-642-83204-8, 978-3-642-83202-4.

[165] B. Kollmitzer, P. Heftberger, M. Rappolt, G. Khelashvili, D. Harries, and G. Pabst. "Protein Partitioning in Liquid-Ordered (LO) / Liquid-Disordered (LD) Domains Depends on Lipid Composition and Protein Shape." In: *Biophys. J.* 106.2 (2014), 510a. ISSN: 0006-3495. DOI: 10.1016/j.bpj.2013.11.2853.

[166] A. Ben-Shaul. "Molecular theory of chain packing, elasticity and lipid-protein interaction in lipid bilayers." In: *Handbook of biological physics*. Ed. by R. Lipowsky and E. Sackmann. Vol. 1. North-Holland, 1995, pp. 359–401.

[167] J. Seddon and R. Templer. "Polymorphism of lipid-water systems." In: *Handbook of biological physics*. Ed. by R. Lipowsky and E. Sackmann. Vol. 1. North-Holland, 1995, pp. 97–160. ISBN: 1383-8121.

[168] F. Jahnig. "What is the surface tension of a lipid bilayer membrane?" In: *Biophys. J.* 71.3 (1996), pp. 1348–1349. ISSN: 0006-3495.

[169] R. S. Cantor. "Lateral pressures in cell membranes: a mechanism for modulation of protein function." In: *J. Phys. Chem. B* 101.10 (1997), pp. 1723–1725.

[170] M. Rappolt, A. Hickel, F. Bringezu, and K. Lohner. "Mechanism of the lamellar/inverse hexagonal phase transition examined by high resolution x-ray diffraction." In: *Biophys. J.* 84.5 (2003), pp. 3111–3122.

[171] F. A. Heberle. *X-ray Measurements on POPC/DOPC/DSPC/Chol*. E-mail. 2013.

[172] S. L. Goh, J. J. Amazon, and G. W. Feigenson.
"Toward a Better Raft Model: Modulated Phases in the Four-Component Bilayer, DSPC/DOPC/POPC/CHOL."
In: *Biophys. J.* 104.4 (2013), pp. 853–862. ISSN: 00063495.
DOI: 10.1016/j.bpj.2013.01.003.

[173] G. Khelashvili, B. Kollmitzer, P. Heftberger, G. Pabst, and D. Harries.
"Calculating the Bending Modulus for Multicomponent Lipid Membranes in Different Thermodynamic Phases."
In: *J. Chem. Theory Comput.* 9.9 (2013), pp. 3866–3871. ISSN: 1549-9618.
DOI: 10.1021/ct400492e.

[174] H. M. Berman, J. Westbrook, Z. Feng, G. Gilliland, T. N. Bhat, H. Weissig, I. N. Shindyalov, and P. E. Bourne.
"The Protein Data Bank." In: *Nucl. Acids Res.* 28.1 (2000), pp. 235–242.
ISSN: 0305-1048, 1362-4962. DOI: 10.1093/nar/28.1.235.

[175] N. Johner, D. Harries, and G. Khelashvili.
"Curvature and Lipid Packing Modulate the Elastic Properties of Lipid Assemblies: Comparing HII and Lamellar Phases."
In: *J. Phys. Chem. Lett.* 5.23 (2014), pp. 4201–4206. ISSN: 1948-7185.
DOI: 10.1021/jz5022284.

[176] B. L. L. E. Gauthé, A. J. Heron, J. M. Seddon, O. Ces, and R. H. Templer. "A high pressure cell for simultaneous osmotic pressure and x-ray diffraction measurements."
In: *Rev. Sci. Instrum.* 80.3 (2009), p. 035107. ISSN: 0034-6748, 1089-7623.
DOI: 10.1063/1.3089826.

Soft Matter

RSC Publishing

PAPER

Monolayer spontaneous curvature of raft-forming membrane lipids†

Cite this: *Soft Matter*, 2013, **9**, 10877

Benjamin Kollmitzer,[a] Peter Heftberger,[a] Michael Rappolt[bc] and Georg Pabst*[a]

Monolayer spontaneous curvatures for cholesterol, DOPE, POPE, DOPC, DPPC, DSPC, POPC, SOPC, and egg sphingomyelin were obtained using small-angle X-ray scattering (SAXS) on inverted hexagonal phases (H_{II}). Spontaneous curvatures of bilayer forming lipids were estimated by adding controlled amounts to a H_{II} forming template following previously established protocols. Spontaneous curvatures of both phosphatidylethanolamines and cholesterol were found to be at least a factor of two more negative than those of phosphatidylcholines, whose J_0 values are closer to zero. Interestingly, a significant positive J_0 value was retrieved for DPPC. We further determined the temperature dependence of the spontaneous curvatures $J_0(T)$ in the range from 15 to 55 °C, resulting in a quite narrow distribution of -1 to -3×10^{-3} (nm °C)$^{-1}$ for most investigated lipids. The data allowed us to estimate the monolayer spontaneous curvatures of ternary lipid mixtures showing liquid ordered/liquid disordered phase coexistence. We report spontaneous curvature phase diagrams for DSPC/DOPC/Chol, DPPC/DOPC/Chol and SM/POPC/Chol and discuss effects on protein insertion and line tension.

Received 4th July 2013
Accepted 24th September 2013

DOI: 10.1039/c3sm51829a

www.rsc.org/softmatter

1 Introduction

Curvature is an essential ingredient in a cell's life and occurs most visibly during membrane fusion and fission processes, *e.g.* exocytosis and endocytosis, or when a cell is attacked by an enveloped virus.[1] Such events may be induced by proteins, but are also known to depend strongly on the molecular properties of the constituent membrane lipids.[2] For instance membrane fusion can take place in the absence of proteins.[3] Lipid-driven membrane curvature may result *e.g.* from unequally distributed lipids of the same type in the opposing membrane leaflets or from asymmetric distributions of lipids with different molecular shapes due to their different intrinsic curvatures.[4–9]

In general, lipids with molecular shapes different from cylinders will form monolayers that either curve away or towards the polar/apolar interface.[10] In planar membranes, however, such monolayers are forced into a flat topology, where they lie back-to-back – in order to avoid energetically unfavorable voids – leading to significant curvature elastic stress that is stored within the membrane. This elastic stress may have several functional consequences for membranes and can be viewed as a hidden dimension of membrane curvature. Of particular interest is the role of intrinsic/spontaneous curvature in coupling to protein function[11–18] and in determining the line tension of lipid domains mimicking membrane rafts.[19,20]

As per definition the spontaneous curvature $J_0 = 0$ for cylindrically formed lipids, $J_0 < 0$ for lipids with tail regions of bigger lateral cross-section than the headgroups and *vice versa* for $J_0 > 0$. For example, lipids with a negative spontaneous curvature are prone to form non-planar structures like inverted hexagonal phases H_{II}. More precisely the radius of curvature of an unstressed monolayer at its neutral plane equals $1/J_0$.[21,22] The neutral plane is defined as the position at which bending and stretching modes are decoupled, *i.e.* bending and stretching deformations proceed independently from each other.[23] A second, frequently quoted surface within the monolayer of amphiphiles is the pivotal plane, which occurs where the molecular area does not change upon deformation. Pioneered by the groups of Rand and Gruner during the late 80s and the 90s, the position of this surface and consequently the spontaneous curvature at the pivotal plane J_{0p} have been determined to high accuracy for a couple of membrane lipids,[21,24–30] for review see ref. 31. The basic idea of these experiments is to use H_{II} phases, where the lipid monolayers expose their intrinsic curvature within the individual rods and to determine the pivotal plane by bending and compressing the rods either by gravimetric dehydration or application of osmotic pressure, while measuring the crystalline lattice *via* X-ray scattering. For a limited number of lipids the neutral plane has been estimated from the pivotal surface using area compressibility and bending rigidity data.[21,23,32]

In the present work we determine J_0 under stress-free conditions by locating the neutral plane from electron density

[a]*Institute of Molecular Biosciences, Biophysics Division, University of Graz, Austria. E-mail: Georg.Pabst@uni-graz.at; Fax: +43 316 4120-390; Tel: +43 316 4120-342*

[b]*Institute of Inorganic Chemistry, Graz University of Technology, Austria*

[c]*School of Food Science and Nutrition, University of Leeds, UK*

† Electronic supplementary information (ESI) available: Electron density maps, tieline parameterization, line tension calculations, miscibilities, and temperature dependence of spontaneous curvature. See DOI: 10.1039/c3sm51829a

maps of H_{II} phases. In particular we focus on spontaneous curvature data of lipids which are involved in the formation of membrane rafts. Such data are especially of need for calculating protein partitioning in diverse lipid environments[11–18] or to estimate the line-tension of lipid domains.[19,20] Additionally, the temperature dependence of spontaneous curvature is still barely investigated. We intend to bridge this gap by determining J_0 for cholesterol, DOPC, DPPC, DSPC, POPC, SOPC and egg sphingomyelin within a DOPE matrix from 15 to 55 °C and for POPE at 37 and 55 °C.

2 Materials and methods

2.1 Sample preparation

Cholesterol (Chol), 1,2-dioleoyl-*sn-glycero*-3-phosphocholine (DOPC), 1,2-dioleoyl-*sn-glycero*-3-phosphoethanolamine (DOPE), 1,2-dipalmitoyl-*sn-glycero*-3-phosphocholine (DPPC), 1,2-distearoyl-*sn-glycero*-3-phosphocholine (DSPC), 1-palmitoyl-2-oleoyl-*sn-glycero*-3-phosphocholine (POPC), 1-stearoyl-2-oleoyl-*sn-glycero*-3-phosphocholine (SOPC), and chicken egg sphingomyelin (eggSM) were purchased from Avanti Polar Lipids, Inc., Alabaster, AL, USA and used without further purification. 9-*cis*-Tricosene was obtained from Sigma-Aldrich, Austria.

After weighing, lipids were dissolved in chloroform–methanol 2 : 1 at a concentration of 10 mg ml^{-1}. These lipid stock solutions were mixed in glass vials, 12 wt% tricosene was added and the organic solvent was evaporated under a gentle nitrogen stream. To remove the remaining solvent, the samples were placed in a vacuum overnight. 18 MΩ cm^{-1} water (UHQ PS, USF Elga, Wycombe, UK) was added to 20 μl mg^{-1} lipid and the mixtures with repeated freeze–thaw cycles fully hydrated. The samples were then protected against oxidation with argon, the vials closed and taped, and stored at 4 °C for 6–7 days until the measurement.

2.2 X-ray measurements

Small-angle X-ray scattering (SAXS) was performed at the Austrian SAXS beamline at ELETTRA, Trieste.[33,34] A mar300 Image Plate 2D detector from Marresearch, Norderstedt, Germany was used covering a q-range from 0.2–6.1 nm^{-1} and calibrated with silver-behenate ($CH_3(CH_2)_{20}COOAg$) with a d-spacing of 5.838 nm.[35] Sample temperatures were controlled with a bath thermostat from Huber, Offenburg, Germany to a precision of ±0.1 °C. The samples were equilibrated for 10 min at given temperatures before exposure. The exposure time was set to 30 s.

2.3 X-ray data analysis

Image integration was performed with FIT2D[36,37] and cross-checked with MATLAB®.[38] For further data analysis, homemade MATLAB scripts were used and their function verified with FIT2D,[39] IDL®,[40] and IGOR Pro®.[41]

Standard procedures were used to determine the lattice parameters and calculate electron-density maps of the H_{II} (for further details, see S1 of the ESI†). In brief, we applied Lorentzians and additive linear background estimators to fit the Bragg peaks. Typically 5–7 peaks were discernible in the patterns, although for higher temperatures and some samples only three or four peaks could be detected. This was considered in the uncertainty estimations.

The lattice parameter a was determined *via* the reflection law, taking into account the information from all Lorentzians. Fourier synthesis yielded the electron density $\rho(\vec{r})$ in real-space, with the phasing condition (+ − − + + + + −) known from the literature for DOPE-rich, fully hydrated H_{II} phases.[42–44] Other phase combinations were tested, but yielded electron densities incompatible with the known structure.

2.4 Spontaneous curvature estimation

2.4.1 Finding the neutral plane. Instead of bending and compressing lipid monolayers with osmotic pressures to determine the position $R_0 = 1/J_0$ of the neutral plane,[21] we applied the following procedure, assuming that the neutral plane coincides with the glycerol backbone of phospholipids. This assumption is supported by bending/compression experiments, which always found the pivotal plane to be close to the glycerol backbone of lipid molecules, but slightly within the hydrocarbon region,[21,24–30,44,45] while the neutral plane was estimated to be closer to the backbone.[21,32] The proximity of both surfaces to the backbone can be rationalized by the high rigidity in this region.[22] In general, the positions of the neutral and pivotal planes differ by less than 10% and can even coincide when monolayers are bent in the absence of compression.[21,22]

We first locate the position R_p of the lipid headgroup by fitting a Gaussian to a radial section of the electron density map in a region of ∼1 nm around the maximum value (see S1 in the ESI† for further details). Then, the neutral surface is simply given by $R_0 = R_p + d_{H1}$, where d_{H1} is the distance between the headgroup and the glycerol backbone. Using a joint refinement of X-ray and neutron data on lamellar phases, Kučerka and coworkers reported high-resolution structural data for a series of phospholipids.[46–49] The reported d_{H1} values range between 0.37 and 0.50 nm at temperatures from 20 to 50 °C. We apply the average of these values for our R_0 calculations $d_{H1} = (0.44 \pm 0.05)$ nm. To test the applicability of this procedure, we compare $J_0 = (-0.387 \pm 0.011)$ nm^{-1} retrieved from the present analysis for DOPE at 25 °C with $J_0 = (-0.367 \pm 0.010)$ nm^{-1} estimated from measurements of the pivotal surface.[21] A small difference is expected due to the presence of tricosene in the present experiments in order to reduce packing frustration (see Section 2.4.2) as compared to the measurements performed by Leikin *et al.*[21]

We also attempted to derive J_0 from the width σ_p of the Gaussian fitted to the headgroup region of the radial electron density profiles, *i.e.* $R_0 = R_p + \sigma_p$. However, the resolution of the electron density maps was too poor for some lipid mixtures, yielding $\sigma_p > 0.7$ nm and hence unrealistic locations of the glycerol backbone.

2.4.2 Relaxation of hexagonal packing frustration. Stress free monolayers, which are necessary for measuring the monolayer spontaneous curvature J_0, are usually obtained by adding free alkanes or alkenes to inverted hexagonal phases

H_{II}.[26,30,50,51] By taking up the interstitial spaces, they can reduce the frustration of packing circular objects in a hexagonal manner. This effect is impressively seen for POPE, which forms in the absence of any additive a H_{II} phase only above 74 °C.[52] Addition of tricosene reduced the frustration to such an amount that already at 37 °C the H_{II} phase was preferred. The total tricosene content of all our samples was 12 wt%. The value was obtained from a test series of varying tricosene concentrations and is close to the 10 wt% used in ref. 45.

2.4.3 Spontaneous curvature of bilayer-forming lipids. Because monolayer J_0 is not accessible in bilayers due to symmetry constraints, bilayer-forming lipids have to be incorporated into other structures, see Fig. 1. Usually H_{II} phases (we use the H_{II} forming lipid DOPE) are used as templates by mixing the lipid of interest ("guest") with a H_{II}-forming "host" lipid.[17,26,29,45,53] As long as both lipids mix well, the guest lipid can be expected to modify the curvature of the mixture linearly with respect to its concentration χ[54–57]

$$J_0^{\mathrm{mix}} = \chi J_0^{\mathrm{guest}} + (1-\chi) J_0^{\mathrm{host}}, \quad (1)$$

and extrapolation towards 100% gives the spontaneous curvature of the guest lipid.[21] A more sophisticated description of spontaneous curvature calculations for lipid mixtures has been reported.[58] However, the experimental determination of several model parameters in this theory remains unclear and experiments seem to contradict with these calculations.[59]

All bilayer-forming lipids were measured at concentrations of 10, 20, 30, 40 and 50 mol% in DOPE. The extrapolation according to eqn (1) was performed using all concentrations below a critical value χ_{crit}, at which:

- immiscibility was directly observed because non-hexagonal Bragg peaks were visible,
- eqn (1) did not obviously hold anymore, or
- the lattice parameter a did not change smoothly with χ.

Entropic contributions get more pronounced at higher temperatures, which generally leads to improved miscibilities. Accordingly, we observed a monotonic increase of χ_{crit} with T for all samples. An example of the occurrence of non-hexagonal peaks is given in Fig. 2.

Good miscibility was observed for Chol and all unsaturated lipids. For saturated lipids χ_{crit} was not equally satisfactory, but improved above the melting transition of the guest lipid with the exception of eggSM, where only 10 mol% could be incorporated into the DOPE matrix at all temperatures. The number of useful data points (where $\chi < \chi_{\mathrm{crit}}$) is taken into account for determining the uncertainty of the resulting J_0. Extrapolation plots and $\chi_{\mathrm{crit}}(T)$ for all lipids are reported in S4 of the ESI.†

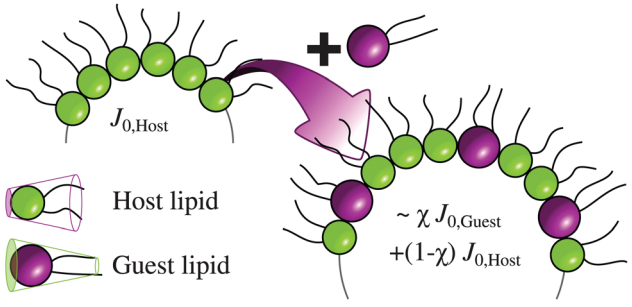

Fig. 1 Guest lipid is incorporated at a concentration χ within the host's template phase. Note the change of the curvature upon mixing.

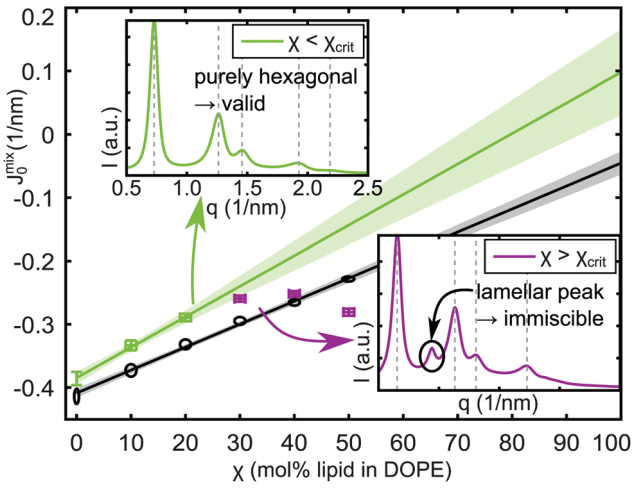

Fig. 2 Determination of J_0^{DPPC} at 25 °C (crosses) and J_0^{POPC} at 45 °C (ellipses) by extrapolation of J_0^{mix} towards $\chi = 100\%$. The insets show X-ray patterns for the last valid (top left) and the first immiscible DPPC data points (bottom right).

2.4.4 Temperature dependence. We performed synchrotron SAXS measurements at 10 °C intervals from 15–55 °C for all lipids except POPE to quantify the spontaneous curvature's temperature dependence $J_0(T)$. The results could be well described within experimental errors by a straight line

$$J_0(T) = k(T - T_{\mathrm{m}}) + J_0^{\mathrm{m}} \quad (2)$$

$$\Delta J_0(T) = \sqrt{(\Delta k)^2 (T - T^{\mathrm{m}})^2 + \left(\Delta J_0^{\mathrm{m}}\right)^2}, \quad (3)$$

where we introduced a mean temperature $T^{\mathrm{m}} = 35$ °C, the coefficient of thermal curvature change k, and J_0^{m} the spontaneous curvature at T^{m}, while ΔX denotes the uncertainty of the quantity X. POPE was measured at 37 and 55 °C. Note that POPE forms a H_{II} phase at these temperatures only in the presence of an agent such as tricosene that relaxes the packing frustration. Fits of $J_0(T)$ in comparison to literature data are plotted in S5 of the ESI.†

3 Results

Chol, DOPC, DPPC, DSPC, POPC, SOPC and eggSM were mixed with DOPE and measured as detailed in the previous section. The pure lipids' monolayer spontaneous curvatures for each temperature were obtained by eqn (1) (data in S4 of the ESI†). Linear fits of the temperature dependence of J_0 yielded the values listed in Table 1 (fits in S5 of the ESI†). By inserting these parameters in eqn (2) and (3), J_0 and its uncertainty are readily available for any temperature from 15 to 55 °C.

POPE was measured with 12 wt% tricosene and excess water at 37 and 55 °C in the absence of DOPE. The slope and offset of a straight line through the two points following eqn (2) with $T^{\mathrm{m}} =$ 37 °C are given in Table 1.

Table 1 Parameters describing $J_0(T)$ according to eqn (2) and (3) with $T^m = 35$ °C, except (*) where $T^m = 37$ °C

Lipid	$J_0{}^m \pm \Delta J_0{}^m$ (1 nm)	$k \pm \Delta k$ (10^{-3}/nm °C)
DOPE	−0.399 ± 0.005	−1.3 ± 0.4
POPE (*)	−0.316 ± 0.007	−2.7 ± 0.7
Chol	−0.494 ± 0.013	−3.5 ± 0.9
DOPC	−0.091 ± 0.008	−1.1 ± 0.6
DPPC	+0.068 ± 0.032	−3.5 ± 2.3
DSPC	−0.100 ± 0.044	−0.2 ± 3.4
POPC	−0.022 ± 0.010	−1.8 ± 0.7
SOPC	−0.010 ± 0.018	−2.2 ± 1.3
eggSM	−0.134 ± 0.072	+1.4 ± 5.1

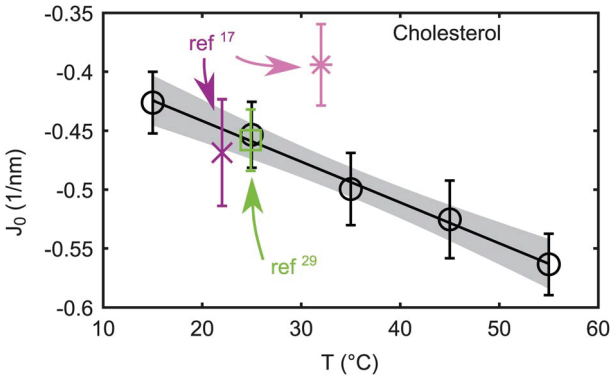

Fig. 3 Comparison between cholesterol spontaneous curvature from the literature (ref. 17 and 29) and new data (circles). The straight line corresponds to linear fit. Literature data at 32 °C have been determined in a DOPC host matrix, and the other two in DOPE.

Fig. 3 compares our results for cholesterol with literature data.‡ Although it seems like the literature data has a positive slope of $J_0(T)$, this is probably a coincidence and due to the uncorrelated experiments in different lipid host systems. Generally, one would expect the chains to be more flexible and therefore also occupy more space at higher temperature, corresponding to a more negative spontaneous curvature. This behavior corresponds to $k < 0$, which is the case for all lipids except for eggSM. This is most likely an artifact due to the limited miscibility of eggSM with DOPE. The limited miscibility also affected other saturated lipids leading to significant experimental uncertainties in k. The overall k varied in a quite narrow window from -1 to -3.5×10^{-3} (nm °C)$^{-1}$, *cf.* Table 1, in good agreement with $k = (-1.7 \pm 0.3) \times 10^{-3}$ (nm °C)$^{-1}$, reported for DOPE at temperatures from 15 to 30 °C.[27]

Interestingly, DPPC is the only bilayer-forming lipid with a significant positive J_0. DSPC, for example, with the same headgroup but longer chains has $J_0 = -0.1$ nm^{-1} at 35 °C. Thus, the headgroup contribution to the molecular shape dominates the cross-sectional area and hence J_0 of DPPC, whereas chain contributions dominate in the case of DSPC. Mismatch in lateral areas of heads and chains is known to cause chain tilt and the ripple phase for saturated phosphatidylcholines in a certain range of chain lengths.[60] Surprisingly, $J_0 \sim -0.1$ nm^{-1} also for eggSM, which similar to PCs has a choline moiety in the headgroup and is predominantly composed of the same hydrocarbons as DPPC. Here the sphingosine backbone of eggSM seems to make the difference by taking up more lateral space than the glycerol backbone of PCs. A detailed investigation of this effect is, however, beyond the scope of the present work.

‡ Reported values for J_{0p}[17,29] were rescaled to J_0 using $J_0 \sim J_{0p}(1+\beta)$, with $\beta = 0.065 \pm 0.035$ determined in ref. 21. Data reported by Boulgaropoulos *et al.*[17] were additionally corrected from $J_{0p} = -0.38$ nm^{-1} to -0.43 nm^{-1} prior to the scaling due to a flaw in their data analysis.

4 Discussion

4.1 Monolayer spontaneous curvature of phase separated systems

For known compositions, monolayer spontaneous curvatures of mixtures are readily computable by generalization of eqn (1) to more components, resulting in

$$J_0{}^{mix} = \sum_i \chi_i J_0{}^{(i)}. \quad (4)$$

As already mentioned, miscibility is required for the linear additivity of spontaneous curvatures. We assume that this criterion is fulfilled within individual domains of a phase separated system, *i.e.* non-ideal mixing is not considered. Thus if the compositions of coexisting phases are known, eqn (4) can be applied to determine their spontaneous curvatures. In the case of non-ideal mixing, which may occur for example by a preferred location of lipids at the domain boundary, energetic contributions from lipid–lipid interactions and mixing entropies need to be considered (see *e.g.* ref. 58). However, this is beyond the scope of the present paper.

Compositional phase diagrams including tielines have been published recently for ternary lipid mixtures exhibiting liquid disordered (L_d)/liquid ordered (L_o) phase coexistences.[61–63] These mixtures are simple lipid-only models for membrane rafts, complex platforms which are thought to enable cellular communication and material transport.[64] We parameterized the proposed coexistence regions and tieline fields according to the method introduced by Smith and Freed[65] and slightly modified by Heberle *et al.*,[62] whose notation we adopted. Briefly, a given phase coexistence region is approximated *via* a Bézier curve of degree five, while a single variable takes care of the tieline fanning. The parameter $u \in [0, 1]$ identifies a particular tieline, with the critical point (tieline of length 0) at $u = 0$ and the tieline farthest away from the critical point at $u = 1$. More details on this parameterization and the explicit values can be found in S2 of the ESI.†

Fig. 4 compares the spontaneous curvatures for coexisting L_o/L_d phases. The mixture POPC/eggSM/Chol behaves as expected, *i.e.* due to the negative intrinsic curvature of cholesterol, the L_o phase, which contains about twice as much cholesterol as L_d domains, exhibits a more negative J_0. Also DOPC/DSPC/Chol shows a similar behaviour, although the measurement uncertainty limits a clear distinction of the spontaneous curvatures of L_o and L_d. For DOPC/DPPC/Chol,

however, J_0 of the liquid ordered phase at high values of u is less negative than for the L_d phase, and within the measurement uncertainty it could even be slightly positive. This results from a more positive J_0 of DPPC as compared to DSPC with $J_0 \sim -0.1$ nm^{-1} (Table 1). We note that the quantitative difference between monolayer spontaneous curvatures of L_o and L_d depends on the exact location of the coexistence region and the tieline orientation, which both contain some uncertainties.

It is instructive to consider the effects of these J_0 differences on the insertion probability of simple membrane proteins. Barrel-like transmembrane proteins, which have a thicker cross-section at the center of the bilayer than near the bilayer-water interface, would generally prefer phases with positive spontaneous curvatures, where the effective lipid cross-section at the tail region is smaller than for the headgroup (Fig. 5). In the DOPC/DPPC/Chol case, this simple argument would mean that the L_o phase is more attractive for such proteins. However, a lower-order expansion of the lateral pressure profile already reveals a dependence of protein partitioning on further elastic parameters, specifically bending elasticities and Gaussian curvature moduli of L_o and L_d.[11,12] The literature suggests furthermore hydrophobic mismatch[66] and disturbance of lipid packing[67,68] as important factors for determining protein-insertion energies in membranes. The treatment of these effects is beyond the scope of the present work.

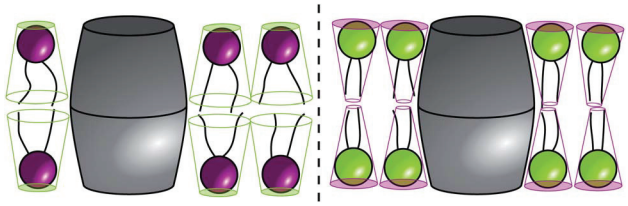

Fig. 5 Barrel shaped transmembrane protein within a bilayer composed of lipids with negative (left) and positive (right) monolayer spontaneous curvatures. For the latter scenario, the protein shape reduces the packing frustration within the bilayer.

4.2 Line tension calculation

Another parameter that is affected by J_0 is the line tension γ between two coexisting phases, which influences the size and shape of domains.[69,70] Theory predicts an elastic contribution to γ by the monolayer bending moduli, tilt moduli, and thickness difference of L_o/L_d domains (γ_{el}) and a second term γ_{J_0}, which includes contributions from the spontaneous curvatures.[19] In the following paragraphs, we give results for the line tension of ternary and quaternary lipid mixtures and discuss the effect of J_0. Calculation details, lipid compositions of L_o and L_d phases, as well as elastic parameters are given in S3 of the ESI.† It is important to note that Helfrich's definition of spontaneous curvature,[71] which has been applied for deriving γ_{J_0} in ref. 19, differs from the quantity J_0 which we determine in the present work. However, in the case of linear bending behavior, or for small deviations from a flat monolayer, *i.e.* if the spontaneous curvature is much smaller than the inverse monolayer thickness h, the two values are approximately equal.[22] In S3 of the ESI,† we show that indeed $|J_0| < 1/h$ for the following calculations.

Just recently, bending and tilt moduli, as well as structural parameters, have been determined with molecular dynamics

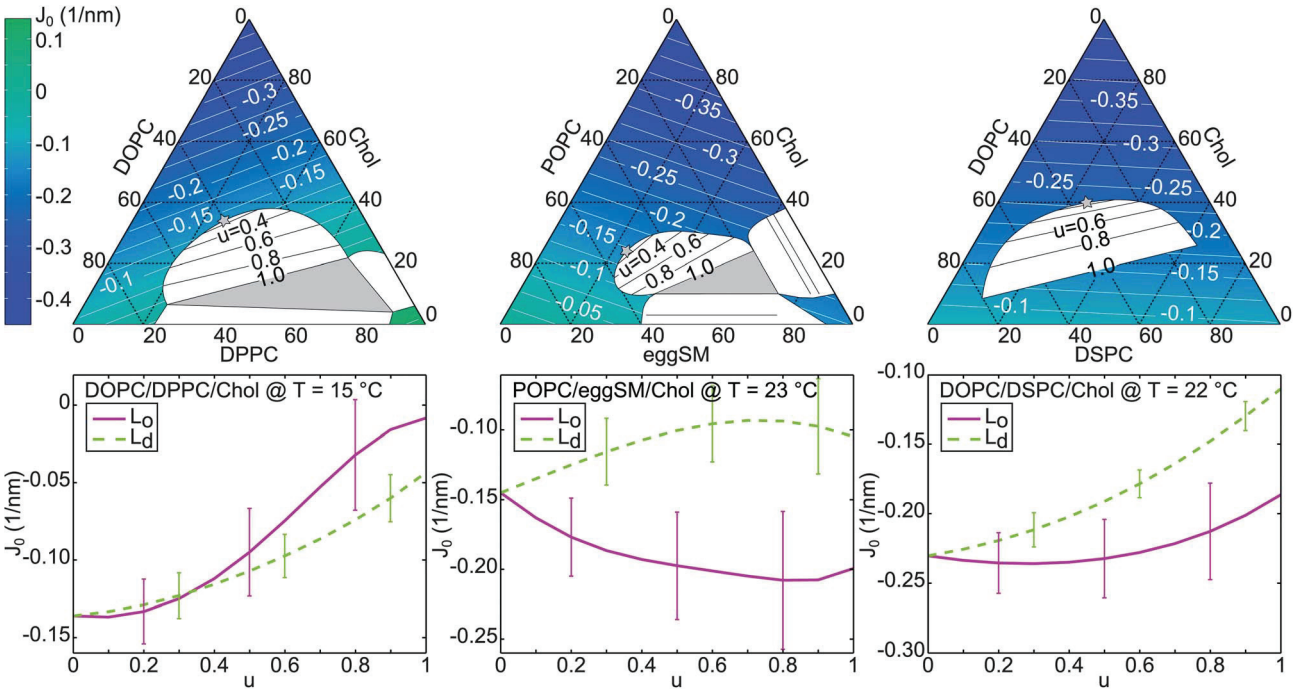

Fig. 4 Spontaneous curvature J_0 (white contours and false-color) for three ternary mixtures within the phase diagrams taken from ref. 61–63. White segments are two-phase coexistence regions with tielines, gray triangles are three-phase coexistence regions, and gray stars are critical points (top row). The spontaneous curvature J_0 is plotted for coexisting L_o/L_d phases along the boundary of the fluid–fluid phase coexistence regime (bottom row) parameterized by u (see text).

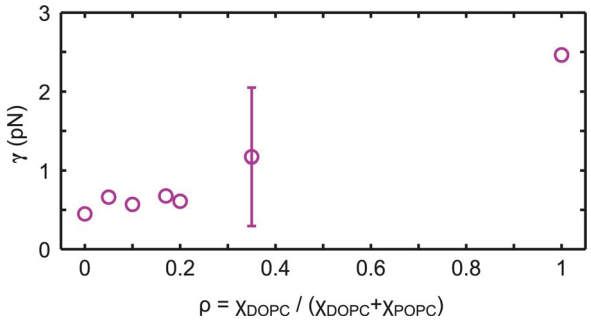

Fig. 6 Calculated line tension γ between L_o and L_d domains in DOPC/POPC/DSPC/Chol. Uncertainties of all data points are comparable.

(MD) simulations supported by SAXS, for two ternary mixtures showing L_o/L_d phase separation.[72] By combining this information with our new curvature data, we calculate $\gamma = 1.4$ pN for DOPC/DPPC/Chol and $\gamma = 1.6$ pN for DOPC/DSPC/Chol at given L_o/L_d compositions. These values are in the typical range reported from either experiment or theory (see, *e.g.* ref. 73–76). Because of the positive curvature of DPPC, J_0 values for both phases of DOPC/DPPC/Chol are close to zero, leading to vanishing contributions of γ_{J_0} to the line tension. For DOPC/DSPC/Chol, however, the L_o and L_d phases feature a negative J_0, leading to $\gamma_{J_0} = -1.8$ pN, *i.e.* the line tension between the coexisting domains is decreased due to the contribution of J_0.

The same theory has been applied to rationalize the transition from nanoscopic to microscopic domains, recently reported for the quaternary mixture DOPC/POPC/DSPC/Chol.[77] Starting from nanometer sized domains in POPC/DSPC/Chol, replacing POPC with DOPC has lead to increasing domain sizes, and finally to domains in the micrometer regime for DOPC/DSPC/Chol. Parameterized by the ratio $\rho = \chi_{DOPC}/(\chi_{DOPC} + \chi_{POPC})$, the original calculation of the line tension has explained this behavior; but apart from information on the bilayer thickness only estimated values for the parameters influencing γ were available. By applying bending and tilt moduli from MD simulations,[72] spontaneous curvatures from the current work, and structural information from Heberle *et al.*,[77] we were able to calculate the line tension for $\rho = 1$ and give improved estimations for $\rho < 1$ (Fig. 6). Because of compositional differences for L_o/L_d domains between experiments and MD simulations, the present calculations still rely on considerable assumptions for $\rho < 1$. In general, the change of nanoscopic to microscopic domains is accompanied by an increase of line tension. This agrees well with our results of $\gamma \sim 0.5$ pN for the nanoscopic regime, $\gamma \sim 2.5$ pN for the microscopic regime, and intermediate in between. The contribution of spontaneous curvature to γ stays nearly constant for all compositions, meaning that the transition from nanoscopic to microscopic domains is mainly driven by bilayer thickness differences in this case, in agreement with the conclusions of the original report.[77]

5 Conclusions

By evaluating synchrotron SAXS data of DOPE-rich lipid mixtures in the H_{II} phase, we were able to estimate monolayer spontaneous curvatures J_0 for several biologically relevant phospholipids, cholesterol and egg sphingomyelin at temperatures ranging from 15 to 55 °C. Within experimental accuracy, our results are in good agreement with values from more in-depth studies by other groups, conducted at room temperature on DOPE, DOPC, and cholesterol.

Our measurements extend the J_0-list of lipid species and add their temperature dependence.[31] These data will be useful for numerous applications in membrane biophysics.

In the present work we discuss three examples: (i) the monolayer spontaneous curvatures of raft-like lipid mixtures, (ii) line tension of L_o/L_d phases and (iii) evaluation of the line tension during a transition from nanoscopic to microscopic domains. For the studied mixtures of POPC/eggSM/Chol and DOPC/DSPC/Chol, J_0 of the L_o phase was found to be more negative than that of the coexisting L_d phase. DOPC/DPPC/Chol however shows a contrary behavior, with a more positively curved liquid ordered phase due to the positive J_0 of DPPC. This would favor partitioning of barrel-shaped proteins into the L_o phase. Regarding line tension, we found only significant contributions of J_0 for coexisting domains in DOPC/DSPC/Chol. In DOPC/DPPC/Chol and also for the transition from nanoscopic to microscopic domains, γ seems to be dominated by elastic moduli and thickness differences.

Acknowledgements

This work is supported by the Austrian Science Fund FWF, Project no. P24459-B20. The authors thank Karl Lohner, George Khelashvili, Siewert-Jan Marrink, and Ilya Levental for valuable discussions and in particular Daniel Harries for pointing us at the literature explaining delicate differences in spontaneous curvatures.

References

1 K. N. Burger, *Traffic*, 2000, **1**, 605–613.
2 L. V. Chernomordik and M. M. Kozlov, *Nat. Struct. Mol. Biol.*, 2008, **15**, 675–683.
3 L. K. Tamm, J. Crane and V. Kiessling, *Curr. Opin. Struct. Biol.*, 2003, **13**, 453–466.
4 M. P. Sheetz and S. J. Singer, *Proc. Natl. Acad. Sci. U. S. A.*, 1974, **71**, 4457–4461.
5 E. Evans, *Biophys. J.*, 1974, **14**, 923–931.
6 S. Svetina, A. Ottova-Leitmannová and R. Glaser, *J. Theor. Biol.*, 1982, **94**, 13–23.
7 S. Svetina and B. Žekš, *Eur. Biophys. J.*, 1989, **17**, 101–111.
8 B. Bozic, S. Svetina, B. Zeks and R. E. Waugh, *Biophys. J.*, 1992, **61**, 963–973.
9 L. Miao, U. Seifert, M. Wortis and H.-G. Döbereiner, *Phys. Rev. E: Stat. Phys., Plasmas, Fluids, Relat. Interdiscip. Top.*, 1994, **49**, 5389–5407.
10 J. Seddon and R. Templer, *Handbook of biological physics*, North-Holland, 1995, vol. 1, pp. 97–160.
11 R. S. Cantor, *J. Phys. Chem. B*, 1997, **101**, 1723–1725.
12 R. S. Cantor, *Chem. Phys. Lipids*, 1999, **101**, 45–56.
13 S. A. Safran, *J. Stat. Phys.*, 1995, **78**, 1175–1177.

14 R. Brewster and S. A. Safran, *Biophys. J.*, 2010, **98**, L21–L23.
15 J. A. Lundbæk, P. Birn, J. Girshman, A. J. Hansen and O. S. Andersen, *Biochemistry*, 1996, **35**, 3825–3830.
16 D. Marsh, *Biophys. J.*, 2007, **93**, 3884–3899.
17 B. Boulgaropoulos, M. Rappolt, B. Sartori, H. Amenitsch and G. Pabst, *Biophys. J.*, 2012, **102**, 2031–2038.
18 G. Pabst, B. Boulgaropoulos, E. Gander, B. R. Sarangi, H. Amenitsch, V. A. Raghunathan and P. Laggner, *J. Membr. Biol.*, 2009, **231**, 125–132.
19 P. I. Kuzmin, S. A. Akimov, Y. A. Chizmadzhev, J. Zimmerberg and F. S. Cohen, *Biophys. J.*, 2005, **88**, 1120–1133.
20 S. A. Akimov, P. I. Kuzmin, J. Zimmerberg and F. S. Cohen, *Phys. Rev. E: Stat., Nonlinear, Soft Matter Phys.*, 2007, **75**, 011919.
21 S. Leikin, M. M. Kozlov, N. L. Fuller and R. P. Rand, *Biophys. J.*, 1996, **71**, 2623–2632.
22 M. M. Kozlov, *Methods in Membrane Lipids*, Springer, 2007, pp. 355–366.
23 M. M. Kozlov and M. Winterhalter, *J. Phys. II*, 1991, **1**, 1077–1084.
24 S. M. Gruner, V. A. Parsegian and R. P. Rand, *Faraday Discuss.*, 1986, **81**, 29–37.
25 M. W. Tate and S. M. Gruner, *Biochemistry*, 1989, **28**, 4245–4253.
26 R. P. Rand, N. L. Fuller, S. M. Gruner and V. A. Parsegian, *Biochemistry*, 1990, **29**, 76–87.
27 M. M. Kozlov, S. Leikin and R. P. Rand, *Biophys. J.*, 1994, **67**, 1603–1611.
28 R. P. Rand and N. L. Fuller, *Biophys. J.*, 1994, **66**, 2127–2138.
29 Z. Chen and R. P. Rand, *Biophys. J.*, 1997, **73**, 267–276.
30 Z. Chen and R. P. Rand, *Biophys. J.*, 1998, **74**, 944–952.
31 J. Zimmerberg and M. M. Kozlov, *Nat. Rev. Mol. Cell Biol.*, 2005, **7**, 9–19.
32 M. M. Kozlov and M. Winterhalter, *J. Phys. II*, 1991, **1**, 1085–1100.
33 H. Amenitsch, M. Rappolt, M. Kriechbaum, H. Mio, P. Laggner and S. Bernstorff, *J. Synchrotron Radiat.*, 1998, **5**, 506–508.
34 S. Bernstorff, H. Amenitsch and P. Laggner, *J. Synchrotron Radiat.*, 1998, **5**, 1215–1221.
35 T. C. Huang, H. Toraya, T. N. Blanton and Y. Wu, *J. Appl. Crystallogr.*, 1993, **26**, 180–184.
36 A. P. Hammersley, *European Synchrotron Radiation Facility Internal Report ESRF97HA02T*, 1997.
37 A. P. Hammersley, S. O. Svensson, M. Hanfland, A. N. Fitch and D. Hausermann, *High Pressure Res.*, 1996, **14**, 235–248.
38 MATLAB v. 7.12 (R2011a), 2011.
39 A. P. Hammersley and C. Riekel, *Syn. Rad. News*, 1989, **2**, 24–26.
40 IDL (Interactive Data Language) v. 6.1.
41 IGOR Pro v. 6.2.2.2, 2011.
42 D. C. Turner and S. M. Gruner, *Biochemistry*, 1992, **31**, 1340–1355.
43 P. E. Harper, D. A. Mannock, R. N. Lewis, R. N. McElhaney and S. M. Gruner, *Biophys. J.*, 2001, **81**, 2693–2706.
44 M. Rappolt, A. Hodzic, B. Sartori, M. Ollivon and P. Laggner, *Chem. Phys. Lipids*, 2008, **154**, 46–55.
45 S. H. Alley, O. Ces, M. Barahona and R. H. Templer, *Chem. Phys. Lipids*, 2008, **154**, 64–67.
46 N. Kučerka, S. Tristram-Nagle and J. F. Nagle, *Biophys. J.*, 2006, **90**, L83–L85.
47 N. Kučerka, S. Tristram-Nagle and J. F. Nagle, *J. Membr. Biol.*, 2006, **208**, 193–202.
48 N. Kučerka, J. F. Nagle, J. N. Sachs, S. E. Feller, J. Pencer, A. Jackson and J. Katsaras, *Biophys. J.*, 2008, **95**, 2356–2367.
49 N. Kučerka, M.-P. Nieh and J. Katsaras, *Biochim. Biophys. Acta, Biomembr.*, 2011, **1808**, 2761–2771.
50 G. L. Kirk and S. M. Gruner, *J. Phys.*, 1985, **46**, 761–769.
51 H. Vacklin, B. J. Khoo, K. H. Madan, J. M. Seddon and R. H. Templer, *Langmuir*, 2000, **16**, 4741–4748.
52 M. Rappolt, A. Hickel, F. Bringezu and K. Lohner, *Biophys. J.*, 2003, **84**, 3111–3122.
53 E. E. Kooijman, V. Chupin, N. L. Fuller, M. M. Kozlov, B. de Kruijff, K. N. J. Burger and R. P. Rand, *Biochemistry*, 2005, **44**, 2097–2102.
54 S. A. Safran, P. Pincus and D. Andelman, *Science*, 1990, **248**, 354–356.
55 M. M. Kozlov and W. Helfrich, *Langmuir*, 1992, **8**, 2792–2797.
56 S. L. Keller, S. M. Bezrukov, S. M. Gruner, M. W. Tate, I. Vodyanoy and V. A. Parsegian, *Biophys. J.*, 1993, **65**, 23–27.
57 G. Khelashvili, D. Harries and H. Weinstein, *Biophys. J.*, 2009, **97**, 1626–1635.
58 S. May and A. Ben-Shaul, *J. Chem. Phys.*, 1995, **103**, 3839.
59 M. Gradzielski, D. Langevin, T. Sottmann and R. Strey, *J. Chem. Phys.*, 1997, **106**, 8232–8238.
60 R. Koynova and M. Caffrey, *Biochim. Biophys. Acta, Rev. Biomembr.*, 1998, **1376**, 91–145.
61 P. Uppamoochikkal, S. Tristram-Nagle and J. F. Nagle, *Langmuir*, 2010, **26**, 17363–17368.
62 F. A. Heberle, J. Wu, S. L. Goh, R. S. Petruzielo and G. W. Feigenson, *Biophys. J.*, 2010, **99**, 3309–3318.
63 I. V. Ionova, V. A. Livshits and D. Marsh, *Biophys. J.*, 2012, **102**, 1856–1865.
64 D. Lingwood and K. Simons, *Science*, 2010, **327**, 46–50.
65 A. K. Smith and J. H. Freed, *J. Phys. Chem. B*, 2009, **113**, 3957–3971.
66 A. Ben-Shaul, *Handbook of biological physics*, North-Holland, 1995, vol. 1, pp. 359–401.
67 L. V. Schäfer, D. H. de Jong, A. Holt, A. J. Rzepiela, A. H. de Vries, B. Poolman, J. A. Killian and S. J. Marrink, *Proc. Natl. Acad. Sci. U. S. A.*, 2011, **108**, 1343–1348.
68 J. Domański, S. J. Marrink and L. V. Schäfer, *Biochim. Biophys. Acta, Biomembr.*, 2012, **1818**, 984–994.
69 A. J. García-Sáez, S. Chiantia and P. Schwille, *J. Biol. Chem.*, 2007, **282**, 33537–33544.
70 D. W. Lee, Y. Min, P. Dhar, A. Ramachandran, J. N. Israelachvili and J. A. Zasadzinski, *Proc. Natl. Acad. Sci. U. S. A.*, 2011, **108**, 9425–9430.
71 W. Helfrich, *Z. Naturforsch., C: J. Biosci.*, 1973, 693–703.
72 G. Khelashvili, B. Kollmitzer, P. Heftberger, G. Pabst and D. Harries, *J. Chem. Theory Comput.*, 2013, **9**, 3866–3871.

73 H. J. Risselada and S. J. Marrink, *Proc. Natl. Acad. Sci. U. S. A.*, 2008, **105**, 17367–17372.
74 A. Tian, C. Johnson, W. Wang and T. Baumgart, *Phys. Rev. Lett.*, 2007, **98**, 208102.
75 C. Esposito, A. Tian, S. Melamed, C. Johnson, S.-Y. Tee and T. Baumgart, *Biophys. J.*, 2007, **93**, 3169–3181.
76 A. R. Honerkamp-Smith, P. Cicuta, M. D. Collins, S. L. Veatch, M. den Nijs, M. Schick and S. L. Keller, *Biophys. J.*, 2008, **95**, 236–246.
77 F. A. Heberle, R. S. Petruzielo, J. Pan, P. Drazba, N. Kučerka, R. F. Standaert, G. W. Feigenson and J. Katsaras, *J. Am. Chem. Soc.*, 2013, **135**, 6853–6859.

Supplementary Material for: Monolayer Spontaneous Curvature of Raft-Forming Membrane Lipids

Benjamin Kollmitzer, Peter Heftberger, Michael Rappolt, and Georg Pabst

September 23, 2013, Graz

S1 Electron density calculation

All recognizable peaks of the intensity $I(q)$ were individually fitted using least-squares plus a linear background estimator, yielding peak intensities $I_{h,k}$ and positions $q_{h,k}$. The (1,1) and (2,0) peaks are close and were fitted together with a common linear background (Fig. S1).

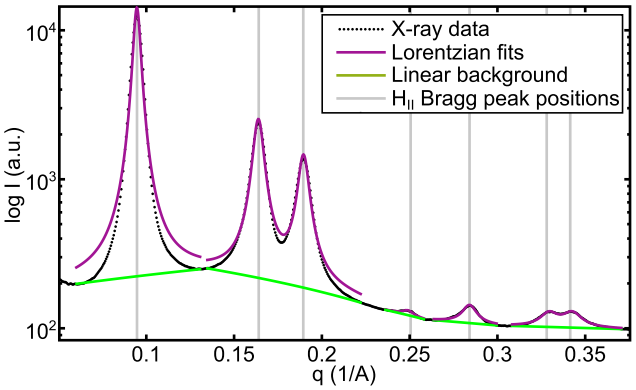

Figure S1: Analysis of DOPE at 35 °C.

We followed the procedure described by Rappolt *et al.* [1] for calculating electron maps. The lattice parameter a was determined via the reflection law $\sqrt{3}\,a\,q_{h,k}/4\pi = 1,\sqrt{3},2,\sqrt{7},\ldots$. Fourier synthesis yielded the electron density in real-space

$$\rho(\vec{r}) = \sum_{h,k} \alpha_{h,k} \sqrt{\frac{I_{h,k}\,q_{h,k}^2}{m_{h,k}}} \cdot \cos\left(2\pi\,\vec{q}_{h,k}\cdot\vec{r}\right), \tag{S1}$$

where multiplication of the intensity with $q_{h,k}^2$ is known as Lorentz correction [2], $m_{h,k}$ is the multiplicity of the equivalent diffraction planes (6 for $(1,0),(1,1),(3,0)\ldots$; 12 for $(2,1),(3,1),(3,2)\ldots$)

and $\alpha_{h,k}$ is the phase (± 1 for centrosymmetric structures as in this work). Literature[3–5] suggests $(+--++++-)$ as phasing condition for DOPE-rich, fully hydrated H_{II} phases. Figure S2 gives an example for a calculated electron density map. Other phase combinations were tested, but yielded electron densities incompatible with the known structure.

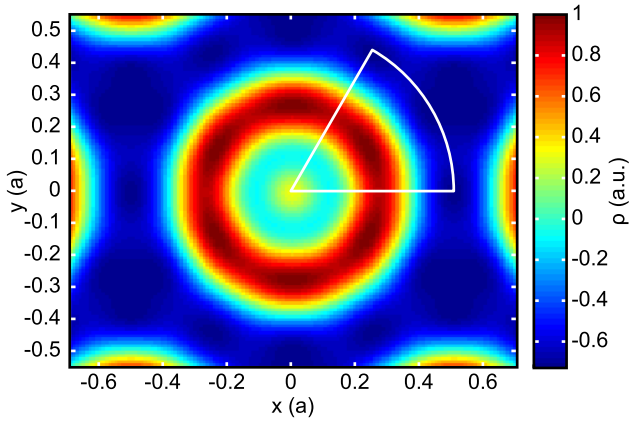

Figure S2: 2D electron density map $\rho(x,y)$ for DOPE at 35 °C. The white circular segment indicates the region, where the radial cross sections of ρ are evaluated for the location of the pivotal plane. Coordinates are normalized by the unit cell parameter a.

A Gaussian fit to the radial cross section of the electron density yielded position R_p and width σ_p of the headgroup (Fig. S3). We averaged these quantities over azimuthal angles ranging from 0° (x-axis) to 60°, as indicated by the circular segment in Fig. S2.

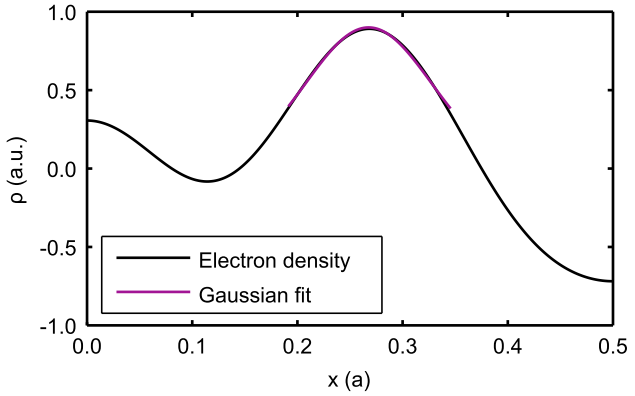

Figure S3: Radial cross section of the electron density from Fig. S2 along the x-axis with Gaussian fit for the headgroup region.

S2 Tieline parameterization

For parameterizing coexistence regions and tieline fields, we applied the method described in[6,7]. Ternary phase diagram coordinates (x,y,z) with $x+y+z=1$ and $\{x,y,z\} \in [0,1]$ are transformed into a two-dimensional vector $\vec{\Psi} = (\xi, \eta)$ with components $\xi = z\sqrt{3}/2$ and $\eta = y + z/2$. Bézier curves

$$\vec{B}(t) = \sum_{l=0}^{n} \binom{n}{l} (1-t)^{n-l} t^l \vec{P}_l \tag{S2}$$

of degree $n = 5$ were reported to describe phase boundaries well in the (ξ, η)-space. To relate these curves to the tieline fields, Smith and coworkers[6] introduced the relationships

$$t_{Lo}(u) = \tau_c + (1-\tau_c)\, u \tag{S3}$$

$$t_{Ld}(u) = \tau_c - \frac{\tau_c\, u}{u + c\,(1-u)}, \tag{S4}$$

where τ_c characterizes the critical point and c takes care of tieline fanning. Equations (S3) and (S4) allow to express the tieline endpoint compositions in 2D as $\vec{\Psi}_{Lo}(u) = \vec{B}(t_{Lo}(u))$ and $\vec{\Psi}_{Ld}(u) = \vec{B}(t_{Ld}(u))$, where $\vec{\Psi}_{Lo}(0) = \vec{\Psi}_{Ld}(0)$ describes the critical point.

We determined the 6 control points $\{\vec{P}_l\}$ from a least squares fit of the Bézier curves to the boundary coordinates of previously published compositional phase diagrams[7–9]. The fitting was performed with the MATLAB® function `grad7.m` listed in[10]. Having determined the control points, we calculated τ_c, by minimizing the distance from the critical point to $\vec{B}(\tau_c)$. Analogously, the auxiliary points $\{\tau_{Lo,i}, \tau_{Ld,i}\}$ were computed by minimizing the distance from $\vec{B}(\tau_{Lo/d,i})$ to the intersection of the i-th tieline with the phase boundary on the L_o/L_d side. The parameter c describing the tieline fanning was calculated by solving

$$c = \frac{(\tau_{Lo,i} - \tau_c)\, \tau_{Ld,i}}{(\tau_{Ld,i} - \tau_c)\, (\tau_{Lo,i} - 1)} \tag{S5}$$

in the least squares sense. Equation (S5) follows directly from eliminating u in Eqs. (S3) and (S4). The resulting parameters describing the reported tielines from[7–9] are listed in Tab. S1.

S3 Line tension calculations

Based on elastic deformations of monolayers, Kuzmin *et al.*[11] derived an expression for the line tension γ between two coexisting phases L_o and L_d

$$\gamma = \frac{1}{Z}\sqrt{B_d K_d B_o K_o}\,\frac{\delta^2}{h_0^2} - \frac{1}{2Z}\left(J_{0,d} B_d - J_{0,o} B_o\right)^2, \tag{S6}$$

with $Z = \sqrt{B_d K_d} + \sqrt{B_o K_o}$, monolayer bending moduli B, tilt moduli K, monolayer spontaneous curvatures J_0, and structural parameters $\delta = h_o - h_d$ and $h_0 = (h_o + h_d)/2$ relating the positions h of the monolayer neutral planes. We refer to the first term of Eq. (S6) as elastic γ_{el} and to the second as curvature contribution γ_{J0} to the line tension. It was already pointed out in 4.2, that

Table S1: Parameters describing the tieline fields of published phase diagrams.

	DOPC/DPPC/Chol[§]	POPC/eggSM/Chol[¶]	DOPC/DSPC/Chol[‖]
$\vec{P}_0$	(0.268, 0.568)	(0.438, 0.087)	(0.155, 0.074)
$\vec{P}_1$	(0.204, 0.174)	(0.112, 0.029)	(0.176, 0.265)
$\vec{P}_2$	(0.361, 0.252)	(0.531, 0.510)	(0.300, 0.380)
$\vec{P}_3$	(0.603, 0.554)	(0.468, 0.126)	(0.624, 0.365)
$\vec{P}_4$	(0.778, 0.196)	(0.671, 0.320)	(0.646, 0.391)
$\vec{P}_5$	(0.780, 0.189)	(0.718, 0.208)	(0.764, 0.224)
τ_c	0.429	0.297	0.506
c	1.115	0.832	1.000

[§] Phase diagram from[8]
[¶] Phase diagram from[9]
[‖] Values taken from[7], fits yielded similar results

these relations hold for $|J_0|$ much smaller than $1/h$. In the following examples, we therefore verify that $|J_0| \cdot h < 1$.

We calculate the spontaneous curvatures $J_{0,d}$ and $J_{0,o}$ according to Eq. (4) using known compositions of L_o and L_d. The moduli in Eq. (S6) are effective moduli of the domains and normalized by cross-sectional area. Per-lipid tilt moduli κ_j reported in[14] were taken, normalized by the lipid areas and averaged over the corresponding phase. Averaging was achieved by defining for each phase an average lipid, of volume $\bar{V} = \sum_j \chi_j V_j$ and area $\bar{A} = \bar{V}/h$, where V_j is the volume of constituent lipid j and h the monolayer thickness of a given domain. We further assumed that the effective tilt modulus can be expressed as $K = \sum_j \chi_j \kappa_j / \bar{A}$.

Lipid volumes needed in this section are available in the literature:[12,13]

	DOPC	POPC	DPPC	DSPC	Chol
V (nm^3)	1.30	1.26	1.23	1.35	0.63

Example 1: Ternary mixtures

All parameters used for calculations are listed in Tab. S2. The magnitude of the spontaneous curvature J_0 is at least by a factor of 2 smaller than the monolayer thickness, meaning that the use of Eq. (S6) is justified. The resulting line tensions obtained by Eq. (S6) are reported in Tab. S3.

Example 2: Varying domain sizes

For the quaternary mixture DOPC/POPC/DSPC/Chol, a similar calculation has already been used to rationalize the domain size behavior as a function of $\rho = \chi_{DOPC}/(\chi_{DOPC} + \chi_{POPC})$.[15] It was found, that the nanoscopic domains in POPC/DSPC/Chol grew bigger by replacing POPC with DOPC, until finally microscopic domains for DOPC/DSPC/Chol were detected. We repeat

Table S2: Compositions χ, temperatures T, and elastic and structural parameters for Example 1.

	DOPC/DPPC/Chol		DOPC/DSPC/Chol	
	L_d	L_o	L_d	L_o
$\chi_1 : \chi_2 : \chi_3$	0.66:0.19:0.15	0.12:0.58:0.30	0.74:0.09:0.17	0.12:0.56:0.32
T (°C)	15	15	22	22
B (kT) *	17±2	49±3	15±1	53±4
κ_1 (kT) *	11±1	34±3	9±1	44±3
κ_2 (kT) *	14±1	53±3	10±1	60±4
κ_3 (kT) *	15±1	48±3	15±2	49±2
h (nm) *,†	1.5	1.8	1.5	2.0
$\bar{V}$ (nm^3)	1.2	1.1	1.2	1.1
$\bar{A}$ (nm^2)	0.77	0.58	0.80	0.57
K (kT nm^{-2})	15	85	13	97
J_0 (nm^{-1})	-0.08	-0.05	-0.14	-0.21
$\lvert J_0 \rvert \cdot h$	0.13	0.22	0.10	0.42

* Taken from [14]

† Although the thickness was not reported explicitly, it was used in the SAXS evaluation of [14]

Table S3: Resulting line tensions γ, and elastic γ_{el} and curvature contributions γ_{J0} for Example 1.

	DOPC/DPPC/Chol	DOPC/DSPC/Chol
γ_{el} (pN)	1.4	3.4
γ_{J0} (pN)	0.0	-1.8
γ (pN)	1.4	1.6

Table S4: Bilayer thickness t and spontaneous curvature J_0 for Example 2.

ρ (%)	0	5	10	17	20	35	100
t_{Ld} (nm) ‡	3.84	3.80	3.80	3.76	3.77	3.67	3.51
t_{Lo} (nm) ‡	4.48	4.48	4.48	4.46	4.46	4.46	4.48
$J_{0,Ld}$ (nm^{-1})	-0.06	-0.06	-0.06	-0.07	-0.07	-0.08	-0.12
$J_{0,Lo}$ (nm^{-1})	-0.16	-0.16	-0.17	-0.17	-0.17	-0.18	-0.19
$\lvert J_{0,Ld}\rvert \cdot h_{Ld}$	0.09	0.10	0.10	0.11	0.11	0.12	0.18
$\lvert J_{0,Lo}\rvert \cdot h_{Lo}$	0.30	0.31	0.32	0.32	0.33	0.34	0.38

‡ Taken from [15]

Table S5: Domain radii R and resulting line tensions γ with elastic γ_{el} and curvature contributions γ_{J0} for Example 2.

ρ (%)	0	5	10	17	20	35	100
R (nm) ‡	68	85	98	111	124	162	>225
γ_{el} (pN)	1.7	1.9	1.9	2.1	2.0	2.7	4.1
γ_{J0} (pN)	-0.6	-0.6	-0.6	-0.6	-0.6	-0.7	-0.7
γ (pN)	1.1	1.4	1.3	1.4	1.4	2	3.4

‡ Taken from [15]

that calculation, but with better determined values for bending moduli, tilt moduli and spontaneous curvature.

The compositions for DOPC/DSPC/Chol from Example 1 are similar to the compositions for $\rho = 1$. We use therefore these MD results [14] also for the current example. We further assume the per-lipid tilt moduli of POPC and DOPC to be equal. This means, that the results for $\rho = 1$ should be reliable, but become more imprecise with increasing POPC content. Bilayer thickness t informations are taken from [15]. To obtain the height of the neutral plane h, which should be close to the apolar/polar interface [16], we subtract 0.3 nm from the monolayer thickness. This value is a reasonable guess for the distance between the Luzzatti position and the apolar/polar interface.[12] The applied bilayer thicknesses and monolayer spontaneous curvatures are listed in Tab. S4. Equation (S6) yields with these values the line tensions given in Tab. S5. Results are shown in Fig. 6. The magnitude of the spontaneous curvature J_0 is at least by a factor of 2 smaller than the monolayer thickness, meaning that the use of Eq. (S6) is justified.

S4 Spontaneous curvature extrapolation

The dependence of $J_0^{mix}(T,\chi)$ on temperature T and concentration χ is given in Tabs. S6–S12 and plotted in Figs. S4–S10. In the figures, black crosses depict valid data points used for extrapolation, while green data points were not considered because there $\chi > \chi_{crit}$.

Table S6: Spontaneous curvature J_0^{mix} as function of temperature $T\,[^\circ\mathrm{C}]$ and concentration $\chi\,[\mathrm{mol}\%]$ Chol in DOPE. Numbers above χ_{crit} are untrustworthy

	10 mol%	20 mol%	30 mol%	40 mol%	50 mol%	$\chi_{crit}\,(mol\%)$
15 °C	−0.38	−0.39	−0.39	−0.39	−0.39	> 40
25 °C	−0.40	−0.40	−0.41	−0.41	−0.41	> 40
35 °C	−0.41	−0.42	−0.43	−0.44	−0.45	> 40
45 °C	−0.43	−0.44	−0.45	−0.46	−0.47	> 40
55 °C	−0.44	−0.45	−0.46	−0.48	−0.50	> 50

Table S7: Spontaneous curvature J_0^{mix} as function of temperature $T\,[^\circ\mathrm{C}]$ and concentration $\chi\,[\mathrm{mol}\%]$ DOPC in DOPE. Numbers above χ_{crit} and NaN are untrustworthy

	10 mol%	20 mol%	30 mol%	40 mol%	50 mol%	$\chi_{crit}\,(mol\%)$
15 °C	−0.34	−0.30	NaN	−0.24	−0.22	> 50
25 °C	−0.35	−0.31	NaN	−0.26	−0.23	> 50
35 °C	−0.36	−0.33	NaN	−0.27	−0.25	> 50
45 °C	−0.38	−0.34	NaN	−0.29	−0.26	> 50
55 °C	−0.39	−0.36	NaN	−0.30	−0.27	> 50

Table S8: Spontaneous curvature J_0^{mix} as function of temperature $T\,[^\circ\mathrm{C}]$ and concentration $\chi\,[\mathrm{mol}\%]$ DPPC in DOPE. Numbers above χ_{crit} are untrustworthy

	10 mol%	20 mol%	30 mol%	40 mol%	50 mol%	$\chi_{crit}\,(mol\%)$
15 °C	−0.32	−0.30	−0.31	−0.31	−0.33	> 10
25 °C	−0.33	−0.29	−0.26	−0.25	−0.28	> 20
35 °C	−0.35	−0.31	−0.27	−0.24	−0.41	> 20
45 °C	−0.37	−0.32	−0.28	−0.25	−0.24	> 30
55 °C	−0.39	−0.34	−0.30	−0.28	−0.25	> 30

Table S9: Spontaneous curvature J_0^{mix} as function of temperature $T\,[^\circ\mathrm{C}]$ and concentration $\chi\,[\mathrm{mol}\%]$ DSPC in DOPE. Numbers above χ_{crit} and NaN are untrustworthy

	10 mol%	20 mol%	30 mol%	40 mol%	50 mol%	$\chi_{crit}\,(mol\%)$
15 °C	−0.35	−0.35	−0.35	−0.35	NaN	> 10
25 °C	−0.35	−0.34	−0.35	−0.36	NaN	> 10
35 °C	−0.36	−0.34	−0.34	NaN	NaN	> 20
45 °C	−0.37	−0.35	−0.35	−0.37	NaN	> 20
55 °C	−0.39	−0.36	−0.34	−0.34	−0.27	> 20

Table S10: Spontaneous curvature J_0^{mix} as function of temperature $T\,[^\circ\mathrm{C}]$ and concentration $\chi\,[\mathrm{mol}\%]$ POPC in DOPE. Numbers above χ_{crit} and NaN are untrustworthy

	10 mol%	20 mol%	30 mol%	40 mol%	50 mol%	$\chi_{crit}\,(mol\%)$
15 °C	−0.33	−0.29	−0.25	−0.22	NaN	> 40
25 °C	−0.34	−0.31	−0.26	−0.24	NaN	> 40
35 °C	−0.36	−0.32	−0.28	−0.25	−0.22	> 40
45 °C	−0.37	−0.33	−0.29	−0.27	−0.23	> 50
55 °C	−0.38	−0.34	−0.30	−0.27	−0.24	> 50

Table S11: Spontaneous curvature J_0^{mix} as function of temperature $T\,[^\circ\mathrm{C}]$ and concentration $\chi\,[\mathrm{mol}\%]$ SOPC in DOPE. Numbers above χ_{crit} and NaN are untrustworthy

	10 mol%	20 mol%	30 mol%	40 mol%	50 mol%	$\chi_{crit}\,(mol\%)$
15 °C	−0.32	−0.28	−0.25	−0.22	−0.19	> 30
25 °C	−0.34	−0.30	−0.27	−0.23	NaN	> 30
35 °C	−0.35	−0.31	−0.28	−0.25	−0.22	> 30
45 °C	−0.37	−0.33	−0.30	−0.27	−0.22	> 30
55 °C	−0.39	−0.34	−0.31	−0.28	−0.24	> 30

Table S12: Spontaneous curvature J_0^{mix} as function of temperature $T\,[^\circ\mathrm{C}]$ and concentration $\chi\,[\mathrm{mol}\%]$ eggSM in DOPE. Numbers above χ_{crit} and NaN are untrustworthy

	10 mol%	20 mol%	30 mol%	40 mol%	50 mol%	$\chi_{crit}\,(mol\%)$
15 °C	−0.35	−0.28	−0.29	NaN	NaN	> 10
25 °C	−0.37	−0.35	−0.28	NaN	NaN	> 10
35 °C	−0.38	−0.36	−0.30	NaN	NaN	> 10
45 °C	−0.39	−0.38	−0.30	NaN	NaN	> 10
55 °C	−0.39	−0.39	−0.33	NaN	NaN	> 10

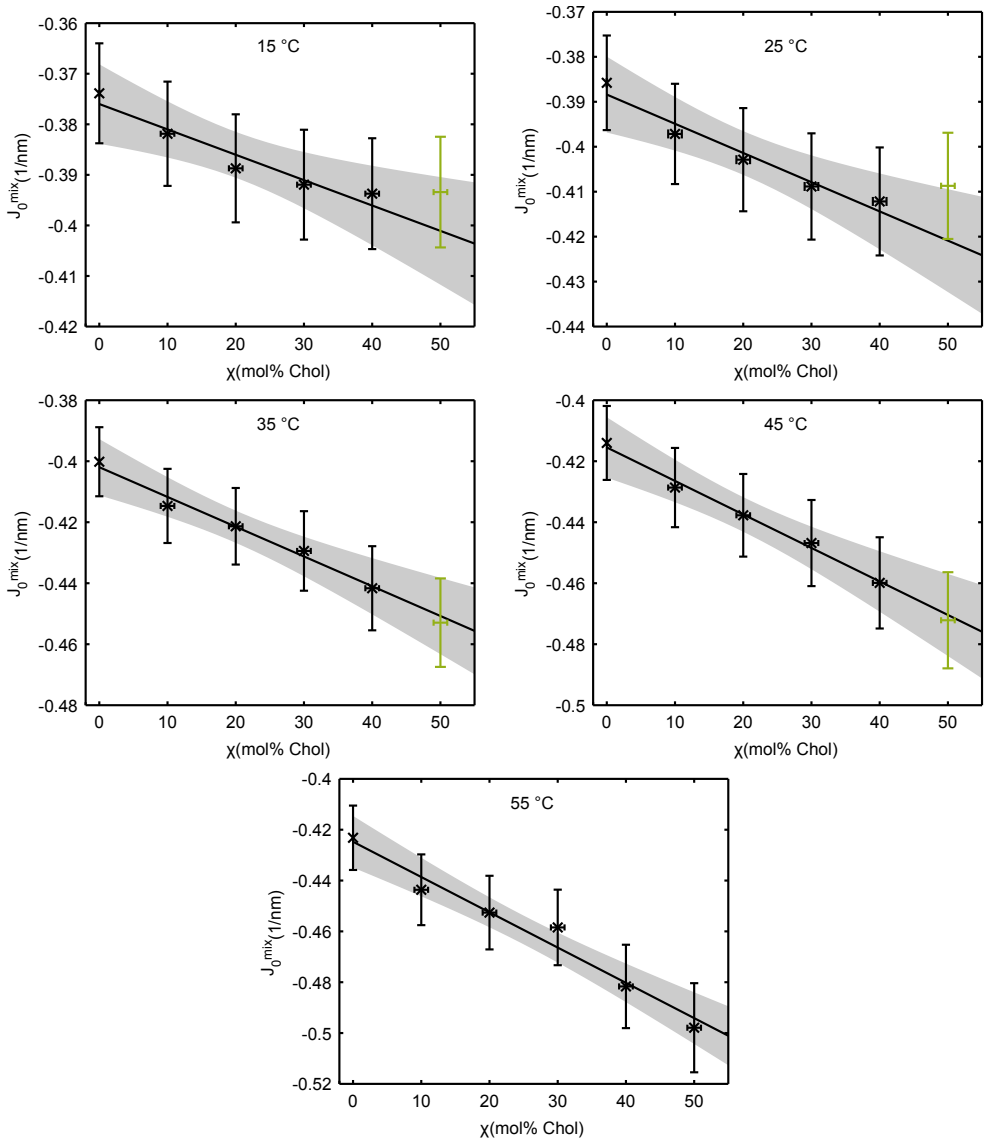

Figure S4: Determination of J_0 for Chol.

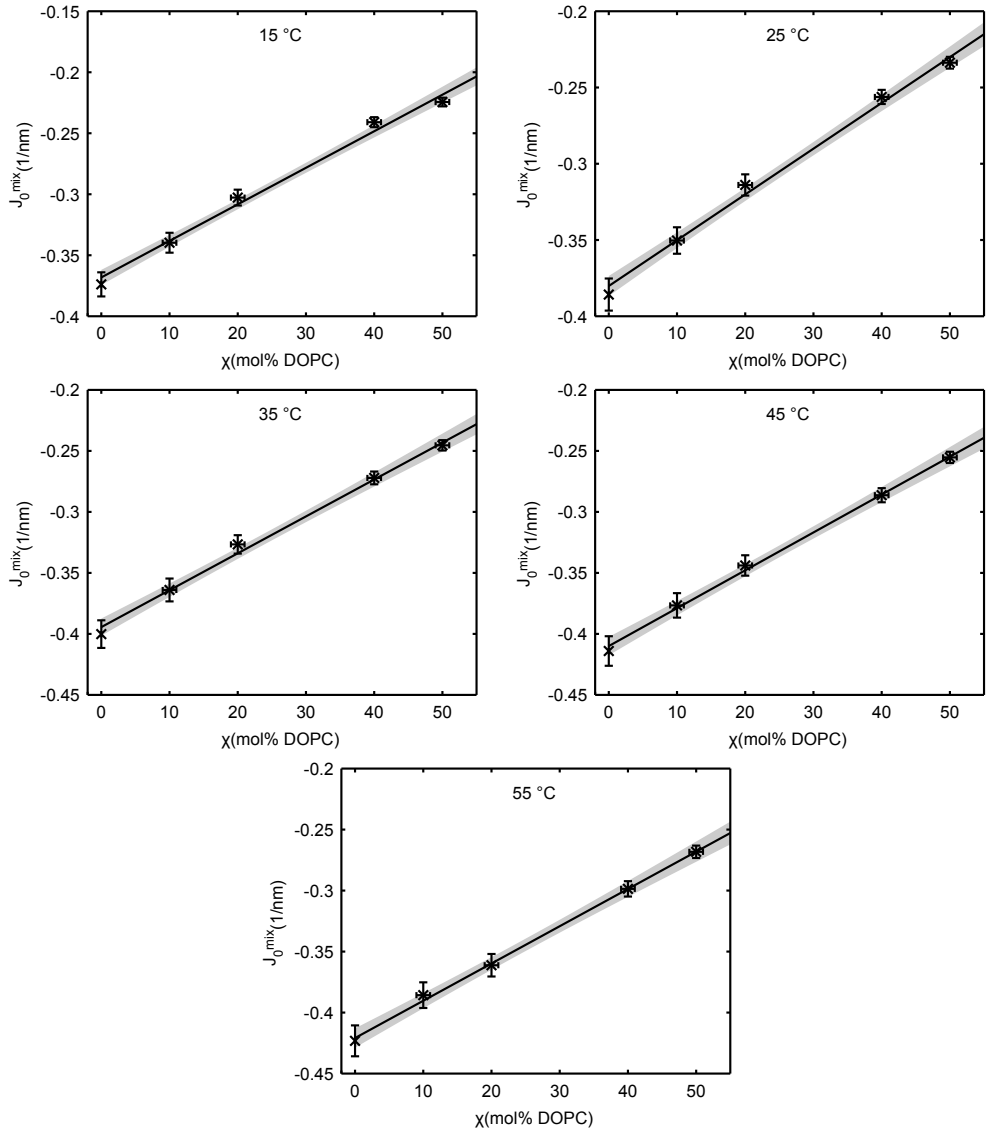

Figure S5: Determination of J_0 for DOPC.

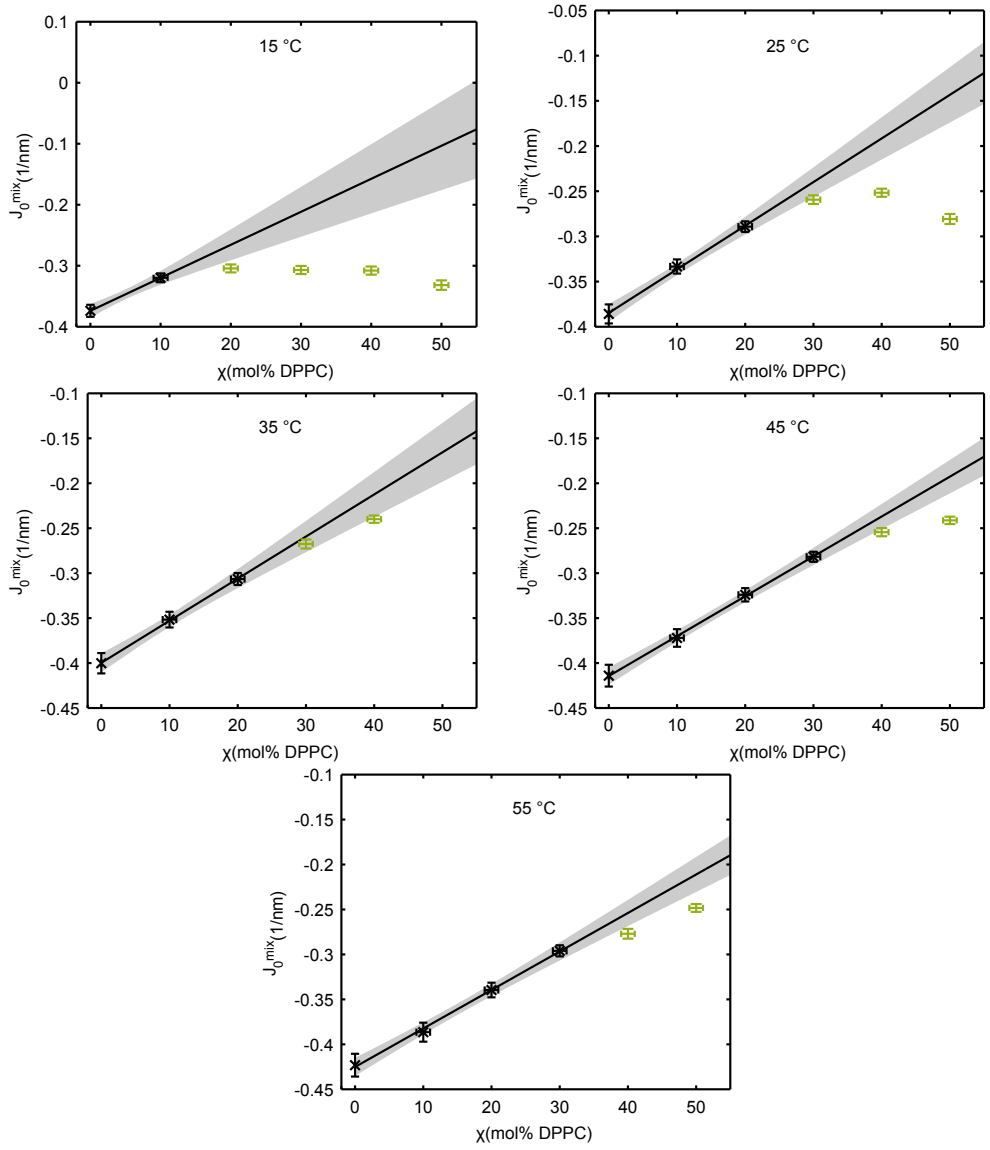

Figure S6: Determination of J_0 for DPPC.

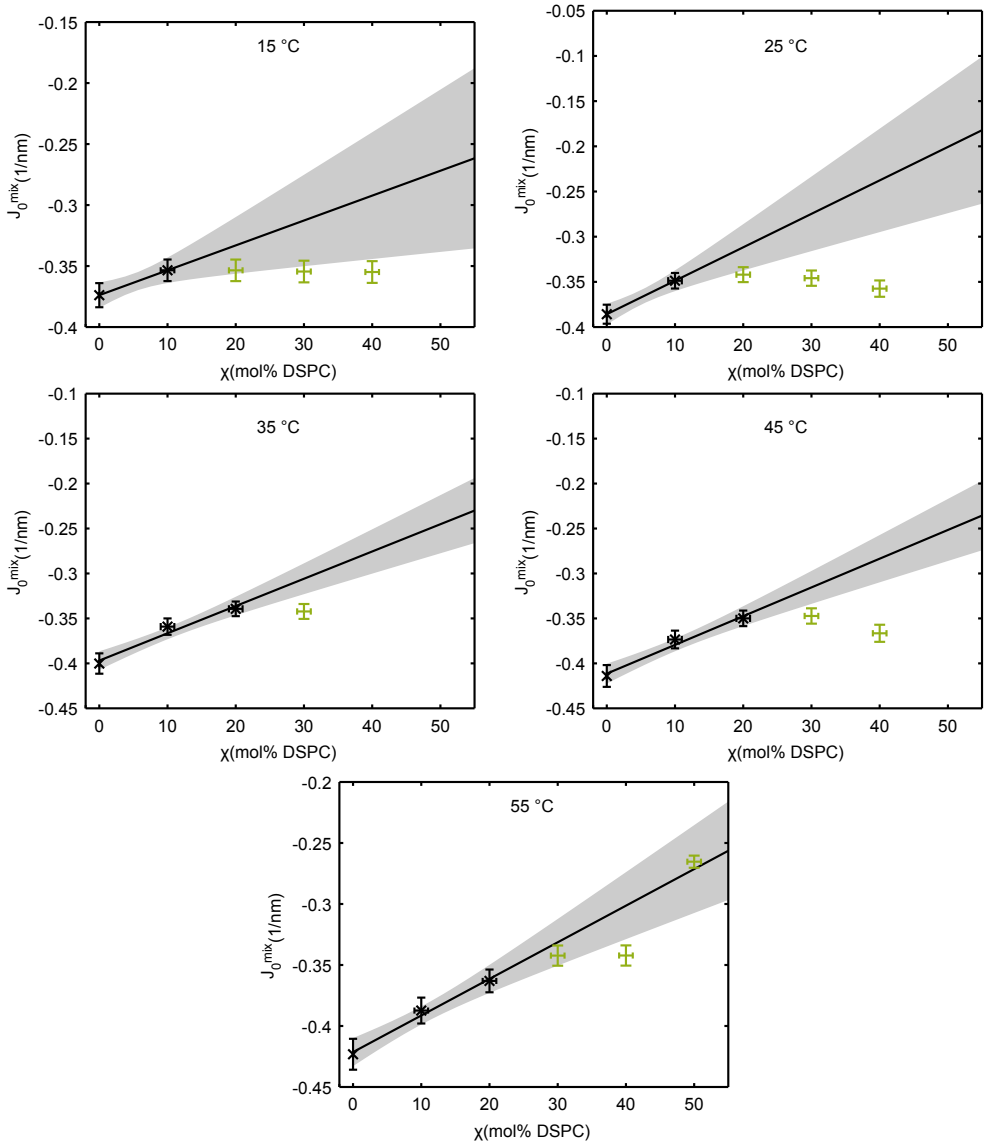

Figure S7: Determination of J_0 for DSPC.

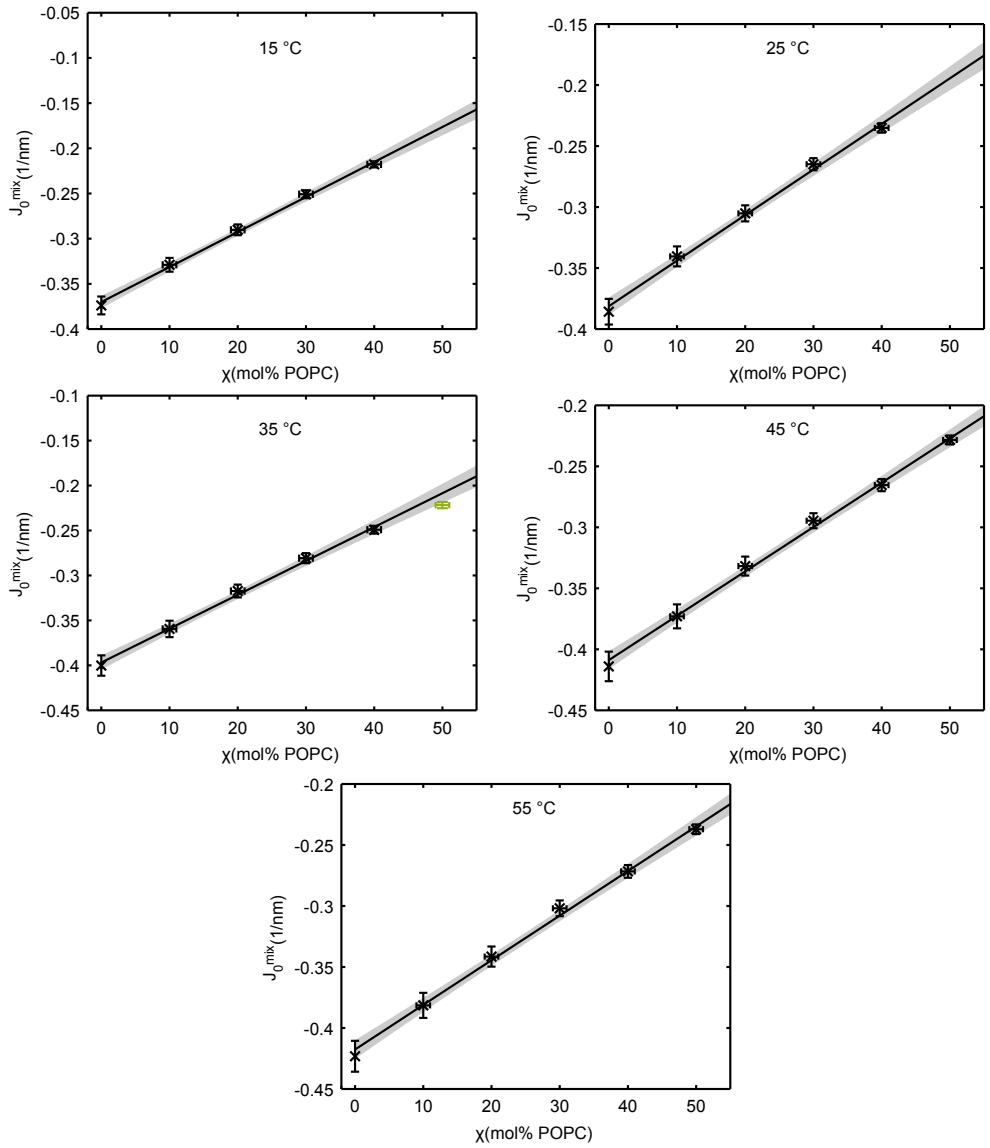

Figure S8: Determination of J_0 for POPC.

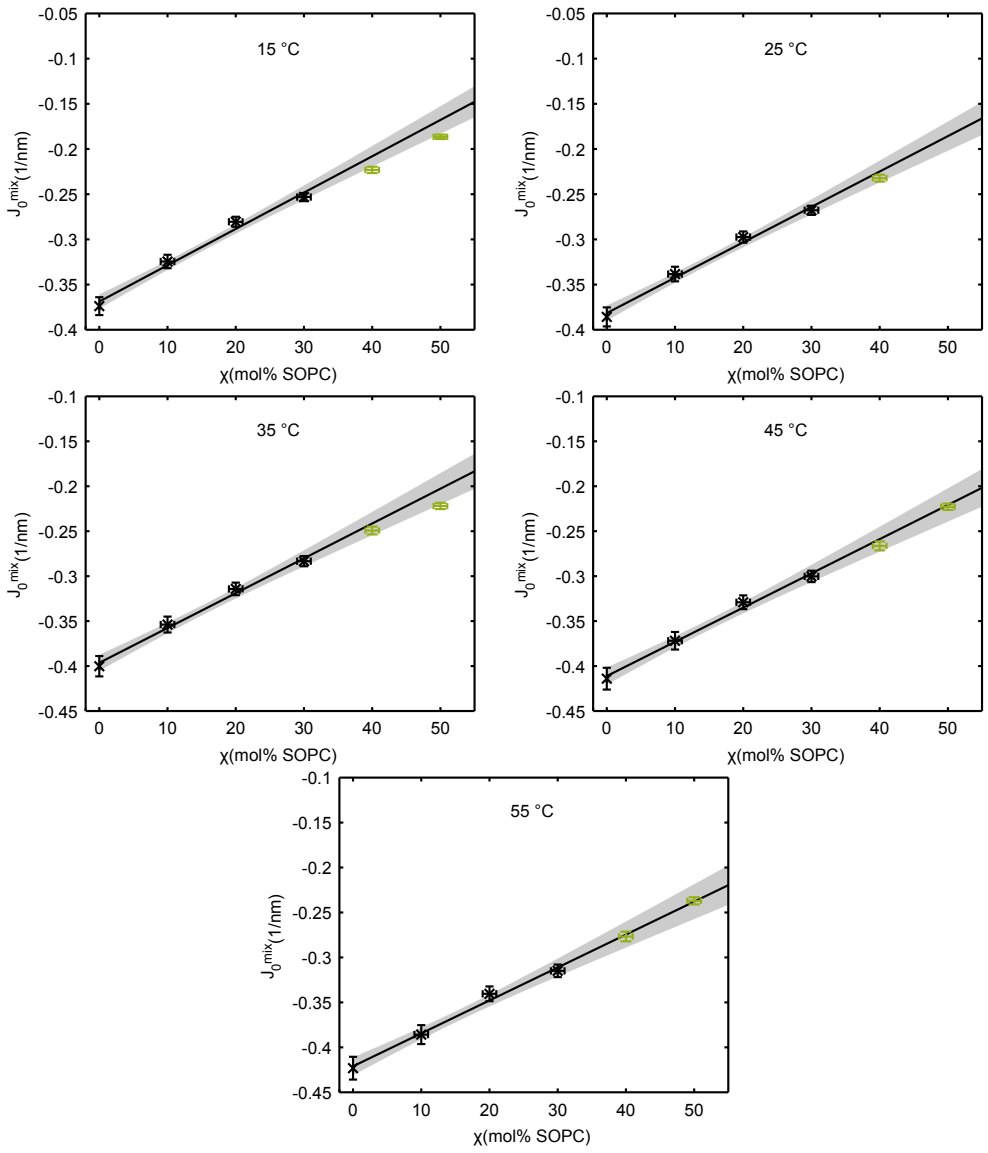

Figure S9: Determination of J_0 for SOPC.

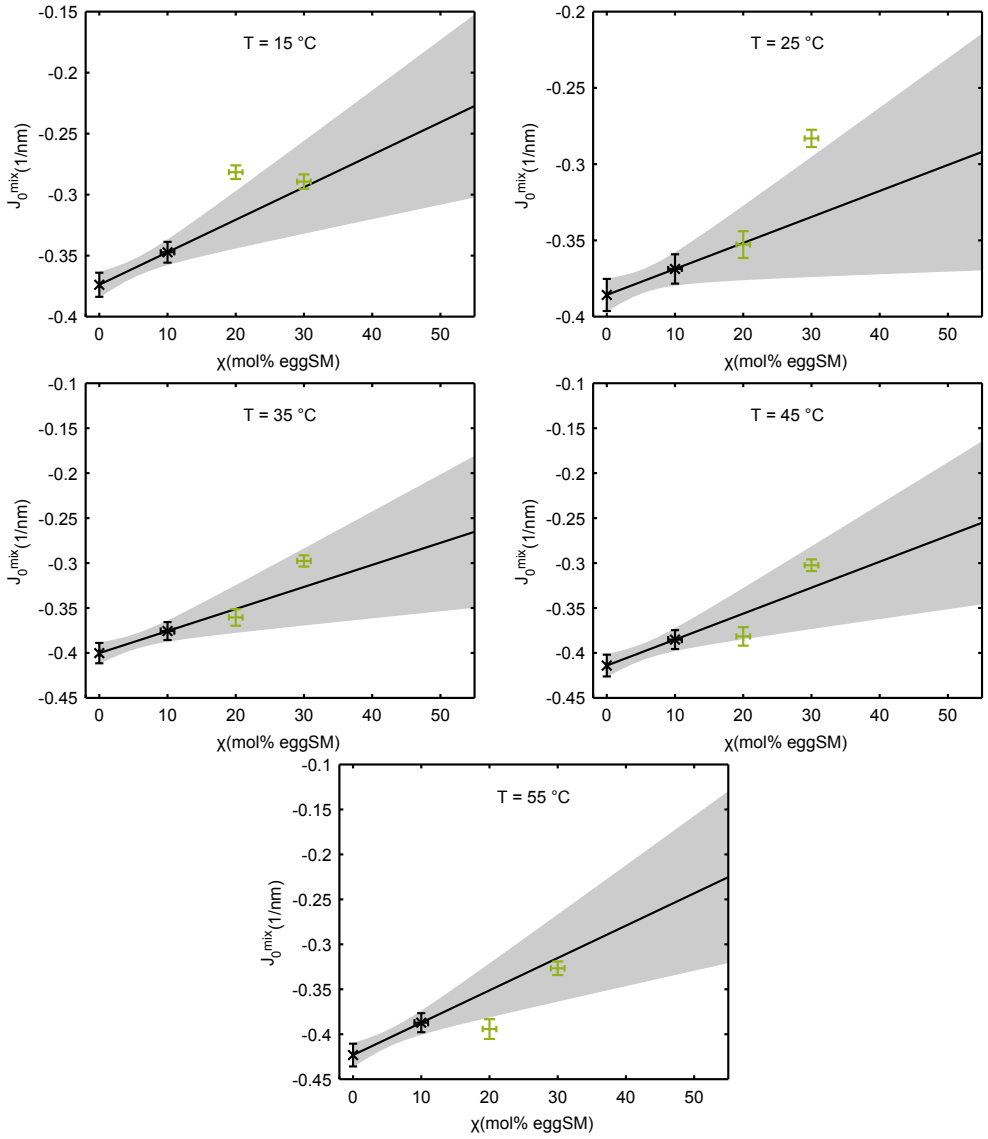

Figure S10: Determination of J_0 for eggSM.

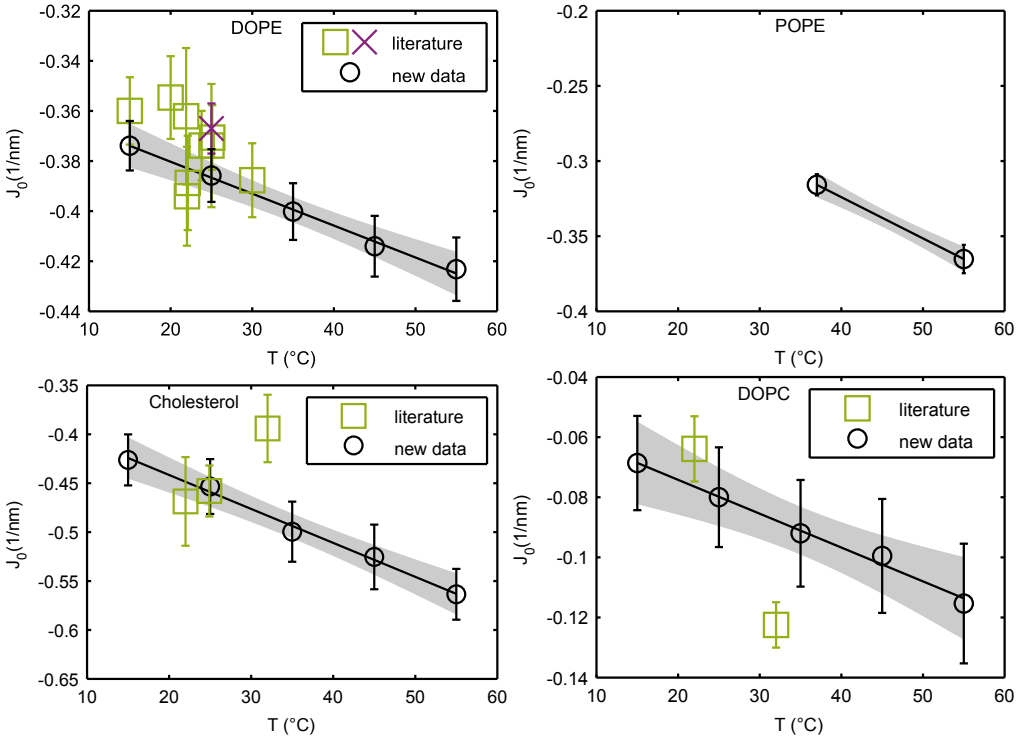

Figure S11: Temperature dependence of $J_0(T)$ compared with literature data.[16–24]

S5 Temperature dependence of spontaneous curvature

Each lipid's spontaneous curvature $J_0(T)$ as a function of temperature T is presented in Figs. S11–S12 (black circles) in comparison with literature data determined at the pivotal plane* (green squares) and the neutral plane (violet crosses). The black straight line is the result of the linear fit according to Eq. (2), while the gray band depicts its error via Eq. (3).

*Similar to Fig. 3, we rescaled reported values to $J_0 \sim J_{0p}(1+\beta)$, with $\beta = 0.065 \pm 0.035$ determined in [17].

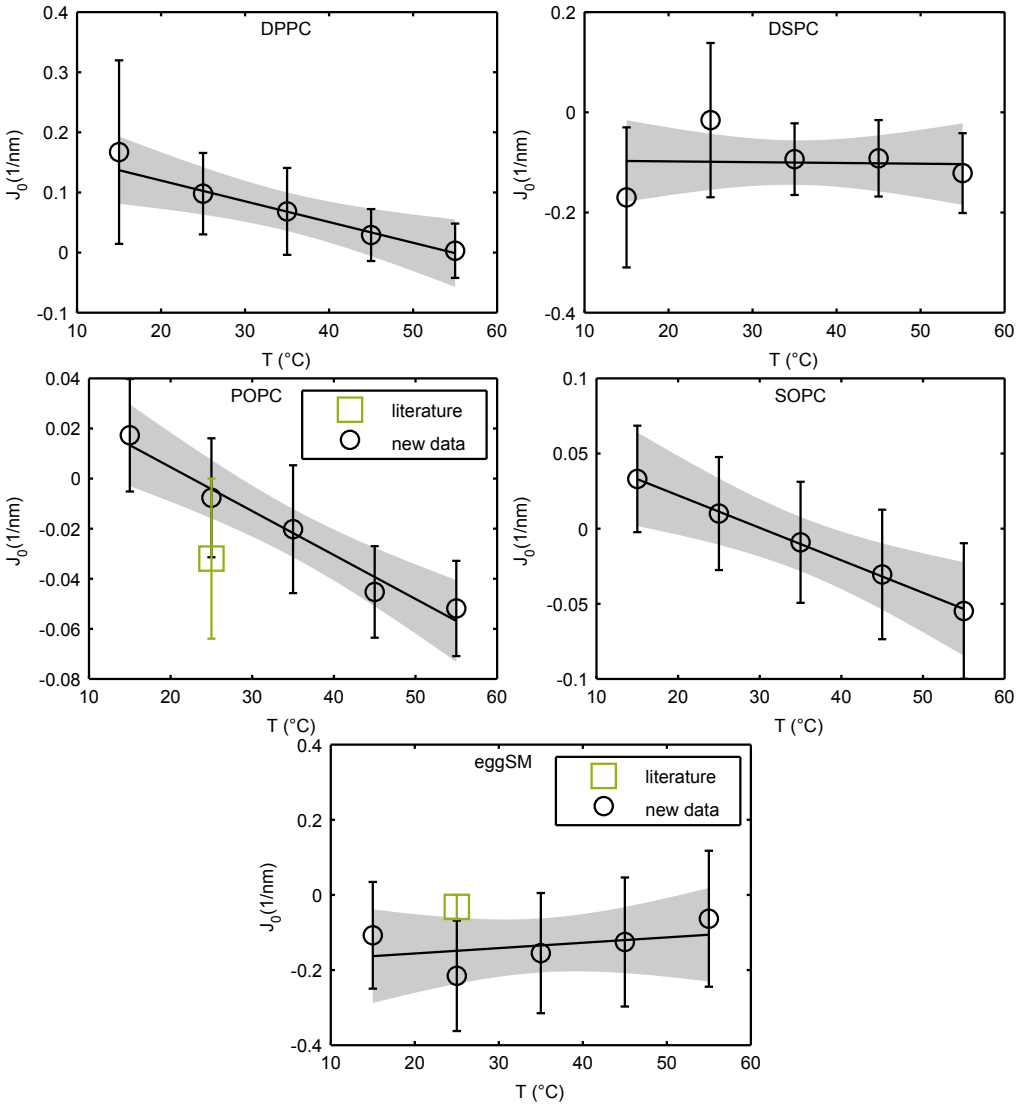

Figure S12: Temperature dependence of $J_0(T)$ compared with literature data.[22]

References

[1] M. Rappolt, A. Hickel, F. Bringezu and K. Lohner, *Biophys. J.*, 2003, **84**, 3111–3122.

[2] B. E. Warren, *X-ray diffraction*, Addison-Wesley Pub. Co., Reading, Mass., 1969.

[3] D. C. Turner and S. M. Gruner, *Biochemistry*, 1992, **31**, 1340–1355.

[4] P. E. Harper, D. A. Mannock, R. N. Lewis, R. N. McElhaney and S. M. Gruner, *Biophys. J.*, 2001, **81**, 2693–2706.

[5] M. Rappolt, A. Hodzic, B. Sartori, M. Ollivon and P. Laggner, *Chem. Phys. Lipids*, 2008, **154**, 46–55.

[6] A. K. Smith and J. H. Freed, *J. Phys. Chem. B*, 2009, **113**, 3957–3971.

[7] F. A. Heberle, J. Wu, S. L. Goh, R. S. Petruzielo and G. W. Feigenson, *Biophys. J.*, 2010, **99**, 3309–3318.

[8] P. Uppamoochikkal, S. Tristram-Nagle and J. F. Nagle, *Langmuir*, 2010, **26**, 17363–17368.

[9] I. V. Ionova, V. A. Livshits and D. Marsh, *Biophys. J.*, 2012, **102**, 1856–1865.

[10] T. A. Pastva, *Master's thesis*, Naval Postgraduate School, Monterey, California, 1998.

[11] P. I. Kuzmin, S. A. Akimov, Y. A. Chizmadzhev, J. Zimmerberg and F. S. Cohen, *Biophys. J.*, 2005, **88**, 1120–1133.

[12] N. Kučerka, M.-P. Nieh and J. Katsaras, *Biochim. Biophys. Acta, Biomembr.*, 2011, **1808**, 2761–2771.

[13] A. I. Greenwood, S. Tristram-Nagle and J. F. Nagle, *Chem. Phys. Lipids*, 2006, **143**, 1–10.

[14] G. Khelashvili, B. Kollmitzer, P. Heftberger, G. Pabst and D. Harries, *J. Chem. Theory Comput.*, 2013.

[15] F. A. Heberle, R. S. Petruzielo, J. Pan, P. Drazba, N. Kučerka, R. F. Standaert, G. W. Feigenson and J. Katsaras, *J. Am. Chem. Soc.*, 2013, **135**, 6853–6859.

[16] R. P. Rand and N. L. Fuller, *Biophys. J.*, 1994, **66**, 2127–2138.

[17] S. Leikin, M. M. Kozlov, N. L. Fuller and R. P. Rand, *Biophys. J.*, 1996, **71**, 2623–2632.

[18] E. E. Kooijman, V. Chupin, N. L. Fuller, M. M. Kozlov, B. de Kruijff, K. N. J. Burger and R. P. Rand, *Biochemistry*, 2005, **44**, 2097–2102.

[19] N. Fuller, C. R. Benatti and R. P. Rand, *Biophys. J.*, 2003, **85**, 1667–1674.

[20] Z. Chen and R. P. Rand, *Biophys. J.*, 1997, **73**, 267–276.

[21] M. M. Kozlov, S. Leikin and R. P. Rand, *Biophys. J.*, 1994, **67**, 1603–1611.

[22] B. Boulgaropoulos, M. Rappolt, B. Sartori, H. Amenitsch and G. Pabst, *Biophys. J.*, 2012, **102**, 2031–2038.

[23] J. A. Szule, N. L. Fuller and R. P. Rand, *Biophys. J.*, 2002, **83**, 977–984.

[24] R. P. Rand, N. L. Fuller, S. M. Gruner and V. A. Parsegian, *Biochemistry*, 1990, **29**, 76–87.

Bending rigidities and interdomain forces in membranes with coexisting lipid domains

Benjamin Kollmitzer,[†,‡] Peter Heftberger,[†,‡] Rudolf Podgornik[§,¶,‖], John F. Nagle[**], and Georg Pabst[†,‡ *]

[†] *University of Graz, Institute of Molecular Biosciences, Biophysics Division, NAWI Graz, Humboldstr. 50/III, A-8010 Graz, Austria.*

[‡] *BioTechMed-Graz, Austria.*

[§] *Department of Theoretical Physics, Jozef Stefan Institute, Ljubljana, Slovenia.*

[¶] *Department of Physics, Faculty of Mathematics and Physics, University of Ljubljana, Ljubljana, Slovenia.*

[‖] *Department of Physics, University of Massachusetts, Amherst, Massachusetts, USA.*

[**] *Department of Physics, Carnegie Mellon University, Pittsburgh, Pennsylvania, USA.*

[*] Correspondence: georg.pabst@uni-graz.at

Abstract

In order to precisely quantify the fundamental interactions between heterogeneous lipid membranes with coexisting liquid-ordered (Lo) and liquid-disordered (Ld) domains, we performed detailed osmotic stress SAXS experiments by exploiting the domain alignment in raft-mimicking lipid multibilayers. Performing a Monte Carlo (MC) based analysis allowed us to determine with high reliability the magnitude and functional dependence of interdomain forces concurrently with the bending elasticity moduli. In contrast to previous methodologies, this approach enabled us to consider the entropic undulation repulsions on a fundamental level, without having to take recourse to crudely justified mean-field like additivity assumptions. Our detailed Hamaker coefficient calculations indicated only small differences in the van der Waals attractions of coexisting Lo and Ld phases. In contrast, the repulsive hydration and undulation interactions differed significantly, with the latter dominating the overall repulsions in the Ld phase. Therefore, alignment of like domains in multibilayers originates from both, hydration and undulation repulsions, and cannot be exclusively attributed to the variability of the hydration interaction between Lo and Ld domains, as proposed recently [Tayebi et al., Nat. Mat. 11, 1074, 2012].

Key words: osmotic stress experiments; interbilayer forces; liquid ordered phase; liquid disordered phase; membrane rafts; Monte Carlo simulations

Introduction

Diverse physiological processes in living systems depend on fundamental physical interactions between lipid membranes acting on the nanoscopic length scale. Of particular interest in this context are forces acting between membrane domains/rafts across the aqueous phase, involved also in their correlated mutual alignment. Such positional correlations are well established for liquid-ordered (Lo)/liquid-disordered (Ld) domains in model lipid multibilayers (1–8), and are also biologically relevant in the context of e.g. the immune response, where organization of receptor–ligand domains occurs during T-cell adhesion (9, 10). Both, the formation of such domains as well as the adhesion affinity depend strongly on thermal fluctuations and consequently on the bending rigidity of membranes (11, 12). It is therefore reasonable to expect that fundamental intermembrane interactions will play an important role also in receptor–ligand domain alignment.

Within the broad DLVO paradigm (13) the fundamental long-range interactions between soft material interfaces, mediated by their molecular environment, such as solvation (hydration) interaction, electrostatic interaction, and van der Waals interaction, can be treated independently and additively. However, this additivity *Ansatz* is in general not vindicated for entropically driven bending undulation interactions that warrant a more sophisticated approach (13–15).

Besides the fundamental role of entropic membrane undulations, their relation with the membrane bending rigidity K_c (14), and through it their connection with diverse physiological processes, has spurred a sustained scientific interest (16). Shape analysis of giant unilamellar vesicles (GUV) (17), diffuse X-ray scattering from oriented lipid multibilayers (18), and GUV micropipette aspiration (19) are all techniques exploiting this connection, but none of them so far has been able to simultaneously determine the bending moduli for coexisting membrane phases.

On the other hand, macroscopically sized domains form distinct lamellar lattices in multibilayer systems, enabling the application of *osmotic stress experiments* (6, 20). In such experiments, osmotic pressure is maintained by, e.g., large neutral polymers, such as poly-ethylene-glycol (PEG), which do not penetrate into the interbilayer water layer, while the corresponding bilayer separation and more recently also the specific line broadening due to fluctuations are measured by small-angle X-ray scattering (SAXS). Several groups, including ours, have previously applied this approach to study interactions between macromolecules, including lipid bilayers (6, 20–29).

The bare long-range DLVO interaction components, that couple macromolecular surfaces through their molecular environment, get inextricably intertwined through the thermally driven conformational fluctuations of the soft interfaces, making detailed predictions of the overall interaction nearly impossible. Therefore, many studies in the past have resorted to describe such complicated thermal fluctuation effects by different mean-field/additivity approximations, where conformational fluctuation effects on the bare interaction potentials are included self-consistently (14, 15, 30–32). In contrast, additivity/mean-field approximations can be altogether avoided in the case of simulations that start from fundamental long-range DLVO interaction components and need no additional approximations to yield an accurate estimate for the total osmotic pressure in the system (33, 34).

In order to understand the coupling between bare interactions and thermal undulations, we apply a gradient-based optimization algorithm to iteratively adjust the parameters entering MC simulations, i.e., the coefficients describing the strength and range of intermembrane interactions as well as the bending rigidity characterizing the thermal undulations, in order to best match simulation results with the experimental osmotic stress data for Ld as well as Lo phases. This

simulation-driven analysis allows us to report for the first time experimental values for bending rigidities and interdomain interactions of coexisting raft-like phases in multilamellar vesicles (MLV).

Materials and methods

Sample preparation

Cholesterol (Chol), 1,2-dioleoyl-*sn*-glycero-3-phosphocholine (DOPC), and 1,2-distearoyl-*sn*-glycero-3-phosphocholine (DSPC) were purchased from Avanti Polar Lipids, Inc., Alabaster, AL, USA and used without further purification. Poly-(ethylene glycol) (PEG) with an average MW of 8000 was obtained from Fluka Chemie AG, Buchs, Switzerland and used as received.

After weighing, lipids were dissolved in chloroform/methanol 2:1 at concentrations of $10\,\mathrm{mg\,ml^{-1}}$ (35). We prepared the ternary lipid-only mixture DOPC/DSPC/Chol (0.42:0.37:0.21), which is known to separate into Lo and Ld domains (36), in a glass vial and evaporated the organic solvent under a gentle nitrogen stream at 30 °C. Remaining solvent traces were removed by placing the samples in vacuum overnight. $18\,\mathrm{M\Omega\,cm^{-1}}$ water (UHQ PS, USF Elga, Wycombe, UK) was added at 20 µl water/mg lipid and the mixtures fully hydrated at 50 °C for 4 hours with repeated freeze-thaw cycles.

To exert osmotic pressure on MLVs, sample aliquots were overlayed after hydration with PEG dissolved in water, yielding final concentrations of 1–42 wt% PEG in water. Samples were protected against oxidation with argon, the vials closed and taped, and stored at 4 °C for 7–10 days until the measurement. The osmotic equation of state for PEG, connecting its osmotic pressure with its solution concentration is well known (37) and allows for an accurate determination of the

PEG osmotic pressure P by using previously reported high resolution data (38).

X-ray measurements

Small-angle X-ray scattering (SAXS) was performed at the Austrian SAXS beamline at ELETTRA, Trieste, Italy (39, 40), at a wavelength of 1.54 Å and an energy-dispersion $\Delta E/E$ of 2.5×10^{-3}. A mar300 Image Plate 2D detector from mar-research, Norderstedt, Germany was used, covering a q-range from 0.2–7.1 Å^{-1} and calibrated with silver-behenate ($CH_3(CH_2)_{20}-COOAg$) with a d-spacing of 5.838 nm (41). Samples were filled into reusable quartz-glass capillaries and kept in a brass sample holder connected to a circulating water bath from Huber, Offenburg, Germany. The samples were equilibrated for 10 min at $(20.0 \pm 0.1)\,^{\circ}\text{C}$ before exposing them for 30 s to the X-ray beam.

The two dimensional detector signal was radially integrated with FIT2D (42, 43). Water background subtraction for samples without PEG was performed with Primus (44). For osmotically stressed samples however, additional scattering from PEG made a standard background subtraction impractical. Since the essential informations in this case were just the Bragg peaks' shapes and positions, we subtracted approximative backgrounds, obtained by interpolating between SAXS signals of pure water and PEG/water mixtures. Alternatively, one could just subtract an arbitrary smooth function from the measured data.

The reduced data were then fitted using a recently published, full q-range analysis method for coexisting liquid/liquid membrane domains (45). This method models each phase's contribution individually with a bilayer-structure and a superimposed membrane lattice. The lattice description is based on a modified Caillé theory (46, 47) and therefore yields the average membrane periodicity d and the line shape parameter η, which is connected to the mean square fluctuation of the

membrane spacing via $\Delta^2 = \eta d^2/\pi^2$ (27). The bilayer-structure of each phase is then modeled separately via probability distributions of quasi-molecular fragments (48).

Most importantly, the full q-range analysis allowed us to quantify the magnitude of fluctuations for coexisting domains. For both phases of stress-free samples, this also yields accurate electron density profiles, from which the bilayer thickness could be obtained; but this was not possible when osmotic pressure was applied. Instead, the osmotic thickening of d_B was calculated using $d_B(P) = d_B(0) \cdot (K_A + P \cdot d(P))/(K_A + P \cdot d_B(0))$ (26), where the area extension modulus K_A was estimated from published micropipette aspiration experiments on single lipids and binary lipid mixtures (49, 50), as detailed in Sec. S1 of the Supporting Material. The overall analysis was rather insensitive to uncertainties in K_A because the maximal change in bilayer thickness was only slightly larger than the uncertainty of the fit ($\pm 2\%$). The definition of the bilayer thickness d_B was found to be more important. In principle one could determine optimal values of d_B via a joint fit with free MC parameters, but this problem is under-determined and led to bizarre values of d_B for different data sets (51). Instead, we defined d_B as the distance between the remotest lipid atoms (52), also known as the steric bilayer thickness (24); this yielded good fits and comparable results, while being directly accessible from the SAXS analysis.

Membrane Monte-Carlo simulation

The simulation code used has been described previously in detail for a single membrane between two walls and for a stack of membranes (33, 34, 51). For completeness, but also to highlight our modifications, we briefly summarize its basic elements.

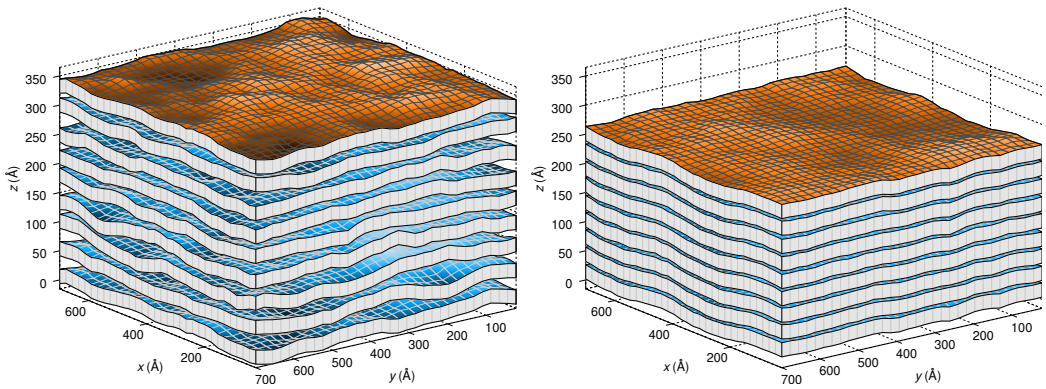

Figure 1: Real space snapshots of equilibrated Ld simulations at zero (left) and finite (5.5 MPa, right) osmotic pressure. Membranes are drawn with their average thickness. Deviations from the periodic lattice are color coded. Due to 3D periodic boundary conditions, the top-most (orange) and bottom-most membranes are equal. The most prominent effects of external pressure, a compression of the stack and a reduction of the fluctuations, are clearly visible.

The system under consideration consists of a stack of M fluctuating and interacting membranes of size $L \times L$, as depicted in Fig. 1. The m-th membrane's displacement from its average plane is denoted as $u_m(x, y)$, the average distance between membranes $\bar{a}$, and the bending rigidity as K_c. Imposing periodic boundary conditions in all directions yields the Hamiltonian of a stack of membranes

$$\mathcal{H} = \sum_{m=0}^{M-1} \int \left(\frac{K_c}{2} (\nabla^2 u_m)^2 + \Phi(a_m) \right) dx\, dy, \tag{1}$$

where Φ denotes the bare interaction potential, given here by the hydration repulsion and the van der Waals attraction, and $a_m(x, y) = u_{m+1}(x, y) - u_m(x, y) + \bar{a}$ denotes the local distance between two membranes. We furthermore require $a_m \geq 0$, meaning that membranes cannot interpenetrate.

To reduce the system's degrees of freedom to a finite amount, the membranes are discretized on a square $N \times N$ lattice. The simulation is performed in the constant pressure ensemble,(53) which converges for this model faster than con-

stant volume simulations (34). Monte-Carlo updates are proposed in $\bar{a}$ and in the complex coefficients $u_m(q_x, q_y)$ of the Fourier transformation of $u_m(x, y)$. Simulating in Fourier space allows for larger moves, thereby accelerating equilibration (34). After every Monte Carlo step (MCS), which corresponds to degree of freedom (N^2M+1) update proposals, we re-centered the coordinate system to correct for small center of mass movement as a new feature in the calculations.

Simulations were performed for $L = 700\,\text{Å}$, several different N (6, 8, 12, 16, 24 and 32), $M = 8$, equilibration lengths of 3×10^3 MCS, and collection lengths of 10^4 MCS, which typically exceeded the autocorrelation time by a factor of 100. Simulations were started with step sizes estimated from an approximative theory (15) and then subsequently optimized during equilibration, applying either dynamically optimized Monte Carlo (DOMC), or – as a new feature – the acceptance ratio method (ARM) as a backup if DOMC fails (51, 54).

Several observables can be determined from converged simulations, but the two most important quantities for comparison with SAXS experiments are the temporally- and spatially-averaged distance between membranes $d_W = \langle \bar{a} \rangle$ and the time average of its fluctuations

$$\Delta^2 = \langle \overline{(z_{m+1}(x,y) - z_m(x,y) - d_B - d_W)^2} \rangle, \tag{2}$$

where the long bar denotes spatial averaging over (m, x, y), $\langle . \rangle$ denotes time averaging, and $z_m(x, y) = u_m(x, y) + m \cdot (\bar{a} + d_B)$ is the m-th membrane's position in real-space. Specifically, d_W corresponds to the experimental thickness of the water layers separating the lipid bilayers, while Δ is related to the experimental Caillé parameter η as detailed above.

It should be emphasized that our explicit purpose of making contact with the X-ray structure factor and the interactions between bilayers, requires much larger

systems than can be presently envisioned either for all-atom simulations, used to obtain electron density profiles, or even for the most coarse grained molecular simulations (55). We require M bilayers in a stack, each bilayer having a large lateral size L. It has been shown in previous work (33), that $L = 700\,\text{Å}$ and $M = 8$ are sufficient to obtain accuracies of 1% for d_W and Δ, and that would require about 130 000 lipids with associated water in typical molecular simulations. Apart from simulation size, also the necessary timescales, which scale with the fourth power of the undulation wavelength (56, pp. 77–78), render molecular dynamics simulations for that purpose unfeasible. Furthermore, to fit the experimental data requires on the order of 100 separate simulations, distributed on multiple optimizations from different start points. In the membrane MC simulations we employ, each bilayer is reduced to a network consisting of N nodes in each of the two lateral directions and each node has only one degree of freedom. Computed observables change significantly with N/L (33, 34), so simulations were performed for a sequence of values of $N \in \{6, 8, 12, 16, 24, 32\}$ and then the observables were extrapolated towards $N/L \to \infty$. Further details of this finite size convergence are given in Sec. S2.

Bare interaction potentials

For uncharged membranes, the potential at bilayer separation a is modeled canonically by (57)

$$\Phi(a) \simeq A\lambda \exp\left(-\frac{a}{\lambda}\right) - \frac{H}{12\pi a^2}. \tag{3}$$

The first term is the well-established empirical form of the solvent-mediated hydration interaction, which has been argued to originate from changes in various measures of order for the water structure at the membrane interface (58–60), with the strength A and the decay length λ, which is typically in the range of 1–2 Å (27). The second term describes the ubiquitous van der Waals interaction poten-

tial for two planar semi-infinite layers, with H being the Hamaker coefficient that in general also depends on the bilayer separation a, $H = H(a)$ (61, p. 15). This functional form is convenient because it can in fact describe both cases of either two finite-thickness layers interacting across a solvent layer (62), as well as effective pairwise interactions in an infinite stack of finite-thickness layers (63). For large solvent layer thickness the nonpairwise additive effects in the latter case become negligible and the van der Waals interaction potential for the two cases follows exactly the same separation dependence.

Due to the divergence of the van der Waals potential for $a \to 0$, the $1/a^2$ term is cut off for $a < 1\,\text{Å}$ (33). In experiments, the collapse of charge neutral bilayers due to van der Waals forces is avoided by very short range steric interactions established by McIntosh et al. (64), but which occur at significantly higher osmotic pressures than those relevant for the present experiments, see also Fig. S5.

To calculate the Hamaker coefficient H *ab initio*, we had to approximate the lipid bilayers by pure hydrocarbon (65). Specifically, we calculated H for an infinite stack of hydrocarbon layers in water, based on a full multilayer Lifshitz formulation (63). The ranges for the hydrocarbon thicknesses $d_B = 45\,\text{Å}$ to $60\,\text{Å}$ and the water spacings $d_W = 5\,\text{Å}$ to $30\,\text{Å}$ were motivated by our experimental data. In this calculation range, differences in the Hamaker coefficient were within 10%. For our MC simulations the exact value of H matters most when all forces are of comparable magnitude, that is at vanishing external osmotic pressure. We therefore used the H values of $4.08\,\text{zJ}$ for Ld and $4.15\,\text{zJ}$ for Lo domains (Fig. 2).

Optimizing parameters against experimental data

After calculating the Hamaker coefficient H as described in , the remaining free parameters for the simulations are $\vec{\Lambda} = (A, \lambda, K_c)$. We implemented a least squares

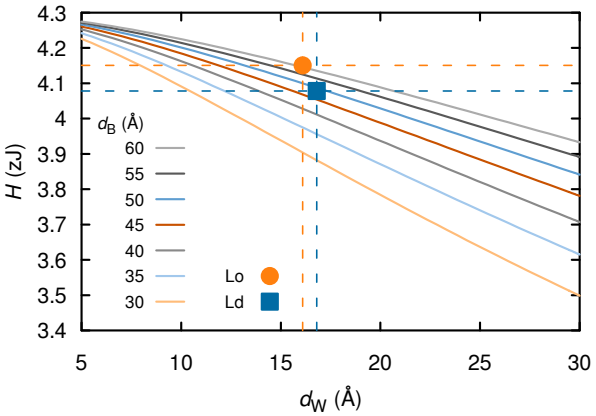

Figure 2: Hamaker coefficient H for hydrocarbon multilayers of height d_B and separation d_W in water. Highlighted are the applied values of H for Ld and Lo, which are described in the main text.

routine with Matlab® (66), utilizing its trust region reflective optimization algorithm to minimize the sum of the squared residues

$$\chi^2(\vec{\Lambda}) = \sum_i \left(\frac{d_{W,i} - d_W(P_i;\vec{\Lambda})}{U_{\text{eff}}(d_{W,i})} \right)^2 + \left(\frac{\Delta_i - \Delta(P_i;\vec{\Lambda})}{U_{\text{eff}}(\Delta_i)} \right)^2, \tag{4}$$

where $d_{W,i}$ and Δ_i are the experimentally determined values at fixed osmotic pressure P_i, $d_W(P_i;\vec{\Lambda})$ and $\Delta(P_i;\vec{\Lambda})$ are simulation results, and $U_{\text{eff}}(f)$ is the effective uncertainty of a given quantity f, derived from

$$U^2_{\text{eff}}(f) = U^2(f_{\text{exp}}) + U^2(f_{\text{sim}}) + \left(\frac{\partial f_{\text{sim}}}{\partial P} \cdot U(P_i) \right)^2. \tag{5}$$

The agreement between model and data was evaluated by the reduced $\chi^2_{red} = \chi^2/\tilde{N}$, where $\tilde{N}$ equals the number of data points minus the number of free parameters (67, p. 268). The Jacobian for this gradient based algorithm and the derivative in Eq. (5) were computed with the histogram reweighting method described in Sec. S3. Once the iteration converged, the uncertainties of the fit pa-

rameters were determined from the curvature of χ^2_{red}. In order to locate the global optimum, several iterations from randomly chosen initial parameter sets were performed.

To test our implementation, we fitted simulation results determined for one reasonable parameter set $\vec{\Lambda}'$, by starting the least squares from several different initial starting points $\vec{\Lambda}$. Within 3–5 iterations, these optimizations converged towards the correct values $\vec{\Lambda}'$, thereby indicating that the weighted histogram based differentiation and the fit were correctly implemented. For the experimental data sets, convergence was usually reached within 10 iterations. However, due to the stochastic nature of the simulations and the consequential randomness of results and derivatives, the optimization algorithm propagated poorly in flat regions, i.e. small $\vec{\nabla}\chi^2_{red}$. Because $\chi^2_{red}(\vec{\Lambda})$ is a smooth function and its gradient has to vanish at extrema, the optimization algorithm's efficiency decreased, the closer it got to the optimum. This was another reason for starting several independent iterations (68).

As a further test case, we re-analyzed previously published osmotic pressure data of pure dimyristoyl-phosphocholine (DMPC) bilayers (27), yielding very reasonable values and a good agreement between simulations and experiments. Details are given in Sec. S4.

Results and Discussion

X-ray analysis

SAXS patterns were analyzed as detailed previously (8). Figure 3 showcases the analysis for two samples at osmotic pressures of 34 kPa and 2.4 MPa, demonstrating that shapes and positions of Bragg reflections are well reproduced. Fits for all

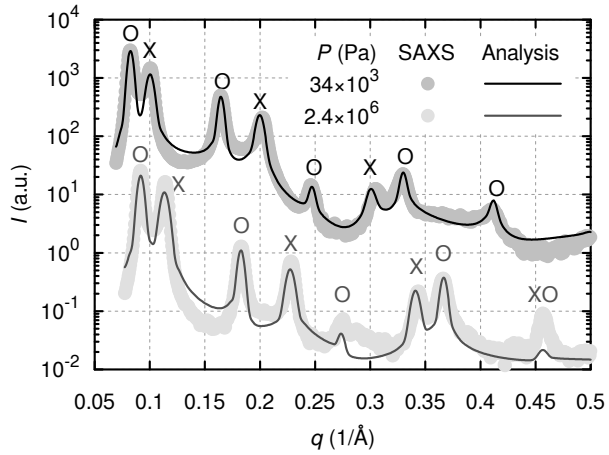

Figure 3: Calculated scattering intensities (solid lines) from full q-range analyses, compared with recorded SAXS data from coexisting phases (dots) for two different osmotic pressures P. Bragg reflections from aligned Lo and Ld domains are indicated by symbols O and X, respectively.

other samples are shown in Sec. S5. For increased pressures, Bragg peaks shifted towards higher q's and became more prominent. This is due to the decrease of bilayer separation which goes in hand with a reduction of bending fluctuations in agreement with previous reports (27, 69). Although the fits are superb for low osmotic pressures, we see stronger differences at increased osmotic pressures, see Fig. 3 or Sec. S5. It seems as if the underlying Caillé theory loses its applicability for the increased order experienced at elevated pressures. This is consistent with reports that the Caillé theory is unsuited to describe the even more ordered gel phase (70).

The effect of osmotic pressure on the lamellar repeat spacing d, as determined from the SAXS analysis, is plotted in Fig. 4. At high osmotic stress, the distance between bilayers is effectively set by the repulsive hydration interaction which dominates the repulsive fluctuation interaction and the attractive van der Waals interaction. As osmotic pressure is decreased, the water spacing between bilayers

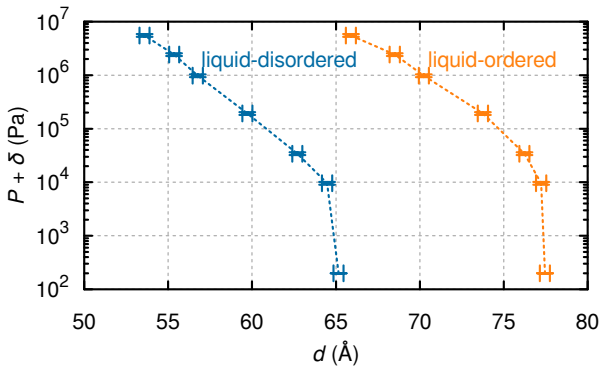

Figure 4: Osmotic pressure P vs membrane periodicity d for Ld and Lo determined by SAXS analysis (71). Dashed lines are meant solely as a guide for the eye.

d_W increases and the fluctuation interaction eventually dominates the hydration interaction. As the osmotic pressure is reduced to zero, the attractive van der Waals force balances the total repulsive forces, resulting in finite d_W and d values.

Within experimental uncertainty, the two isotherms in Fig. 4 are rather similar when the difference in membrane thickness is taken into account ($d_B^{Ld} = (48.5 \pm 1.0)$ Å and $d_B^{Lo} = (61.3 \pm 1.2)$ Å). Of course, identical isotherms would imply that all the interactions are identical. However, significant experimental differences were observed in the fluctuation behavior as detailed below, corroborating the crucial advantage of jointly analyzing fluctuations and osmotic pressure isotherms in order to obtain the interaction parameters (27).

Optimized simulations

The experimental data and the results of optimized simulations are compared in Fig. 5, while Tab. 1 lists the corresponding simulation parameters. Experimental errors for d_W and η were obtained from the SAXS analysis and for P were estimated to equal the pipetting error of 6% for viscous PEG solutions. To quantify the

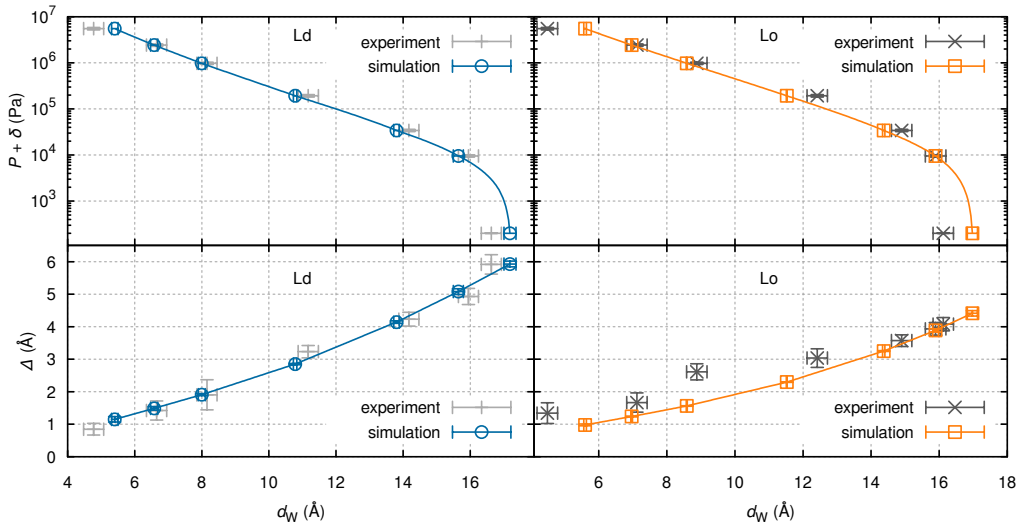

Figure 5: Pressure (top) and fluctuations (bottom) vs water-layer thickness for best fit of membrane MC simulation (cyan/orange) against SAXS data (gray) (71). Solid lines were obtained by exponentially interpolating fluctuation contributions.

agreement between data and simulations, we report χ^2_{red}, which becomes ca. 1 if the differences are compatible with experimental errors (67, p. 268). This is the case for the Ld phase, where simulations and experimental data match ideally, but the mismatch for Lo is bigger than expected ($\chi^2_{red} = 6$).

We are inclined to attribute this discrepancy for Lo at least partially to the limited applicability of the Caillé theory for highly ordered systems, as described in the previous section. Indeed, deviations in Δ are especially pronounced for small bilayer separations, i.e. at high osmotic pressures. In light of these discrepancies, we suggest that the experimental uncertainties determined for the Lo phase are rather too small because they do not take into account the decreasing applicability of the Caillé theory for more ordered phases whose fluctuations are suppressed by low hydration.

While differences in $P(d_W)$ are insignificant between Ld and Lo (see also

Table 1: Optimal parameters determined for describing the coexisting Lo/Ld phases in DOPC/DSPC/Chol (0.42:0.37:0.21). Errors as obtained from the fitting routine, see text for further details.

	Ld	Lo
K_c/zJ	44 ± 10	120 ± 20
A/Pa	$10^{8.3 \pm 0.2}$	$10^{8.1 \pm 0.2}$
λ/Å	1.37 ± 0.15	1.74 ± 0.15
χ^2_{red}	1.5 ± 0.5	5.8 ± 0.5

Fig. 4), fluctuations of the Lo phase, containing most of the DSPC and about thrice as much cholesterol as Ld, are evidently smaller (Fig. 5). In the continuum mechanics treatment used in the simulations, this increase in bilayer stiffness is captured by a threefold higher K_c for Lo, see Tab. 1.

The values obtained by us for K_c compare well with previously reported results from different techniques. Bending rigidities of binary DOPC/cholesterol mixtures have been measured by several groups, ranging from (60 ± 8) to (100 ± 25) zJ and were found to be largely unchanged by the cholesterol content (72–75). This supports the $K_c = (44 \pm 10)$ zJ obtained for Ld, where DOPC is the main constitutent (36). In contrast, a larger concentration of saturated lipids, for which K_c does increase with cholesterol (72), is present in the Lo phase, so a larger bending rigidity would be expected for Lo than for Ld. Our finding of $K_c = (120 \pm 20)$ zJ for the Lo phase is consistent with this expectation.

Furthermore, molecular dynamics (MD) simulation results are available for comparison. Khelashvili et al. (76) used the reported tie-line endpoint compositions (36) to separately simulate the liquid-disordered and -ordered phases, obtaining bending moduli of 80–130 zJ for Ld and 340–440 zJ for Lo. Although these values are large compared to our results, both methods find a strong increase of K_c between Ld and Lo.

In agreement with Ref. 77, we find that a rather simple model suffices to relate

bending to area extension moduli for cholesterol-rich samples (78). Based on the assumption that the main contribution to membrane rigidity comes from the stiff cholesterol ring of size δ', Pan et al. used the relationship $\delta'^2 = 12K_c/K_A$. For our samples, with $K_A = 430\,\mathrm{mN\,m^{-1}}$ and $2100\,\mathrm{mN\,m^{-1}}$ (see Sec. S1 for details), this equation yields $\delta' = 11$ Å and 8 Å for Ld and Lo, respectively, in good agreement to actual cholesterol ring sizes of about 9 Å, giving additional support to our analysis.

Interdomain forces

As stated before, the differences between Ld and Lo in the P vs d_W data sets are small. However, a more thorough investigation of these quantities yields interesting insights. Because good fits to these data were obtained, the total pressure P is readily dissected into its individual contributions from the fundamental surface forces (79). Their functional dependence is plotted in Fig. 6.

The thicker Lo bilayer causes an increase in the Hamaker coefficient, but only by 3% compared to the Ld phase; this is a minor difference in the van der Waals interaction that is hardly noticeable in the P_{vdW} curve in Fig. 6. For small bilayer separations, the hydration interactions are of similar magnitude and represent, as expected, the dominant contribution to the total interaction potential for both phases. Despite these similarities, the fluctuation pressure starts to surpass the hydration pressure already at much smaller separations d_W for Ld than for Lo. This difference implies, in contrast to the ordered phase, that the undulation interaction becomes the most important repulsive interaction over a wider range of bilayer separations in the case of the disordered phase. Stronger repulsions due to fluctuation interactions are of course reasonable because thermal undulations were found to be significantly increased for the Ld phase (Fig. 5). Nevertheless, even in the Lo phase, the thermal undulation interaction dominates the hydration

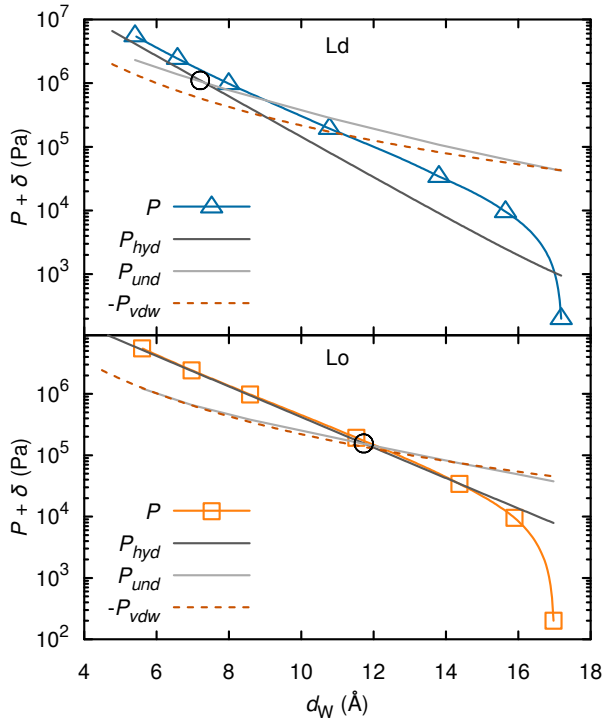

Figure 6: Partitioning of total pressure P into contributions from hydration P_{hyd}, van der Waals P_{vdw}, and undulations P_{und} for Ld (top) and Lo (bottom) (71). The large open black circles show the values of the separation d_W, at which hydration and undulation pressure are equal. Due to the additive constant δ, the hydration pressure deviates from a straight line at low P.

force over the most important, well hydrated range of d_W, starting at separations of 12 Å.

We obtained almost exponentially decreasing fluctuation forces of the scaling form $\propto \exp(-z/\lambda_{und})$, with effective decay lengths $\lambda_{und} \approx 3.3$ Å and 3.7 Å for Ld and Lo, respectively (80). The ratio of fluctuation to hydration decay length λ_{und}/λ is obtained as 2.4 for Ld and 2.1 for Lo. While the mean-field theory predicted its value as 2.0 (15), values of 2.4 have been reported for simulations (33, 34), and 2.0–3.0 from other experiments (6, 27, 28).

Compared to Lo, a significantly shorter decay length for the hydration interaction pressure was found for the Ld phase. At present, the origin for this difference is unclear. However, it is this difference combined with the larger fluctuation force that gives P versus d_W curves that are nearly the same for Lo and Ld, both with fully hydrated d_W close to 17 Å.

Domain alignment across interlamellar aqueous phases has recently been hypothesized to be caused by water network mismatch due to the different hydration properties of Lo and Ld phases (1). In support of this postulation, we observed significantly different hydration forces and nearly equal van der Waals forces for both phases. Thermal fluctuations were however neglected in the aforementioned hypothesis, while we now find considerable differences specifically in the undulation forces for coexisting domains. Their importance is especially striking near full hydration, where undulation and van der Waals pressures surpass hydration repulsion by an order of magnitude (see Fig. 6).

Conclusion

We have evaluated the fundamental long-range interactions between bilayers in Lo and in Ld domains in DOPC/DSPC/cholesterol MLV. Because we could do this at concentrations where Lo and Ld domains coexist, we were able to avoid all uncertainties in the phase diagram and its associated tie-lines between Lo and Ld phases. This work combines methodology from three separate inputs: SAXS/ osmotic stress experiments, comprehensive Monte Carlo simulations, and detailed calculations of van der Waals interactions.

The reported values for fundamental surface forces and bending moduli are the first of their kind being, directly obtained from coexisting Lo/Ld domains. The underlying full q-range SAXS analysis allowed us to quantify the extent of fluctuations and capture their dependence on osmotic pressure, which proved essential for determining the bending rigidities of cholesterol-rich phases. We obtained bending moduli of 44 zJ for Ld and a roughly threefold higher value for Lo domains, attributable to their larger concentrations of saturated lipid and cholesterol.

While we obtained almost identical van der Waals interactions for aligned Lo and Ld domains, the remaining interactions, however, turned out to be strikingly different: decay lengths of the hydration pressures differed by 25% between Lo and Ld phases, and repulsions due to thermal fluctuations were found to be significantly increased for Ld. These findings provide evidence that, in addition to hydration repulsion which was previously singled out as the sole mechanism driving domain alignment in multibilayers (1), the fluctuation-driven undulation repulsion must be considered in any quantitative explanation of the long-range positional correlations between aligned Lo and Ld domains.

Author Contributions

B.K. designed and performed research, analyzed data and wrote the paper; P.H. designed and performed research and analyzed data; R.P. and J.F.N. contributed analytic tools and wrote the paper; G.P. designed and performed research and wrote the paper.

Acknowledgments

This work is supported by the Austrian Science Fund FWF, Project no. P24459-B20 to GP. The computational results presented have been achieved using the Vienna Scientific Cluster (VSC). The authors thank Alexander Rieder and Heinz Amenitsch for experimental support and Hans Gerd Evertz for critical review of the simulation and advice regarding finite size convergence. Support for the original development of the MC software was provided to JFN under grant GM44976 from the U.S. National Institutes of Health. RP would like to acknowledge the SLO-A bilateral grant N1–0019 of the Slovene Research Agency.

Supporting Citations

References (81–90) appear in the Supporting Material.

References

1. Tayebi, L., Y. Ma, D. Vashaee, G. Chen, S. K. Sinha, and A. N. Parikh, 2012. Long-range interlayer alignment of intralayer domains in stacked lipid bilayers. *Nat. Mater.* 11:1074–1080.

2. Karmakar, S., and V. A. Raghunathan, 2005. Structure of phospholipid-cholesterol membranes: An x-ray diffraction study. *Phys. Rev. E* 71:061924.

3. Chen, L., Z. Yu, and P. J. Quinn, 2007. The partition of cholesterol between ordered and fluid bilayers of phosphatidylcholine: A synchrotron X-ray diffraction study. *Biochim. Biophys. Acta, Biomembr.* 1768:2873–2881.

4. Mills, T. T., S. Tristram-Nagle, F. A. Heberle, N. F. Morales, J. Zhao, J. Wu, G. E. S. Toombes, J. F. Nagle, and G. W. Feigenson, 2008. Liquid-Liquid Domains in Bilayers Detected by Wide Angle X-Ray Scattering. *Biophys. J.* 95:682–690.

5. Staneva, G., C. Chachaty, C. Wolf, K. Koumanov, and P. J. Quinn, 2008. The role of sphingomyelin in regulating phase coexistence in complex lipid model membranes: Competition between ceramide and cholesterol. *Biochim. Biophys. Acta, Biomembr.* 1778:2727–2739.

6. Pabst, G., B. Boulgaropoulos, E. Gander, B. R. Sarangi, H. Amenitsch, V. A. Raghunathan, and P. Laggner, 2009. Effect of Ceramide on Nonraft Proteins. *J. Membr. Biol.* 231:125–132.

7. Uppamoochikkal, P., S. Tristram-Nagle, and J. F. Nagle, 2010. Orientation of Tie-Lines in the Phase Diagram of DOPC/DPPC/Cholesterol Model Biomembranes. *Langmuir* 26:17363–17368.

8. Heftberger, P., B. Kollmitzer, A. A. Rieder, H. Amenitsch, and G. Pabst, 2015. In Situ Determination of Structure and Fluctuations of Coexisting Fluid Membrane Domains. *Biophysical Journal* 108:854–862.

9. Monks, C. R. F., B. A. Freiberg, H. Kupfer, N. Sciaky, and A. Kupfer, 1998.

Three-dimensional segregation of supramolecular activation clusters in T cells. *Nature* 395:82–86.

10. Grakoui, A., S. K. Bromley, C. Sumen, M. M. Davis, A. S. Shaw, P. M. Allen, and M. L. Dustin, 1999. The Immunological Synapse: A Molecular Machine Controlling T Cell Activation. *Science* 285:221–227.

11. Różycki, B., R. Lipowsky, and T. R. Weikl, 2010. Segregation of receptor–ligand complexes in cell adhesion zones: phase diagrams and the role of thermal membrane roughness. *New J. Phys.* 12:095003.

12. Hu, J., R. Lipowsky, and T. R. Weikl, 2013. Binding constants of membrane-anchored receptors and ligands depend strongly on the nanoscale roughness of membranes. *PNAS* 110:15283–15288.

13. Israelachvili, J. N., 2011. Interactions of Biological Membranes and Structures. *In* Intermolecular and surface forces, Academic Press, Burlington, MA, 577–616.

14. Helfrich, W., 1978. Steric Interaction of Fluid Membranes in Multilayer Systems. *Z. Naturforsch., A: Phys. Sci.* 33:305.

15. Podgornik, R., and V. A. Parsegian, 1992. Thermal-mechanical fluctuations of fluid membranes in confined geometries: the case of soft confinement. *Langmuir* 8:557–562.

16. Pabst, G., 2013. Coupling Membrane Elasticity and Structure to Protein Function. *In* Advances in Planar Lipid Bilayers and Liposomes, Elsevier, volume 18, 81–109.

17. Méléard, P., C. Gerbeaud, T. Pott, L. Fernandez-Puente, I. Bivas, M. D. Mitov, J. Dufourcq, and P. Bothorel, 1997. Bending elasticities of model membranes: influences of temperature and sterol content. *Biophys. J.* 72:2616–2629.

18. Lyatskaya, Y., Y. Liu, S. Tristram-Nagle, J. Katsaras, and J. F. Nagle, 2000. Method for obtaining structure and interactions from oriented lipid bilayers. *Phys. Rev. E* 63:011907.

19. Evans, E., and W. Rawicz, 1990. Entropy-driven tension and bending elasticity in condensed-fluid membranes. *Phys. Rev. Lett.* 64:2094–2097.

20. Boulgaropoulos, B., M. Rappolt, B. Sartori, H. Amenitsch, and G. Pabst, 2012. Lipid Sorting by Ceramide and the Consequences for Membrane Proteins. *Biophys. J.* 102:2031–2038.

21. LeNeveu, D. M., and R. P. Rand, 1977. Measurement and modification of forces between lecithin bilayers. *Biophys. J.* 18:209–230.

22. Parsegian, V. A., N. Fuller, and R. P. Rand, 1979. Measured work of deformation and repulsion of lecithin bilayers. *PNAS* 76:2750–2754.

23. Parsegian, V. A., R. P. Rand, N. L. Fuller, and D. C. Rau, 1986. Osmotic stress for the direct measurement of intermolecular forces. *In* Lester Packer, editor, Methods in Enzymology, Academic Press, volume 127 of *Biomembranes Part O: Protons and Water: Structure and Translocation*, 400–416.

24. McIntosh, T. J., and S. A. Simon, 1986. Hydration force and bilayer deformation: a reevaluation. *Biochemistry* 25:4058–4066.

25. McIntosh, T. J., and S. A. Simon, 1993. Contributions of hydration and steric (entropic) pressures to the interactions between phosphatidylcholine bilayers: Experiments with the subgel phase. *Biochemistry* 32:8374–8384.

26. Rand, R. P., and V. A. Parsegian, 1989. Hydration Forces Between Phospholipid-Bilayers. *Biochim. Biophys. Acta* 988:351–376.

27. Petrache, H. I., N. Gouliaev, S. Tristram-Nagle, R. Zhang, R. M. Suter, and J. F. Nagle, 1998. Interbilayer interactions from high-resolution x-ray scattering. *Phys. Rev. E* 57:7014–7024.

28. Pabst, G., S. Danner, R. Podgornik, and J. Katsaras, 2007. Entropy-Driven Softening of Fluid Lipid Bilayers by Alamethicin. *Langmuir* 23:11705–11711.

29. Pabst, G., N. Kučerka, M.-P. Nieh, M. C. Rheinstädter, and J. Katsaras, 2010. Applications of neutron and X-ray scattering to the study of biologically relevant model membranes. *Chem. Phys. Lipids* 163:460–479.

30. Sornette, D., and N. Ostrowsky, 1986. Importance of membrane fluidity on bilayer interactions. *J. Chem. Phys.* 84:4062–4067.

31. Evans, E. A., and V. A. Parsegian, 1986. Thermal-mechanical fluctuations enhance repulsion between bimolecular layers. *PNAS* 83:7132–7136.

32. Mecke, K. R., T. Charitat, and F. Graner, 2003. Fluctuating Lipid Bilayer in an Arbitrary Potential: Theory and Experimental Determination of Bending Rigidity. *Langmuir* 19:2080–2087.

33. Gouliaev, N., and J. F. Nagle, 1998. Simulations of Interacting Membranes in the Soft Confinement Regime. *Phys. Rev. Lett.* 81:2610–2613.

34. Gouliaev, N., and J. F. Nagle, 1998. Simulations of a single membrane between two walls using a Monte Carlo method. *Phys. Rev. E* 58:881–888.

35. Supplier provided M_W, accounting for an additional water molecule with DOPC, were used for determining stock concentrations.

36. Heberle, F. A., J. Wu, S. L. Goh, R. S. Petruzielo, and G. W. Feigenson, 2010. Comparison of Three Ternary Lipid Bilayer Mixtures: FRET and ESR Reveal Nanodomains. *Biophys. J.* 99:3309–3318.

37. Cohen, J. A., R. Podgornik, P. L. Hansen, and V. A. Parsegian, 2009. A Phenomenological One-Parameter Equation of State for Osmotic Pressures of PEG and Other Neutral Flexible Polymers in Good Solvents†. *J. Phys. Chem. B* 113:3709–3714.

38. Stanley, C. B., and H. H. Strey, 2003. Measuring Osmotic Pressure of Poly(ethylene glycol) Solutions by Sedimentation Equilibrium Ultracentrifugation. *Macromolecules* 36:6888–6893.

39. Amenitsch, H., M. Rappolt, M. Kriechbaum, H. Mio, P. Laggner, and S. Bernstorff, 1998. First performance assessment of the small-angle X-ray scattering beamline at ELETTRA. *J. Synchrotron Radiat.* 5:506–508.

40. Bernstorff, S., H. Amenitsch, and P. Laggner, 1998. High-Throughput Asymmetric Double-Crystal Monochromator of the SAXS Beamline at ELETTRA. *J. Synchrotron Radiat.* 5:1215–1221.

41. Huang, T. C., H. Toraya, T. N. Blanton, and Y. Wu, 1993. X-ray powder diffraction analysis of silver behenate, a possible low-angle diffraction standard. *J. Appl. Crystallogr.* 26:180–184.

42. Hammersley, A. P., 1997. FIT2D: an introduction and overview. *European Synchrotron Radiation Facility Internal Report ESRF97HA02T* .

43. Hammersley, A. P., S. O. Svensson, M. Hanfland, A. N. Fitch, and D. Hausermann, 1996. Two-dimensional detector software: From real detector to idealised image or two-theta scan. *High Pressure Res.* 14:235–248.

44. Konarev, P. V., V. V. Volkov, A. V. Sokolova, M. H. J. Koch, and D. I. Svergun, 2003. PRIMUS: a Windows PC-based system for small-angle scattering data analysis. *J. Appl. Crystallogr.* 36:1277–1282.

45. Ref. 8. We checked the X-ray analysis for coexisting phases by comparing it with PEG-free, homogeneous samples prepared at the published tie-line endpoint concentrations of (0.79:0.09:0.12) for Ld and (0.05:0.65:0.30) for the Lo phase (36). These samples were also helpful for constraining some model details (the widths and distances between molecular subgroups composing the lipid heads) in the X-ray analysis.

46. Zhang, R., R. M. Suter, and J. F. Nagle, 1994. Theory of the structure factor of lipid bilayers. *Phys. Rev. E* 50:5047–5060.

47. Caillé, A., 1972. Physique cristalline: remarques sur la diffusion des rayons X dans les smectiques. *C. R. Acad. Sc. Paris Sie B.* 274:891–893.

48. Kučerka, N., J. F. Nagle, J. N. Sachs, S. E. Feller, J. Pencer, A. Jackson, and J. Katsaras, 2008. Lipid Bilayer Structure Determined by the Simultaneous Analysis of Neutron and X-Ray Scattering Data. *Biophys. J.* 95:2356–2367.

49. Rawicz, W., B. Smith, T. McIntosh, S. Simon, and E. Evans, 2008. Elasticity, Strength, and Water Permeability of Bilayers that Contain Raft Microdomain-Forming Lipids. *Biophys. J.* 94:4725–4736.

50. Rawicz, W., K. C. Olbrich, T. McIntosh, D. Needham, and E. Evans, 2000. Effect of Chain Length and Unsaturation on Elasticity of Lipid Bilayers. *Biophys. J.* 79:328–339.

51. Gouliaev, N., 1998. Monte-Carlo simulations of membrane systems. Ph.D. thesis, Carnegie Mellon University, Pittsburgh, Pennsylvania, USA.

52. Specifically, we use $d_B = 2(z_{CholCH3} + \sigma_{CholCH3})$, where $z_{CholCH3}$ and $\sigma_{CholCH3}$ are the position (measured from the bilayer center) and the width, respectively, of the lipid head choline's CH_3 groups. Within measurement accuracy, the definition used in Ref. 27 yields equal values.

53. McDonald, I., 1972. NpT-ensemble Monte Carlo calculations for binary liquid mixtures. *Mol. Phys.* 23:41–58.

54. Bouzida, D., S. Kumar, and R. H. Swendsen, 1992. Efficient Monte Carlo methods for the computer simulation of biological molecules. *Phys. Rev. A* 45:8894–8901.

55. Cooke, I. R., and M. Deserno, 2005. Solvent-free model for self-assembling fluid bilayer membranes: Stabilization of the fluid phase based on broad attractive tail potentials. *J. Chem. Phys.* 123:224710.

56. Pabst, G., N. Kučerka, M.-P. Nieh, and J. Katsaras, 2014. Liposomes, Lipid Bilayers and Model Membranes: From Basic Research to Application. CRC Press.

57. An additional steric repulsion $A_{st}\lambda_{st}\exp(-a/\lambda_{st})$, with $A_{st} = 3.6\,\mathrm{GPa}$ and $\lambda_{st} = 0.6\,\text{Å}$ according to (64) was used, but proved unimportant for realistic parameters.

58. Marčelja, S., and N. Radić, 1976. Repulsion of interfaces due to boundary water. *Chem. Phys. Lett.* 42:129–130.

59. Kanduč, M., E. Schneck, and R. R. Netz, 2013. Hydration interaction between phospholipid membranes: insight into different measurement ensembles from atomistic molecular dynamics simulations. *Langmuir* 29:9126–9137.

60. Kanduč, M., A. Schlaich, E. Schneck, and R. R. Netz, 2014. Hydration repulsion between membranes and polar surfaces: Simulation approaches versus continuum theories. *Adv. Colloid Interface Sci.* 208:142–152.

61. Parsegian, V. A., 2006. Van der Waals forces. Cambridge university press Cambridge etc.

62. The van der Waals potential for infinitely extended slabs of finite thickness d_B at separation a is $\propto (1/a^2 - 2/(a+d_B)^2 + 1/(a+2d_B)^2)$ (61, p. 15), and was applied for osmotic stress experiments in e.g. Refs 6, 27.

63. Podgornik, R., R. H. French, and V. A. Parsegian, 2006. Nonadditivity in van der Waals interactions within multilayers. *J. Chem. Phys.* 124:044709.

64. McIntosh, T. J., A. D. Magid, and S. A. Simon, 1987. Steric repulsion between phosphatidylcholine bilayers. *Biochemistry* 26:7325–7332.

65. Although this model gives only a first order estimate for the van der Waals interactions of fluctuating lipid bilayers, it is to our knowledge the best available approximation in the absence of data on the dielectric response of PC lipids.

66. 2011. MATLAB v. 7.12 (R2011a).

67. Taylor, J., 1997. Introduction to Error Analysis, the Study of Uncertainties in Physical Measurements, 2nd Edition, volume 1. University Science Books, New York.

68. Alternatively, one could have used optimization algorithms specialized for simulations (91–94), but the existing implementations did not satisfy our needs.

69. Hemmerle, A., L. Malaquin, T. Charitat, S. Lecuyer, G. Fragneto, and J. Daillant, 2012. Controlling interactions in supported bilayers from weak electrostatic repulsion to high osmotic pressure. *PNAS* 109:19938–19942.

70. Pabst, G., 2006. Global properties of biomimetic membranes: perspectives on molecular features. *Biophys. Rev. Lett.* 01:57–84.

71. The small offset $\delta = 200\,\mathrm{Pa}$ is necessary for plotting $P = 0$ on a logarithmic scale.

72. Pan, J., T. T. Mills, S. Tristram-Nagle, and J. F. Nagle, 2008. Cholesterol Perturbs Lipid Bilayers Nonuniversally. *Phys. Rev. Lett.* 100:198103.

73. Sorre, B., A. Callan-Jones, J.-B. Manneville, P. Nassoy, J.-F. Joanny, J. Prost, B. Goud, and P. Bassereau, 2009. Curvature-driven lipid sorting needs proximity to a demixing point and is aided by proteins. *PNAS* 106:5622–5626.

74. Tian, A., B. R. Capraro, C. Esposito, and T. Baumgart, 2009. Bending Stiffness Depends on Curvature of Ternary Lipid Mixture Tubular Membranes. *Biophys. J.* 97:1636–1646.

75. Gracià, R. S., N. Bezlyepkina, R. L. Knorr, R. Lipowsky, and R. Dimova, 2010. Effect of cholesterol on the rigidity of saturated and unsaturated mem-

branes: fluctuation and electrodeformation analysis of giant vesicles. *Soft Matter* 6:1472–1482.

76. Khelashvili, G., B. Kollmitzer, P. Heftberger, G. Pabst, and D. Harries, 2013. Calculating the Bending Modulus for Multicomponent Lipid Membranes in Different Thermodynamic Phases. *J. Chem. Theory Comput.* 9:3866–3871.

77. Pan, J., S. Tristram-Nagle, and J. F. Nagle, 2009. Effect of cholesterol on structural and mechanical properties of membranes depends on lipid chain saturation. *Phys. Rev. E* 80:021931.

78. This relation was suggested by Evan Evans (77).

79. For a given potential Φ, we calculate the bare pressure by $-\partial\Phi(d_W)/\partial d_W$. We found that the difference to the exact relationship $\langle -\partial\Phi(\bar{a})/\partial\bar{a}\rangle$ is smaller than the corresponding uncertainty from the simulations. The fluctuation pressure is calculated directly via $P_{und} = P - P_{hyd} - P_{vdW}$, according to Ref. 34.

80. Effective decay lengths λ_{und} were determined by fitting a straight line to $\ln P_{und}(d_W)$ in the limit of large separations ($d_W \geq 14\,\text{Å}$).

81. Salsburg, Z. W., J. D. Jacobson, W. Fickett, and W. W. Wood, 1959. Application of the Monte Carlo Method to the Lattice-Gas Model. I. Two-Dimensional Triangular Lattice. *J. Chem. Phys.* 30:65–72.

82. Ferrenberg, A. M., and R. H. Swendsen, 1988. New Monte Carlo technique for studying phase transitions. *Phys. Rev. Lett.* 61:2635–2638.

83. Ferrenberg, A. M., and R. H. Swendsen, 1989. Optimized Monte Carlo data analysis. *Phys. Rev. Lett.* 63:1195–1198.

84. Kumar, S., J. M. Rosenberg, D. Bouzida, R. H. Swendsen, and P. A. Kollman, 1992. The weighted histogram analysis method for free-energy calculations on biomolecules. I. The method. *J. Comput. Chem.* 13:1011–1021.

85. Nagle, J. F., 2013. Introductory Lecture: Basic quantities in model biomembranes. *Faraday Discuss.* 161:11.

86. Chu, N., N. Kučerka, Y. Liu, S. Tristram-Nagle, and J. F. Nagle, 2005. Anomalous swelling of lipid bilayer stacks is caused by softening of the bending modulus. *Phys. Rev. E* 71:041904.

87. Bonner, J. C., and M. E. Fisher, 1964. Linear Magnetic Chains with Anisotropic Coupling. *Phys. Rev.* 135:A640–A658.

88. Nagle, J. F., and J. C. Bonner, 1970. Numerical studies of the Ising chain with long-range ferromagnetic interactions. *J. Phys. C: Solid State Phys.* 3:352.

89. Quenouille, M. H., 1956. Notes on Bias in Estimation. *Biometrika* 43:353–360.

90. Tukey, J. W., 1958. Bias and confidence in not quite large samples (abstract). *Ann. Math. Statist.* 29:614.

91. Ben-Tal, A., and A. Nemirovski, 1999. Robust solutions of uncertain linear programs. *Operations Research Letters* 25:1–13.

92. Ben-Tal, A., and A. Nemirovski, 2000. Robust solutions of Linear Programming problems contaminated with uncertain data. *Math. Program.* 88:411–424.

93. Fu, M. C., 2002. Feature Article: Optimization for simulation: Theory vs. Practice. *INFORMS Journal on Computing* 14:192–215.

94. Ben-Tal, A., A. Goryashko, E. Guslitzer, and A. Nemirovski, 2004. Adjustable robust solutions of uncertain linear programs. *Math. Program., Ser. A* 99:351–376.

Supporting information for: Bending rigidities and interdomain forces in membranes with coexisting lipid domains

B. Kollmitzer, P. Heftberger, R. Podgornik,
J. F. Nagle, and G. Pabst

February 25, 2015, Graz

S1 Area extension modulus estimation

The dependence of bilayer thickness on osmotic pressure P is accounted for via the area extension modulus K_A and given by the equation[1]

$$d_B(P) = d_B(0)\frac{K_A + P\,d(P)}{K_A + P\,d_B(0)}. \tag{S1}$$

We estimated K_A for our coexisting liquid phases based on published data for single lipids and binary lipid mixtures by Rawicz *et al.*[2,3] The Ld phase under investigation consists essentially of DOPC, with approximately 10 mol% cholesterol.[4] Interpolating linearly between the two published values for 0 and 50 mol% cholesterol in DOPC[2] yields $K_{A,\mathrm{Ld}} = (430 \pm 30)\,\mathrm{mN\,m^{-1}}$.

In the coexisting Lo phase, the main constituent is the saturated lipid DSPC, which is accompanied by ca. 30 mol% cholesterol.[4] Unfortunately, published K_A values for saturated lipids are sparse. As a compromise, we interpolated linearly between pure DMPC (0 mol% cholesterol) and a 1:1 mixture of sphingomyelin/cholesterol,[2,3] yielding $K_A = (2100 \pm 500)\,\mathrm{mN\,m^{-1}}$ for our Lo phase.

As pointed out in the section *X-ray measurements* of the main text, knowing the magnitude of K_A is more important than getting the precise number. That is because the biggest estimated change in bilayer thickness turned out to be just 0.3 Å. In principle, such a subtle difference in d_B would be resolvable with SAXS, but not with the additional scattering signal due to PEG.

S2 Finite size convergence

With open edges, one generally expects a 'surface' perturbation proportional to the relative size of the boundary to the interior, i.e. proportional to $1/N$ for our systems. As is well known, periodic boundary conditions generally reduce this perturbation. They also speed up the convergence with system size, from $1/N$ to $1/N^2$ in a case well documented by Bonner and Fisher[5] (note their Fig. 1) and in the case of the one-dimensional Ising model the convergence is exponentially fast with periodic boundary condions. While another case with very slow convergence is known,[6] that one is due to very long range interactions not present in our membrane stacks.

For periodic boundary conditions, the exact solution of a harmonic approximation to Eq. (3) suggests that d_W and Δ converge asymptotically like $y(N) \sim c_\infty - c_2/N^2$, i.e. convergence is expected to be faster than $1/N$ and, in agreement with the previous simulations,[7] our results are consistent with a dominant $1/N^2$ asymptotic convergence, allowing, of course, for higher order terms.

We perform simulations for several 'densities' $N \in \{N_{min}, \dots, N_{max}\}$ and fit them with the function $y(N) = c_\infty + \sum_{k=2}^{k_{max}} c_k/N^k$. Together with the originally proposed $k_{max} = 3$ and $N \in \{6, \dots, 32\}$, this method yields sufficiently precise continuum estimators c_∞, compared to the experimental uncertainties.[8] However, we found that varying the arbitrary parameters k_{max} and N_{min} influenced the final estimator stronger for some simulations (e.g. high pressures) than for others. To obtain more reliable uncertainties and perhaps even better continuum estimates, we perform now several extrapolations, with different values for k_{max} and N_{min}, but always using the highest possible N_{max}. By not changing N_{max}, we weight the most significant simulations (with the highest density) stronger. This procedure yields a list of results for $c_{\infty,l}$, which we average for the final estimator. Its uncertainty is then determined by the individual errors of $c_{\infty,l}$ (statistical uncertainty of observables due to finite simulation length) and their standard deviation (error due to finite simulation density). This procedure is closely related to the Jackknife technique.[9,10]

Comparisons between these improved Jackknife estimators and estimators obtained by the original method are given in Fig. S1. The relative difference in the estimators were less than 5% for all performed simulations, but most importantly, Jackknife produces a meaningful uncertainty.

S3 Efficient differentiation

A single simulation of a particular set of parameters $\vec{\Lambda} = (P, A, H, \lambda, K_c, \dots)$ contains more information in the generated time series, than the aforementioned observables which are determined by averaging. By reweighting the simulated histogram of density of states, it is possible to compute these quantities over a certain range of simulation parameters and thereby also derive their gradients.[11–13] [14] This well recognized method was briefly mentioned for membrane MC simulations,[15] but has not been implemented for them previously.

We calculated the expectation value of an observable $f(u, \bar{a})$ for a different set of parameters $\vec{\Lambda}'$ from a simulation performed at $\vec{\Lambda}$ by

$$\langle f \rangle_{\vec{\Lambda}'} = \frac{\sum f_{\vec{\Lambda}'}(u, \bar{a}) \cdot \exp\left(-\delta G/kT\right)}{\sum \exp\left(-\delta G/kT\right)}, \tag{S2}$$

where the sums extend over all realized configurations and δG is the change in the Gibbs energy of each state $(u, \bar{a})$ upon changing $\vec{\Lambda}$ to $\vec{\Lambda}'$. Most parameters could be separated from u and $\bar{a}$ in our case, yielding $\delta G(u, \bar{a}) = \delta\Lambda \cdot \xi(u, \bar{a})$. This allowed us to store only the time series of ξ instead of all realized states. The parameters P, A, H, and K_c were separable in this way, yielding

$$\frac{\delta G}{V} = \delta P\, \xi_P + \delta A\, \lambda\, \xi_A - \frac{\delta H}{12\pi}\, \xi_H + N^2 \frac{\delta K_c}{2}\, \xi_{Kc}, \tag{S3}$$

where $\xi_P = \bar{a}/d_W$, $\xi_A = \overline{\exp(-a/\lambda)}$, $\xi_H = \overline{1/a^2}$, and $\xi_{Kc} = \overline{q^4 |u_m(q_x, q_y)|^2}$. The local distance between membranes is denoted by $a = u_{m+1}(i,j) - u_m(i,j) + \bar{a}$, while the bars denote averages over (m, i, j) or (m, q_x, q_y). $V = L^2 M \bar{a}$ is the membrane stack's volume.

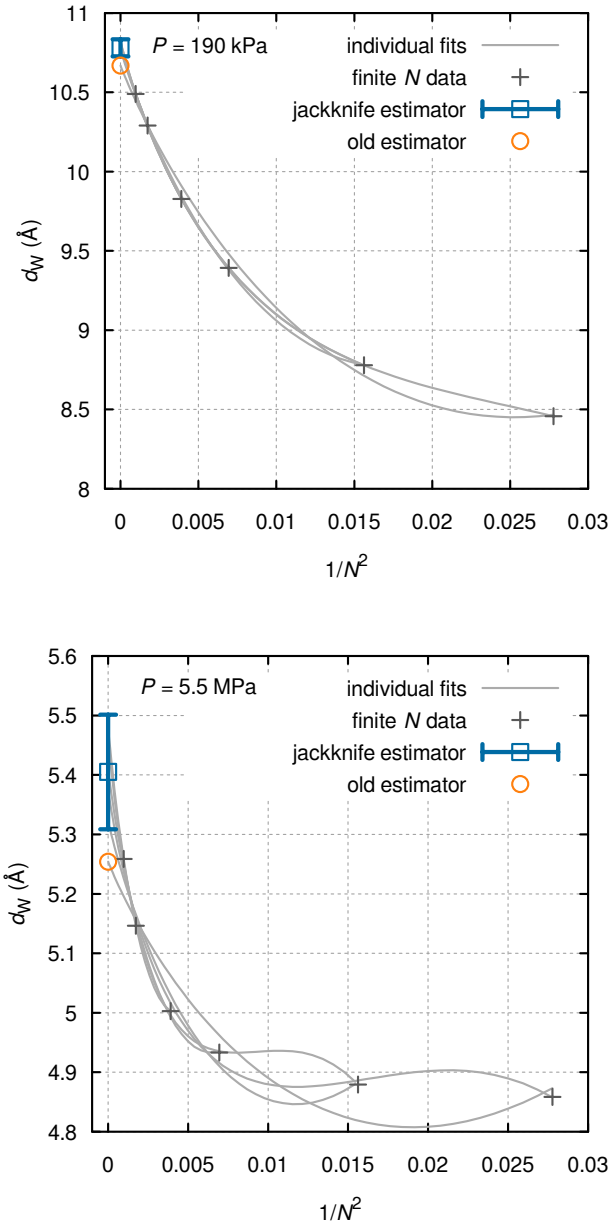

Figure S1: Finite size convergence of membrane spacing d_W vs membrane "density" N of Ld domains according to Tab. 1 at intermediate (top) and high osmotic pressures P (bottom). A variant of Jackknife allows us to obtain reasonable errors for the estimator. Statistical uncertainties for plotted finite N data are less than 10^{-2} Å.

Separating λ from $(u, \bar{a})$ in δG turned out to be impossible, but we were able to calculate gradients of d_W and Δ with respect to λ efficiently. Because d_W and Δ did not depend explicitly on λ (i.e. $\partial f/\partial\lambda = 0$), differentiating Eq. (S2) yielded,

$$\left.\frac{\partial\langle f\rangle_{\lambda'}}{\partial\lambda'}\right|_{\lambda'=\lambda} = -\frac{AV}{kTN^2\Omega}\left(\sum f(u,\bar{a})\xi_\lambda - \langle f\rangle_\lambda \sum \xi_\lambda\right), \tag{S4}$$

where sums extend over all realized states, Ω denotes the collection length and

$$\xi_\lambda = \overline{\left(1+\frac{a}{\lambda}\right)\exp\left(-\frac{a}{\lambda}\right)}. \tag{S5}$$

Up to first order, $\langle f\rangle_{\lambda'}$ was then determined from $\langle f\rangle_{\lambda'} \approx \langle f\rangle_\lambda + (\lambda' - \lambda)\ \partial\langle f\rangle/\partial\lambda$.

Thus, for any observable $f \in \{d_W, \Delta\}$ and parameter $\Lambda \in \{P, A, H, K_c, \lambda\}$, we first determined $\langle f\rangle_{1,2}(N)$ for $\Lambda_{1,2} = \Lambda \pm \delta\Lambda$ as detailed above, extrapolated these expectation values for $N \to \infty$ according to section S2, and finally calculated the finite difference quotient $\partial\langle f\rangle/\partial\Lambda \approx (\langle f\rangle_1 - \langle f\rangle_2)/2\delta\Lambda$. Relative finite differences were set to $\delta\Lambda/\Lambda = 0.03$.

We checked this method against direct numerical differentiation for a couple of reasonable parameters. Errors were always sufficiently small (well below 50%) to lead the optimization routine towards a global minimum (see the section *Optimizing parameters against experimental data* of the main text).

S4 Results for a homogeneous control sample

We tested our analysis on already published SAXS data for homogeneous DMPC MLVs.[16] The Lifshitz calculation of the van der Waals forces yielded a value of $H = 4.11\,\mathrm{zJ}$ for the published bilayer thickness of 44.0 Å. The obtained values describing the intersurface forces are given in Tab. S1, while Fig. S2 compares the simulations with the experimental data. Reassuringly, the simulations fit the experimental pressure data well. While the fit to Δ is excellent for high hydration, the fit becomes relatively poor for Δ as d_W becomes small, similarly to our L_o sample and likely for the same reason given in the main text.

The interaction parameters obtained from the fit are shown in Tab. S1. Literature values for DMPC's bending modulus range from 50–130 zJ at 30 °C.[18] In light of this large variation, comparing only results of related methods is appropriate. Ref. 16 could not determine K_c and the modulus B separately and therefore considered several values of K_c; two of these are shown in Tab. S1. The values of A agree very well with ours. The larger values of λ would have been smaller if the true value of K_A had been known at that time. Two differences from the previous analyses are that here we calculated H and we used simulations; these cause the main differences reflected in the pairs of values for H and K_c in Tab. S1. Table S1 also shows results from another study,[19] that employed the same kind of simulations used here and differed by obtaining X-ray data from oriented stacks of DMPC bilayers, from which K_c was obtained directly. It also used the same P data, but failed to readjust the A and λ values to account for the corrected K_A. Nevertheless, agreement is reasonable.

For completeness, the functional dependence of the individual fundamental surface forces for DMPC is plotted in Fig. S3. The fluctuation force becomes the dominant repulsive force when d_W exceeds 9 Å, intermediate between the values of the Ld and Lo phases in Fig. 7, suggesting that the DMPC bilayer fluctuations are intermediate in this regard between the more fluid Ld phase and the more ordered Lo phase in the studied mixture. This is consistent with the Ld

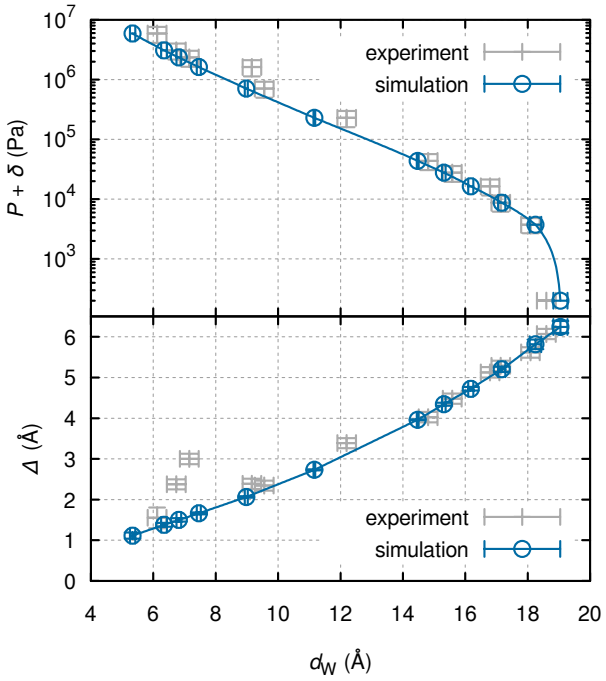

Figure S2: Pressure (top) and fluctuations (bottom) vs water-layer thickness for best fit of membrane MC simulation (cyan) against SAXS data (light gray) obtained from Ref. 16.[17] Solid lines were obtained by exponentially interpolating fluctuation contributions.

Table S1: Optimal parameters found for describing the DMPC data published in Ref. 16.

	Current	1998a [16]	1998b [16]	2005 [19]
H/zJ	4.11	7.13	4.91	6.1
K_c/zJ	57 ± 5	50	80	69
A/Pa	$10^{8.1 \pm 0.2}$	$10^{8.1}$	$10^{8.1}$	$10^{8.1}$
λ/Å	1.66 ± 0.15	1.91	1.97	1.91

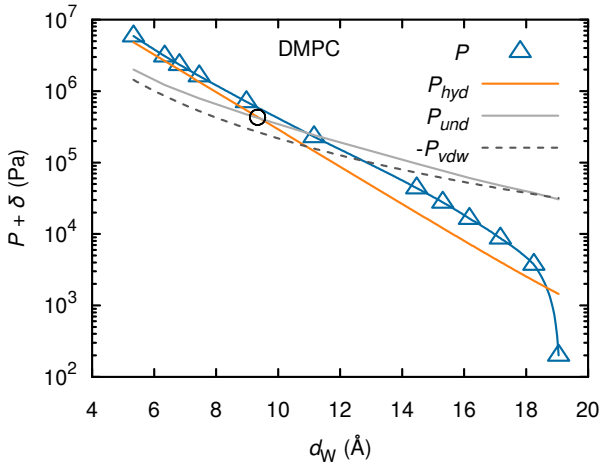

Figure S3: Partitioning of total pressure P into contributions from hydration P_{hyd}, van der Waals P_{vdw}, and undulations P_{und} for DMPC.[17] The large open black circle shows the value of the separation d_W at which hydration and undulation pressure are equal.

phase having a high concentration of the more disordered unsaturated lipids and the Lo phase having longer saturated chains with cholesterol.

S5 SAXS analysis

Comparisons between full q-range SAXS analyses and experimental data are shown in Fig. S4. Deviations between data and fits, especially for higher q ranges, are due to imperfect background subtraction, as explained in the section *X-ray measurements* in the main text.

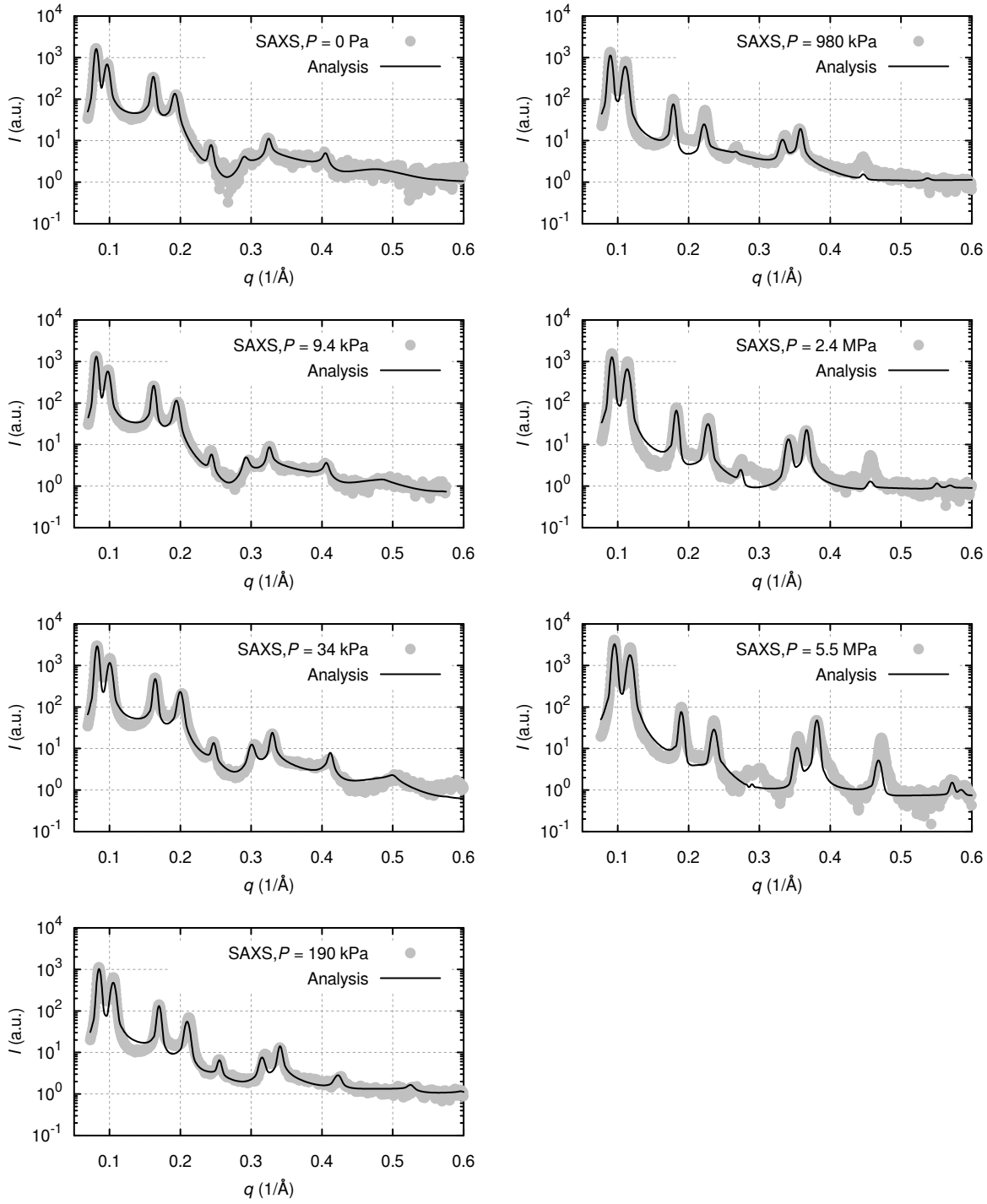

Figure S4: Calculated scattering intensities (solid lines) from full q-range analyses, compared to recorded SAXS data from coexisting phases (dots) of DOPC/DSPC/Chol (0.42:0.37:0.21), for all recorded osmotic pressures P.

S6 Fluctuations of the interbilayer water spacing

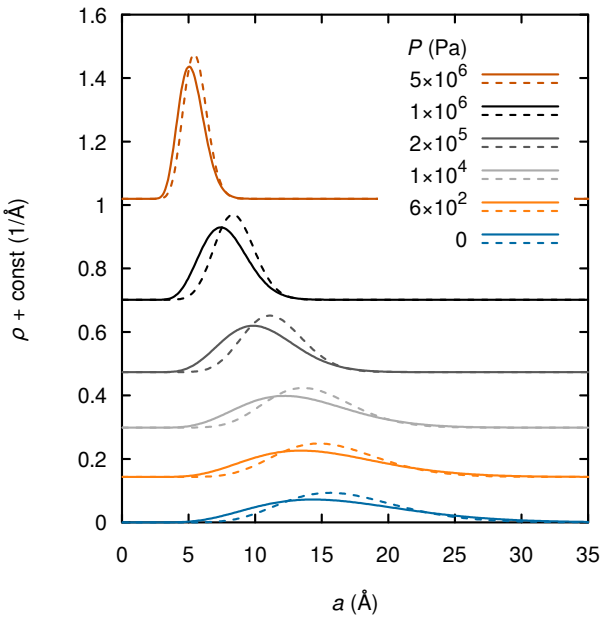

Figure S5: Probability density function ρ of the water spacing a at different external pressures P, for Ld (solid) and Lo (dashed) according to Tab. 1, obtained from $N = 32$ simulations.

References

[1] R. P. Rand and V. A. Parsegian. Hydration Forces Between Phospholipid-Bilayers. *Biochim. Biophys. Acta*, 988(3):351–376, December 1989.

[2] W. Rawicz, B.A. Smith, T.J. McIntosh, S.A. Simon, and E. Evans. Elasticity, Strength, and Water Permeability of Bilayers that Contain Raft Microdomain-Forming Lipids. *Biophys. J.*, 94(12):4725–4736, June 2008.

[3] W. Rawicz, K. C. Olbrich, T. McIntosh, D. Needham, and E. Evans. Effect of Chain Length and Unsaturation on Elasticity of Lipid Bilayers. *Biophys. J.*, 79(1):328–339, July 2000.

[4] Frederick A. Heberle, Jing Wu, Shih Lin Goh, Robin S. Petruzielo, and Gerald W. Feigenson. Comparison of Three Ternary Lipid Bilayer Mixtures: FRET and ESR Reveal Nanodomains. *Biophys. J.*, 99(10):3309–3318, November 2010.

[5] Jill C. Bonner and Michael E. Fisher. Linear Magnetic Chains with Anisotropic Coupling. *Phys. Rev.*, 135(3A):A640–A658, August 1964.

[6] J. F. Nagle and J. C. Bonner. Numerical studies of the Ising chain with long-range ferromagnetic interactions. *J. Phys. C: Solid State Phys.*, 3(2):352, February 1970.

[7] Nikolai Gouliaev and John F. Nagle. Simulations of Interacting Membranes in the Soft Confinement Regime. *Phys. Rev. Lett.*, 81(12):2610–2613, September 1998.

[8] Nikolai Gouliaev and John F. Nagle. Simulations of a single membrane between two walls using a Monte Carlo method. *Phys. Rev. E*, 58(1):881–888, July 1998.

[9] M. H. Quenouille. Notes on Bias in Estimation. *Biometrika*, 43(3/4):353–360, December 1956.

[10] John W. Tukey. Bias and confidence in not quite large samples (abstract). *Ann. Math. Statist.*, 29(2):614, June 1958.

[11] Z. W. Salsburg, J. D. Jacobson, W. Fickett, and W. W. Wood. Application of the Monte Carlo Method to the Lattice-Gas Model. I. Two-Dimensional Triangular Lattice. *J. Chem. Phys.*, 30(1):65–72, January 1959.

[12] Alan M. Ferrenberg and Robert H. Swendsen. New Monte Carlo technique for studying phase transitions. *Phys. Rev. Lett.*, 61(23):2635–2638, December 1988.

[13] Alan M. Ferrenberg and Robert H. Swendsen. Optimized Monte Carlo data analysis. *Phys. Rev. Lett.*, 63(12):1195–1198, September 1989.

[14] A common extension of this method would even allow to combine information from multiple simulations (WHAM)[20].

[15] Nikolai Gouliaev. *Monte-Carlo simulations of membrane systems.* PhD thesis, Carnegie Mellon University, Pittsburgh, Pennsylvania, USA, July 1998.

[16] Horia I. Petrache, Nikolai Gouliaev, Stephanie Tristram-Nagle, Ruitian Zhang, Robert M. Suter, and John F. Nagle. Interbilayer interactions from high-resolution x-ray scattering. *Phys. Rev. E*, 57(6):7014–7024, June 1998.

[17] The small offset $\delta = 200\,\mathrm{Pa}$ is necessary for plotting $P = 0$.

[18] John F. Nagle. Introductory Lecture: Basic quantities in model biomembranes. *Faraday Discuss.*, 161:11, 2013.

[19] Nanjun Chu, Norbert Kučerka, Yufeng Liu, Stephanie Tristram-Nagle, and John F. Nagle. Anomalous swelling of lipid bilayer stacks is caused by softening of the bending modulus. *Phys. Rev. E*, 71(4):041904, April 2005.

[20] Shankar Kumar, John M. Rosenberg, Djamal Bouzida, Robert H. Swendsen, and Peter A. Kollman. The weighted histogram analysis method for free-energy calculations on biomolecules. I. The method. *J. Comput. Chem.*, 13(8):1011–1021, 1992.